STRUCTURAL CONTROLS ON THE EDWARDS AQUIFER/TRINITY AQUIFER INTERFACE IN THE CAMP BULLIS QUADRANGLE, TEXAS

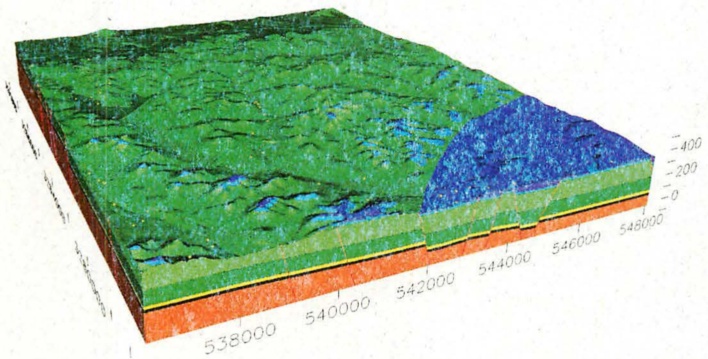

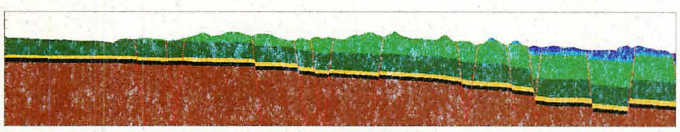

DECEMBER 2003

SOUTHWEST RESEARCH INSTITUTE®
SAN ANTONIO HOUSTON WASHINGTON, DC

Structural Controls on the Edwards Aquifer/Trinity Aquifer Interface in the Camp Bullis Quadrangle, Texas

David A. Ferrill[1], Darrell W. Sims[1], Alan P. Morris[2], Deborah J. Waiting[1], Nathan Franklin[1]

[1] CNWRA, Southwest Research Institute®, San Antonio, TX 78238-5166

[2] Department of Earth and Environmental Science, University of Texas at San Antonio, San Antonio, TX 78249

Prepared for:

Edwards Aquifer Authority

and

U.S. Army Corps of Engineers

December 5, 2003

EXECUTIVE SUMMARY

The purpose of the project reported here is to characterize the structural architecture of the Edwards and Trinity Aquifers for the area of the Camp Bullis 7 ½ minute quadrangle, and extending north to include Cibolo Creek in the southern part of the Bergheim 7 ½ minute quadrangle. Included in this analysis are tasks to generate a three-dimensional computer model of the Trinity and Edwards Aquifer, and perform field investigations to characterize the mechanisms and products of localized fault-related deformation in the Edwards and Trinity Aquifers in and near the study area. An important objective is to analyze the potential for communication between the Edwards Aquifer and the Trinity Aquifers, taking into account fault-related deformation and juxtaposition of the aquifers across key faults.

Results of the project show the aquifer architecture throughout the study area, the location and interpreted geometry of the most important mapped faults in the study area, and the deformation mechanisms and deformation style in fault zones in the rocks of both the Edwards and Trinity Aquifers. The three-dimensional geologic framework model of the Camp Bullis area reveals (i) juxtaposition of permeable and relatively impermeable hydrogeologic units, (ii) structural thinning of the Edwards Aquifer and Trinity Aquifers, (iii) potential for cross-fault communication between the Trinity and Edwards Aquifers, (iv) faults expressed on the surface as potential infiltration pathways, and (v) maximum offset concentrated along a small number (two or three) fault systems. This information, along with an understanding of fault zone deformation mechanisms and the role of fault zones as barriers or conduits, can assist in locating environmentally sensitive areas. It is useful for aquifer water flow path studies and contributes to the identification of areas where communication between the Trinity and the Edwards Aquifers is suspected.

In this geologic framework model, the Edwards and Trinity Aquifers are subdivided into seven stratigraphic horizons which are offset by a network of 40 faults. Vertical offset (fault throw) ranges from near zero to an approximate maximum of 110 meters (361 ft). Displacement sense is normal, commonly down to the southeast, and lateral displacement gradients are small. In map view, fault blocks are elongate, with the long axis oriented NE-SW. Maximum offset is concentrated along three fault systems, the southernmost of which forms the northern boundary of the aquifer recharge zone, where rocks of the Edwards Group are in faulted juxtaposition with rocks of the Glen Rose Formation.

Fault displacements within the Camp Bullis study area are too small to place the base of the Edwards Aquifer (Basal Nodular layer) against the permeable Lower Glen Rose layer. However, each fault decreases the effective aquifer thickness. This structural thinning of aquifer layers can cause flow constrictions, which in turn diverts flow and causes fluctuations in the local water table from fault block to fault block. Areas of such flow constrictions can be identified using a map of fault throw distribution; constriction is greatest where fault throw is greatest.

In the Castle Hills quadrangle, immediately south of the Camp Bullis quadrangle, several faults offset the Edwards Aquifer by distances equal to or greater than its full thickness. Smaller fault

displacements in the Camp Bullis area and the northern part of the Castle Hills quadrangle reduce the amount of direct juxtaposition of Kainer against Lower Glen Rose in these areas to a minimum. The lack of fault juxtaposition of the recognized highly permeable units of the Edwards Group and Glen Rose Formation in the Camp Bullis and Castle Hills areas suggests that simple juxtaposition is not likely to be a major source of aquifer communication in this area.

3DStress™ analysis of measured faults, and regional stratigraphic thicknesses based on published maps yield a stress system during faulting of: vertical effective stress = 15 MPa; minimum horizontal effective stress (σ_3') = 4 MPa with an azimuth of 150°; and an intermediate principal effective stress = 9.5 MPa. When applied to the fault surfaces exported from the three-dimensional geologic framework model, this stress tensor indicates that the dominant, NE-SW striking faults experience high slip tendencies and are well oriented to have accommodated regional strains developed within the inferred stress system. A few NW-SE trending faults experience low slip tendencies and probably formed in response to local stress perturbations, indicating that local perturbations resulting from such effects as displacement-gradient-driven fault block deformation were not widely developed in this area. In addition to experiencing high slip tendencies in the inferred stress system, the predominant faults are also subject to high dilation tendencies. This combination of high slip and dilation tendencies implies that the major faults could have been effective fluid transmission pathways at the time of faulting. If a similar stress system were extant today, the faults would be in favorable orientations for fluid transmissivity.

Fault block deformation calculated using cutoff lines generated from the three-dimensional geologic framework model results in cutoff line elongations that rarely exceed 2% (positive or negative). These small cutoff elongations reflect the low displacement gradients on faults within the Camp Bullis study area. At the scale of the three-dimensional model, competent units exhibit gentle dips, which is consistent with relatively rapid lateral and vertical fault propagation, until intersection with other faults occurs (laterally) or intersection with a weaker mechanical layer occurs. This lack of steep lateral displacement gradients suggests rapid fault propagation with respect to the rate of displacement accumulation on the faults.

Field work reveals interesting contrasts between faults in the Edwards and Trinity Aquifers. Faults with displacements of 5 m (16 ft) to tens of meters in the Glen Rose Formation (Trinity Aquifer) commonly have damage zones with widths on the order of meters, within which small faults and rotated fault blocks are common. Although faults with displacements of 5 m (16 ft) to tens of meters in the Edwards Group limestones typically have numerous associated small faults, block rotation and bed tilting is not common. This characteristic difference in structural style between the Edwards Group limestones and the Glen Rose Formation appears to be related to lithologic differences and the resulting differences in mechanical behavior of the two stratigraphic sections. The Glen Rose Formation contains both competent massive limestone beds and incompetent argillaceous limestone and shale beds. Incompetent beds tend to arrest fault propagation during fault growth. Consequently, with increasing fault displacement, fault tips (terminations) episodically propagate then arrest. Continued displacement on a fault with an arrested fault tipline will produce fault tipline folding and associated local deformation such as intense small scale faulting. Resulting fault damage zones can be quite complex and variable along a fault, related to the structural position (including displacement magnitude) and the associated mechanical stratigraphy. Permeability in fault zones and fault blocks is likely to be strongly influenced by the different deformation styles in mechanical layers, and the deformation progression with increasing fault displacement.

The large fault surfaces that cut multiple layers depicted in the Camp Bullis geologic framework model provide potential pathways for both vertical and lateral movement of water and hydraulic communication between aquifers. These fault surfaces along with localized zones of relatively intense small scale faulting and extension fracturing, and limestone solution (karst conduit formation) provide likely communication pathways between the Trinity and Edwards Aquifers. The structural analyses presented in this report provide the framework for more detailed investigations of groundwater levels, multiwell pumping (drawdown) tests, tracer studies, and geochemical investigations to further investigate potential groundwater communication between the Trinity and Edwards Aquifers in the Camp Bullis and Castle Hills Quadrangles.

Acknowledgments

This work was funded jointly by the Edwards Aquifer Authority and the U.S. Army Corps of engineers. Results reported from three-dimensional geologic framework modeling of the Castle Hills quadrangle and some of the work on stress analysis and fault zone deformation were funded by Southwest Research Institute through the SwRI Internal Research and Development Program (project #R9223.01.001). We thank Steve Johnson, Geary Schindel and John Hoyt for their efforts in planning and executing the project. San Antonio Water System, Bureau of Economic Geology, U.S. Geological Survey, and Edwards Aquifer Authority provided invaluable assistance. We especially thank Alvin Schultz and Allan Clark for their major efforts to supply data and discuss interpretations in preparation for geologic framework modeling. Eddie Collins, Sue Hovorka, Steve Johnson, Kirk Nixon, George Ozuna, Geary Schindel, and John Waugh assisted by providing data and suggestions during the course of this work. We thank Jerry D. Brite for providing access to the Canyon Lake spillway discharge channel area and spillway gorge for research. Japan National Oil Corporation allowed us to use data we collected as part of work for them in 2000 and 2001. Dr. H. Lawrence McKague and Dr. John Russell improved this report by their constructive reviews.

TABLE OF CONTENTS

LIST OF FIGURES

Chapter 1:

Chapter 2:

Chapter 3:

Figure 4-1. Map of the Balcones fault system in the San Antonio area with fault traces colored according to their slip tendencies. Slip tendency analysis was performed using 3DStress™ v. 1.3.2 (see Ferrill et al., 2003a) based on mapped faults of Collins and Hovorka (1994).

Figure 4-2. The effects of faulting on the Trinity and Edwards Aquifers. Different stratigraphic layers are juxtaposed across faults with different displacements; pattern of juxtaposition is related to the amount of displacement on the fault. Faults with 20 m (66 ft), 40 m (131 ft), 60 m (198 ft), 80 m (262 ft), 100 m (328 ft), and 120 m (394 ft) throw are illustrated. In this generalized model, a fault with 40 m (131 ft) of throw could juxtapose the Trinity Aquifer with the lower portion of the Edwards Aquifer. A fault with greater than 100 m (328 ft) of throw would juxtapose the Trinity Aquifer with the upper portion of the Edwards Aquifer.

Figure 4-3. Oblique views of Upper Glen Rose Fm. model layer in (a) Camp Bullis geologic framework model, and (b) Castle Hills geologic framework model. Note that fault displacement is insufficient to completely offset Upper Glen Rose Fm. from itself except in one very localized area as indicated by the arrow in b. Therefore, the overlying Edwards Aquifer and underlying Middle Trinity Aquifer are not in fault juxtaposition in the Camp Bullis and Castle Hills (Ferrill et al., 2003a) study areas except near the NW corner of the Castle Hills quadrangle.

Figure 4-4. Throw map at the top of the Lower Glen Rose Fm. in the Camp Bullis study area (see Section 3) combined with the throw map at the top of the Upper Glen Rose Fm. in the Castle Hills quadrangle (after Ferrill et al., 2003a).

Figure 4-5. Map (after Figure 1-3) with stereonets representing poles to all faults measured in outcrop and road cut exposures in the Glen Rose Formation.

Figure 4-6. (a) Slip tendency plot and (b) dilation tendency plot with poles to all faults measured in the field with different colors and symbols for each field locality.

Figure 4-7. Three-dimensional fault surfaces from geologic framework model color coded according to (a) slip tendency and (b) dilation tendency (σ_1 = 15 MPa, vertical; σ_2 = 9.5 MPa, 60°; σ_3 = 4 MPa, 150°).

Chapter 5:

Figure 5-1. (a) Fault system exposed in Beckmann Quarry in northwest San Antonio (after Ferrill et al., 2003a). Note that faults cut across approximately 65 m (213 ft) exposed thickness of Edwards strata, and show evidence of only very minor tilting of layers adjacent to the fault. (b) Un-annotated and (c) annotated photographs showing striations and grooves, fault rock (yellow patches) and dissolution features (red) on Beckmann Quarry fault.

Figure 5-2. Fault in the dolomitic member of the Kainer Formation tips (terminates) upward into the Kirschberg Evaporite member. Displacement in the dolomitic member is replaced by monoclinal folding in the overlying Kirschberg Evaporite member. Photo from the Beckmann Quarry, San Antonio, Texas. View is to the ENE, along the direction of strike of the fault.

Figure 5-3. Field photographs of faults and dissolution features in the Buda Limestone, exposed near the intersection of Bandera Road (16) and Loop 1604, in northwest San Antonio, Texas. (A) Monoclinal fold developed in the clay-rich Eagle Ford Formation and the base of the Austin Group above the Buda Limestone. View is toward the east. (B) Dissolution cavity developed in a dilational segment of a small-displacement normal fault in the Buda Limestone. View is toward the east. (C) Dissolution cavities developed in extensional faults and fractures accommodating bending in the Buda Limestone. View is approximately toward the southeast. (D) Schematic cross section based on (A), (B), and (C).

Figure 5-4. Faults exposed on Route 46. Red dots indicate fault tips. At this location more than half of the 13 measured faults tip in the shale layer illustrated in this photograph.

Figure 5-5. Photographs of three exposures of major fault in Canyon Lake Spillway Gorge. Fault has tens of meters of down-to-the-southeast displacement. Photographs show detail of fault damage zone which includes many small-displacement faults and fractures that are both synthetic (dipping in same direction) and antithetic (dipping in opposite direction) to the main fault. Conjugate faulting of this style is expected to produce anisotropic permeability as discussed by Ferrill et al. (1999b; 2000). Synthetic dip is present in the footwall of the main displacement fault core in each profile seen of the fault zone. Layer attenuation and shale smear are visible in the exposures shown in (A) and (B), and approximately 50 m (164 ft) northeast of (C). Many of the faults exhibit cross-cutting, conjugate relationships (Ferrill et al., 2000).

Figure 5-6. Lateral and or vertical fault segmentation, along with monoclinal folding associated with arrest of propagating fault tips in weak clay rich layers has led to significant tilting, extension, and thinning of limestone beds in fault zone exposed in the Canyon Lake Spillway Gorge. (A) Unannotated photograph of exposure. (B) Sequence 1 through 7 is the interpreted evolution of the structure in cross section (compare with Figure 5-7), blue layers are more competent than the white. (C) Annotated photograph of exposure, compare with Fig. 5-7.

Figure 5-7. Schematic illustration of the progressive development of the fault zone as seen at location shown in photograph in Figures 5-5a and 5-6. (A) Lateral propagation of two normal faults (propagation direction indicated by chevrons) establishes a relay ramp between the terminal sections of the faults. Bending in the relay ramp causes development of small extensional faults. (B) Continued propagation of the bounding faults causes enlargement and increased bending of relay ramp. Early formed normal faults in ramp become rotated. (C) Continued propagation of one of the bounding faults, propagation of other fault is arrested. (D) Temporarily arrested fault propagates further. Relay ramp has rotated into a synthetic dip panel and faults within it may be reactivated to accommodate down-dip extension.

LIST OF TABLES

1 INTRODUCTION

The Edwards and Trinity Aquifers are the primary source of water for many south-central Texas communities, including the city of San Antonio (Figure 1-1). The Edwards Aquifer supplies residential water for 1.7 million people, serving as primary source of water for San Antonio, and providing water for agriculture, industry, and recreation (Sharp and Banner, 1997; Hovorka et al., 1998; Johnson et al., 2002). Both aquifers are complex karst limestone aquifer systems that have permeability architectures that include a combination of host rock permeability, fractures and fault zones, and dissolution features. Although the strata that make up the Edwards Aquifer are younger and stratigraphically overlie the strata that comprise the Trinity Aquifer (Figure 1-2), displacement along faults of the Balcones fault system has placed the Edwards Aquifer laterally against (side-by-side with) the Trinity Aquifer. The location and amount of fault juxtaposition are sensitive to the location, geometry, and displacement on faults. Along faults that define the structural interface between the Edwards and Trinity Aquifers, caves and some fault zones provide conduits for groundwater flow and potential pathways for interaquifer communication. The occurrence of or degree to which interaquifer communication occurs is controversial and various hydrologic and geochemical studies have attempted to place constraints on the amount of water that the Trinity Aquifer contributes to the Edwards Aquifer.

The general question of the contribution of water from the Trinity Aquifer to the Edwards Aquifer is important as it pertains to both the quantity and quality of water in the Edwards Aquifer. If the Trinity Aquifer is hydraulically connected and provides water to the Edwards Aquifer, then the Edwards Aquifer recharge zone is in effect larger than the (Edwards) aquifer outcrop connected to the confined aquifer. In addition, contaminants in the Trinity Aquifer could potentially threaten the Edwards Aquifer. These issues of quantity and quality of water underlie the importance of understanding potential pathways for hydraulic communication between the Trinity and Edwards Aquifers. Recently the potential for interaquifer communication has received attention in San Antonio because of the recognition and characterization of contamination of the Trinity Aquifer by pollutants from Camp Stanley and Camp Bullis. Groundwater sampling studies on Camp Bullis have demonstrated southward movement of contaminants towards the Edwards Aquifer recharge zone, and have drawn attention to the potential for contamination of the Edwards Aquifer by pollutants in the Trinity Aquifer.

The purpose of the project reported here is to characterize the structural architecture of the Edwards and Trinity Aquifers for the area of the Camp Bullis 7 ½ minute quadrangle, and extending north to include Cibolo Creek in the southern part of the Bergheim 7 ½ minute quadrangle (Figure 1-3). Included in this analysis are tasks to generate a three-dimensional computer model of the Trinity and Edwards Aquifer, and perform field investigations to characterize the mechanisms and products of localized fault-related deformation in the Edwards Aquifer and Trinity Aquifer near the study area. An important objective is to analyze the potential for communication between the Edwards Aquifer and the Trinity Aquifers, taking into account fault-related deformation and juxtaposition of the aquifers across key faults.

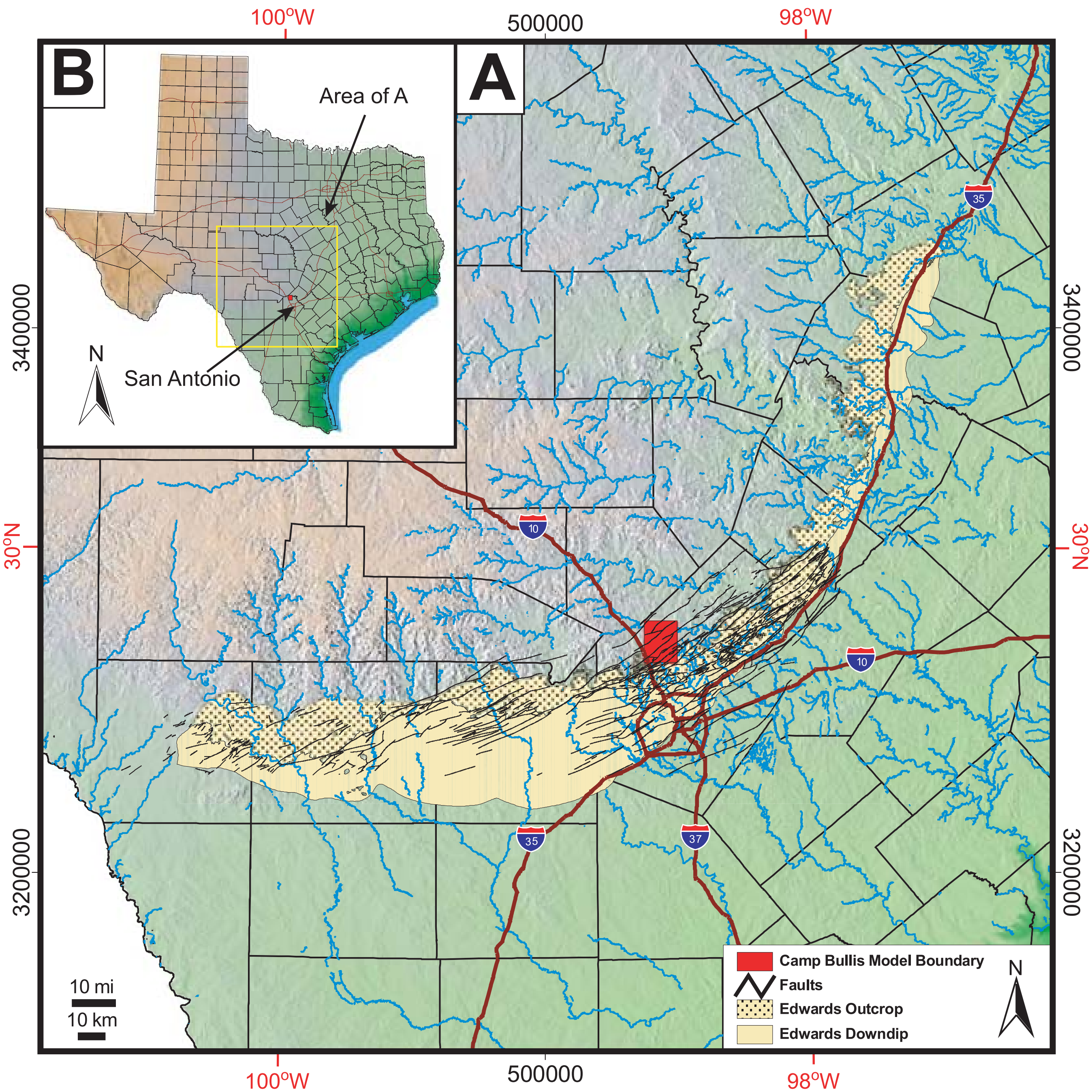

Figure 1-1. (a) Colored topography of south central Texas from 1°x1° tiles (Chalk Butte, Inc., 1994) showing counties, location of Edwards Aquifer (TNRIS, 1997), faults of the Balcones Fault zone (Collins and Hovorka, 1997), and location of model area. (b) Colored topography of Texas (Chalk Butte, Inc., 1994) showing the location of A. A and B base images were reprojected from geographic, decimal degrees to UTM, zone 14, meters.

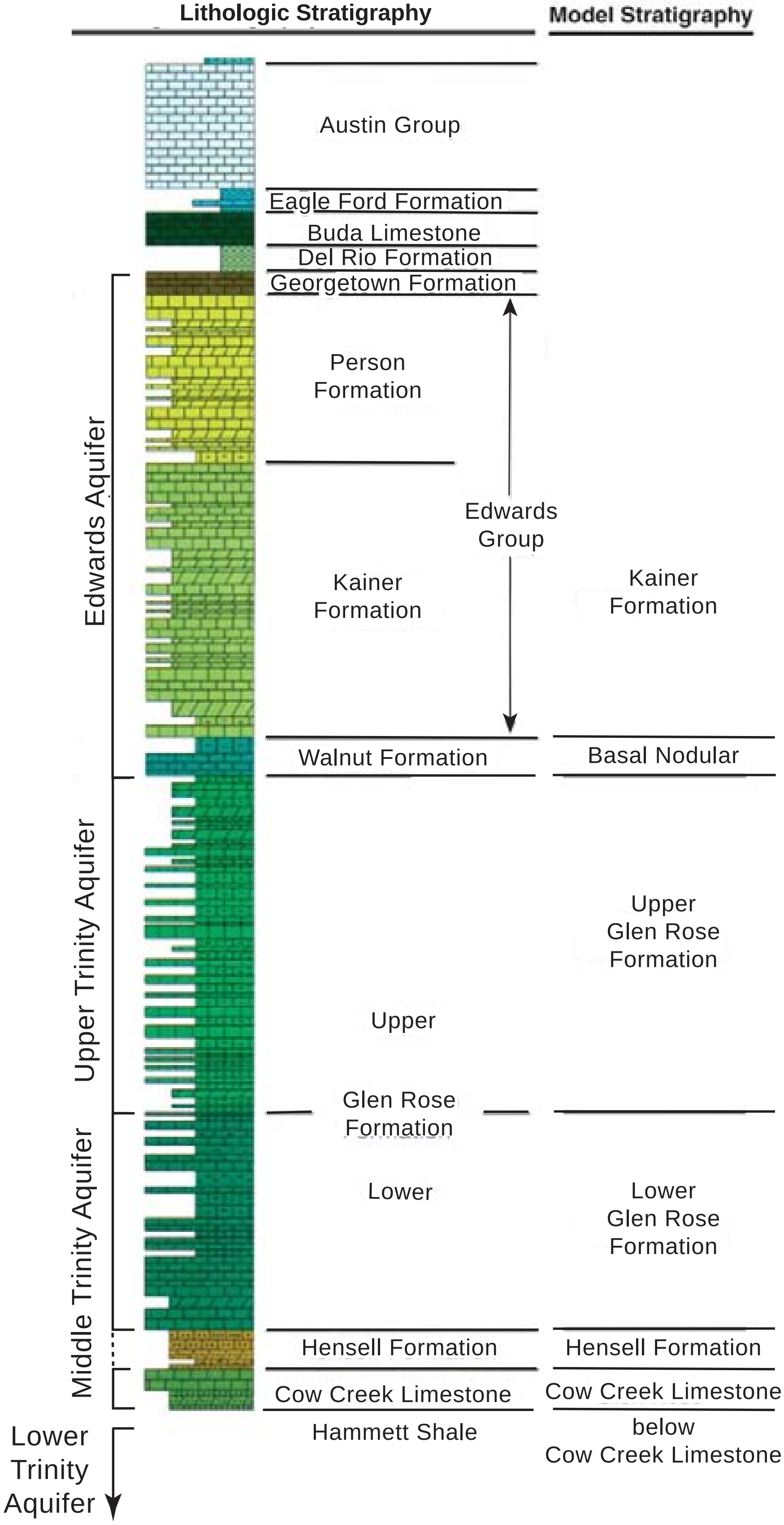

Figure 1-2. Stratigraphic column showing relationship between lithostratigraphic units and units used in the Camp Bullis geologic framework model. Stratigraphic column is after Collins (2000).

The project is organized into six tasks, including five technical tasks (summarized below), plus reporting:

1. 3DStress™ analysis to assess consistency of major faults in the context of the regional stress field at the time of faulting (Morris et al., 1996; Ferrill et al., 1999a).

2. Structural framework modeling (using Earthvision™) to define the 3-dimensional architecture of the study area.

3. Fault block deformation analysis based on assessment of displacement gradients on normal faults, which commonly produce locally intense fault block deformation (faults and fractures; Collins, 1993; Ferrill et al., 1999b), using the approach developed by Ferrill and Morris (2001).

4. Field analysis of fault zone materials and deformation mechanisms in accessible outcrops (primarily outside of the project study area), to determine parameters such as fault zone thicknesses, fault zone materials, and their distribution along faults with an emphasis on understanding the development of fault zone conduits (e.g., monoclines/synthetic dip panels, breccia zones, and dilatant damage zones; Caine et al., 1996; Ferrill and Morris, 2003) versus barriers (e.g., shale smear; Yielding et al., 1997).

5. Structural analysis of potential communication across the interface between the Trinity and Edwards Aquifers (Allan, 1989) taking into account four main considerations: geometry of stratigraphic horizons, fault displacement, fault geometry, and fault zone materials.

Results of the project show the aquifer architecture throughout the study area, the location and interpreted geometry of the most important mapped faults in the study area, and the deformation mechanisms and deformation style in fault zones in the rocks of both the Edwards and Trinity Aquifers. The three-dimensional geologic framework model of the Camp Bullis area reveals (i) juxtaposition of permeable and relatively impermeable hydrogeologic units, (ii) structural thinning of the Edwards Aquifer and Trinity Aquifers, (iii) potential for cross-fault communication between the Trinity and Edwards Aquifers, (iv) faults expressed on the surface as potential infiltration pathways, and (v) maximum offset concentrated along a small number (two or three) fault systems (Maclay and Small, 1983; Maclay, 1995; Ferrill et al., 2003a). This information, along with an understanding of fault zone deformation mechanisms and the role of fault zones as barriers or conduits, can assist in locating environmentally sensitive areas, is useful for aquifer water flow path studies, and contributes to the identification of areas where communication between the Trinity and the Edwards Aquifers is suspected.

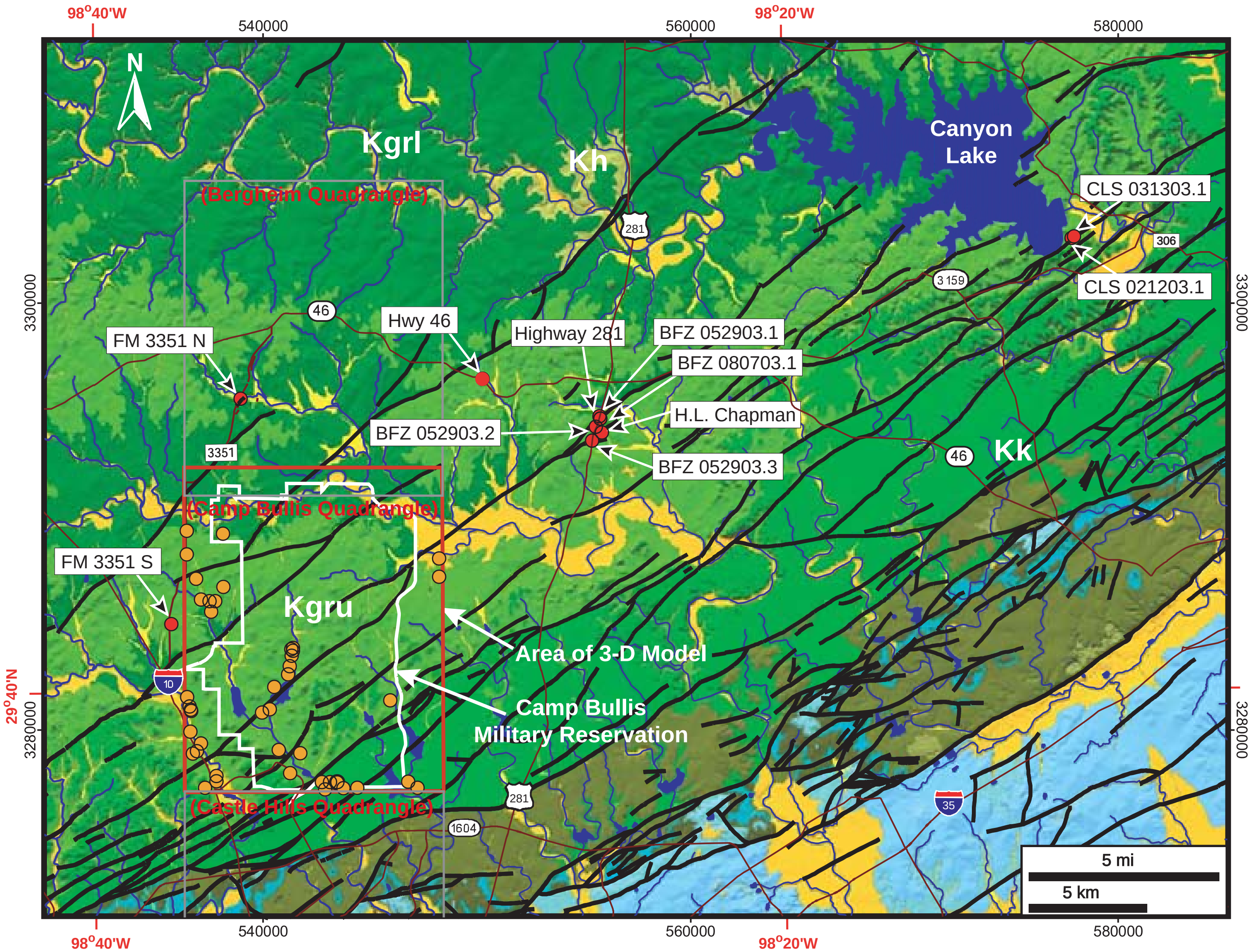

Figure 1-3. Location map showing the Balcones fault system and Edwards Aquifer recharge zone in south central Texas. Geologic map derived from Collins (2000) is draped over hillshaded digital elevation model. Red box shows the location of the Camp Bullis 7 ½ minute quadrangle and extension north into the Bergheim quadrangle to include Cibolo Creek. Castle Hills quadrangle is south of Camp Bullis. Geologic units: Kk = Kainer Fm., Kgru = Upper Glen Rose Fm., Kgrl = Lower Glen Rose Fm., and Kh = Hensell Fm. Fault traces are from Collins (2000). See Fig. 1-2 for stratigraphic column. Orange dots are locations of wellbore data used in construction of geologic framework model of the Camp Bullis Quadrangle. Red dots show the locations of field studies of faulting along state Route. 46, FM 3351 (Ralph Fair Road), Highway 281, and Canyon Lake Spillway Gorge. White outline represents the area of Camp Bullis Military Reservation.

2 BACKGROUND

The Edwards Aquifer is a karst aquifer (Maclay and Small, 1983; Johnson et al., 2002) consisting of porous, highly fractured Lower Cretaceous (Comanchean) limestone. Stratigraphically, the aquifer is in the Kainer and Person Formations of the Edwards Group and the overlying Georgetown Formation of the Washita Group (Maclay and Small, 1983; Figure 1-2). The aquifer is constrained between an upper confining unit consisting of the Del Rio Clay, Buda Limestone, and Eagle Ford Formation and the underlying Upper Glen Rose Formation of the Trinity Group (Figure 1-2; Clark, 2000). The Trinity Aquifer consists of three parts: (i) the upper part consists of the Upper Member of the Glen Rose Formation, (ii) the middle part consists of the Lower Member of the Glen Rose Formation and the Cow Creek Limestone, which are separated by the Hensell Sand or Bexar Shale, and (iii) the lower part consists of the Hosston Formation and overlying Sligo Formation, and is separated from the Cow Creek Limestone by the intervening Hammett Shale (Mace et al., 2000).

The Trinity Aquifer extends across a wide region of the Texas Hill Country to the north and west of the main faults of the Balcones Fault System (Mace et al., 2000). The Edwards Aquifer extends along the Balcones Escarpment from Bell County in the north, curving southwestward through Williamson, Travis, Hays, Comal, Bexar, Medina, Uvalde, and Kinney Counties (TNRIS, 1997; Zahm et al., 1998; Hayes, 2000) (Figure 1-1). Although Trinity Aquifer strata are present beneath the Edwards aquifer through the Balcones fault system, the Trinity is not considered to be a prolific groundwater producer in the area, and production is primarily from the Edwards. Exposures of the Edwards Aquifer strata along the Balcones Fault Zone represent the primary recharge zone, where surface water enters the Edwards Aquifer by way of fractures, faults, caves, sinking streams, and sinkholes (Maclay and Small, 1983, 1984; Maclay, 1995; Collins and Hovorka, 1997; Johnson et al., 2002). High porosity and permeability of the Edwards Aquifer allows for rapid recharge, but also creates opportunities for contamination of the aquifer with little filtration (Johnson et al., 2002). Subsurface flow paths in the Edwards Aquifer are thought to be controlled by structural architecture similar to fluid movement pathways in faulted oil fields (Ferrill et al., 2003a).

Rocks of both the Edwards and Trinity Aquifers crop out in the Edwards Plateau region, and their southern and eastern outcrop boundary is within the Balcones fault system, a zone of Tertiary age, down to the southeast, normal faulting (Foley, 1926; Maclay and Small, 1983, 1984; Stein and Ozuna, 1996; Clark, 2000; Collins, 2000). South and east of the Balcones Fault System, the Edwards Aquifer is confined beneath younger sedimentary rocks and serves as the primary water source for many communities, including the city of San Antonio. Recharge of the aquifer occurs primarily by streamflow loss and infiltration in porous parts of the unconfined Edwards Aquifer recharge zone, responding to rainfall in the recharge zone and upslope catchment area. Water in the unconfined aquifer moves down hydraulic gradient following, in many places, tortuous flow paths controlled by the Balcones Fault System. Natural discharge sites for the aquifer are springs associated with the Balcones Fault System in the vicinity of New Braunfels and San Marcos, Texas. Spring discharge in Bexar County is intermittent and feeds the San Antonio River through San Antonio Springs (Arnow, 1963). Most significant recharge of the aquifer occurs along the Balcones Fault System where faults, fractures, and solution-features such as sink holes and caves are considered to be major sites for groundwater recharge (Clark, 2000). By analogy with surface exposures, the high-volume, high flow-rate subsurface flow is also likely to be controlled primarily by faults, fractures, and solution cavities (Hovorka et al., 1998).

The Balcones Fault System is a broad *en echelon* system of mostly south-dipping normal faults that formed during the middle to late Tertiary (Murray, 1961; Young, 1972). The arcuate zone trends east-northeast and spans much of central Texas. The 25 to 30 km wide Balcones Fault System has a maximum total displacement of 366 m (1201 ft) (Weeks, 1945), and defines the transition from structurally stable flat-lying rocks of the Texas craton to gently coastward-dipping sediments of the subsiding Gulf of Mexico. At the margin of the Texas Hill Country northwest of San Antonio, exposures in Cretaceous-aged platform carbonates include the Edwards Group, a series of carbonate strata that formed along the margin of the Central Texas platform with the ancestral Gulf of Mexico (Rose, 1972). Offset of carbonate strata across the Balcones Fault System resulted in a broad, weathered escarpment of vegetated limestone hills rising from the predominantly clastic coastal plains to the uplands of the Texas Craton. Within the fault system, the dip of bedding varies from gentle coastward dips to nearly horizontal, with occasional localized dip of hanging wall beds northward into some faults. Faulting has been interpreted as being rooted in the deeply buried foreland-basin sediments of the Ouachita orogeny (Murray, 1956).

A primary control on the permeability architecture of stratified rocks is the difference in permeability between rock layers. If a stratigraphic sequence is not deformed, this vertical inhomogeneity and anisotropy produced by layering will dominate bulk permeability. In faulted strata, however, geologic structures (faults and fractures) exert three additional controls on aquifer permeability and flow:

1. Fault offsets alter the overall geometry of and communication between fault blocks (Allan, 1989; Maclay, 1989; Ferrill and Morris, 2001).

2. Fault zones commonly form relatively impermeable barriers to across-fault flow, form permeable pathways for along-fault flow, or form both barriers and pathways (Arnow, 1963; Caine et al., 1996; Knipe, 1997; Yielding et al., 1997; Ferrill and Morris, 2003). This fault and fracture conductivity may be influenced by the current stress field and fault activity (Finkbeiner et al., 1997; Ferrill et al., 1999b).

3. Fault block deformation by formation of small faults and fractures leads to permeability anisotropy (Antonellini and Aydin, 1994; Mayer and Sharp, 1998; Ferrill et al., 2000).

These three controls are listed in generally descending order of scale of influence from regional, to subregional, to local. In carbonate rock layers like those that make up the Trinity and Edwards Aquifers, groundwater flow and limestone dissolution (Deike, 1990) can enhance the permeability effects of fault and fracture systems, producing solution enlargement at scales of individual fractures to cave networks consisting of fissures, angular passages, and fracture controlled networks of passages (Palmer, 1991; Loucks, 1999). Alignment of linear cave segments and cave networks with fracture patterns, and direct observation of association of caves with faults and fractures, indicate fault and fracture control on caves in the Edwards Aquifer recharge zone (Wermund and Cepeda, 1977; Wermund et al., 1978; Kastning, 1981). Modification of faults and fractures by dissolution are thought to produce some of the most important paths for recharge of the Edwards Aquifer (Clark, 2000).

Geologic structures in the Trinity and Edwards Aquifers influence permeability architecture at a range of scales (Ferrill et al., 2003a). At the largest scale, the influence of faults and fractures on the aquifer could be described using one or more permeability tensors. Although not typically incorporated into groundwater flow simulations of the Edwards and Trinity Aquifers, structurally controlled permeability anisotropy has been incorporated with greater hydraulic conductivity parallel to faulting, and less perpendicular to faulting (Kuniansky and Holligan, 1994). At the scale of individual recharge features, flow conduits causing significant heterogeneity are observed. Here we consider the scale range from regional flow models down to that of individual recharge features, flow conduits, and wells. Structural control on permeability architecture is here subdivided into three components (Figure 2-1a). At the largest scale, major faults of the Balcones Fault System control the overall geometry of the aquifer, including its position at the ground surface (recharge zone), dip magnitude and direction, and position of the aquifer in the subsurface. Major faults produce tilting of fault blocks and locally thin the aquifer to some fraction of its original thickness. Thus, aquifer communication is decreased in directions perpendicular to the fault strike because of thinning. Fault zones themselves generally have increased permeability parallel to the fault zone, and relatively reduced permeability perpendicular to the faults. These faults locally serve as conduits for vertical and lateral water movement. Smaller faults and extension fractures within fault blocks produce permeability anisotropy within fault blocks. Fault block deformation by small-scale faulting and extension fracturing is heterogeneously developed within the Edwards Aquifer. High intensities of small faults occur close to large faults (within ~100 m). In the Edwards Aquifer, the role of major faults for geometry and thinning of the aquifer has been identified (Maclay and Small, 1983; Hovorka et al., 1998; Collins, 2000), as has the importance of individual faults as infiltration and subsurface flow pathways (Clark, 2000; Ferrill and Morris, 2003). The role of fault block deformation in the Edwards Aquifer is variable, and is controlled primarily by structural position (Figure 2-1b), specifically, proximity to large (>10 m (33 ft) maximum displacement) faults.

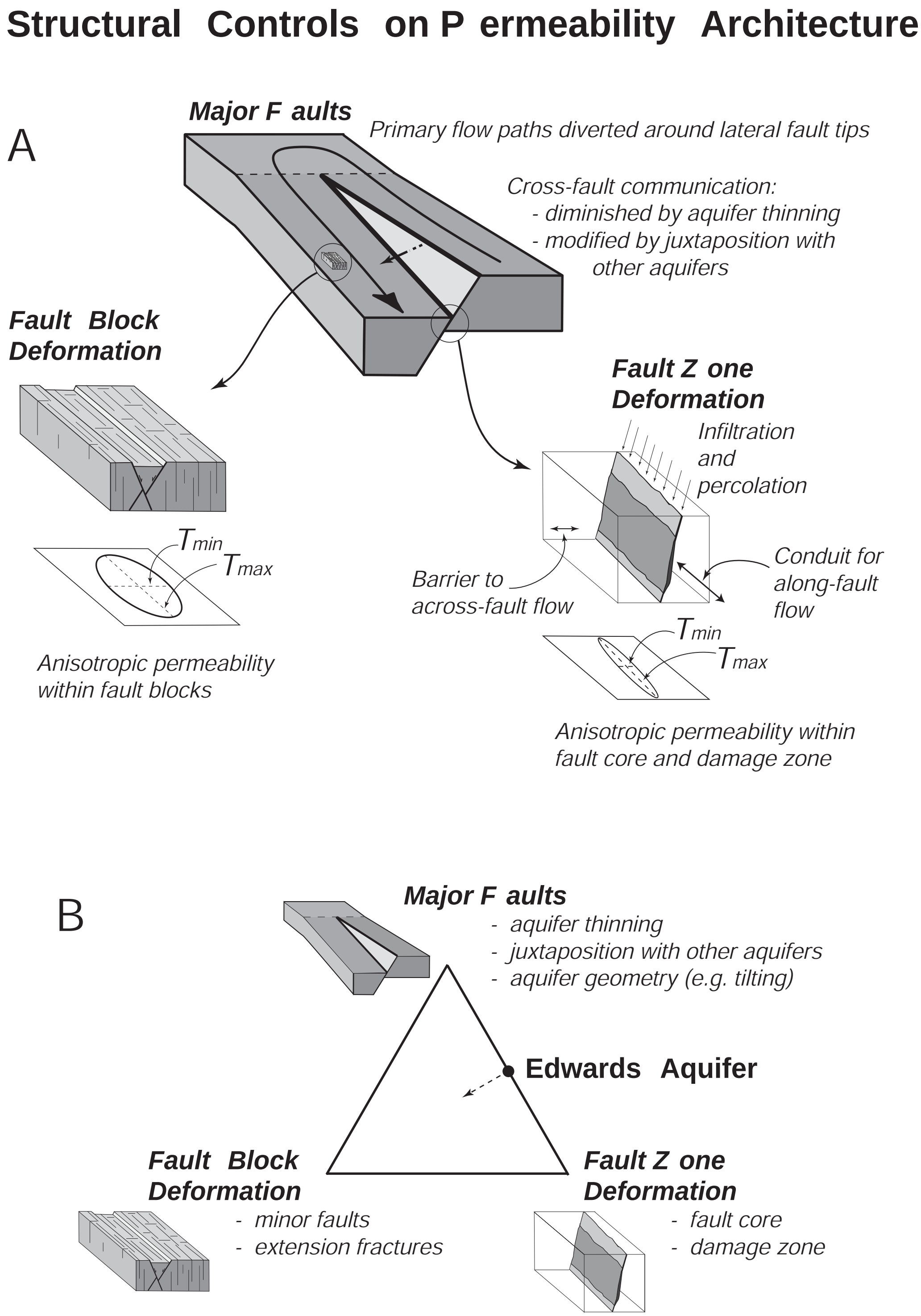

Figure 2-1. (a) Schematic illustration of interplay between the three major elements of structural control on the Edwards Aquifer. Tmin and Tmax refer to minimum and maximum principal transmissivity, respectively. (b) Major structural controls are represented as a ternary system. The geometry and fault zone deformation of major faults are major controls on flow in the Edwards Aquifer, as shown by the filled circle. Fault block deformation is highly variable within the Edwards Aquifer, and is best developed adjacent to mappable faults. Dashed arrow shows that increasing role of fault block deformation tends to place the aquifer nearer the center of the ternary system (after Ferrill et al., 2003a).

An important question with respect to the Edwards Aquifer recharge zone, and related subsurface groundwater flow in the confined Edwards Aquifer, is whether there is subsurface flow communication (i) across faults within the Edwards Aquifer, (ii) between the Edwards Aquifer, Buda Limestone, and Austin Chalk, higher in the stratigraphic section, or (iii) between the Edwards Aquifer and the Glen Rose Limestone (Trinity Aquifer) below. Such flow communication could be the result of flow across faults, laterally or vertically within a fault zone, or a combination of these. Water that infiltrates in other stratigraphic units may be capable of flowing laterally into the Edwards Aquifer. This potential for subsurface aquifer communication is important because it controls the amount and distribution of areas that provide recharge to the Edwards Aquifer, thereby effectively expanding the recharge zone. In addition, communication between aquifers could mean increased threat for contaminant migration into the Edwards Aquifer from other aquifers such as the Trinity Aquifer.

Faults that juxtapose the Edwards Aquifer with itself are not likely to be effective barriers to across-fault aquifer communication, because the Edwards Aquifer stratigraphic section does not contain significant clay-rich sealing layers. Field observations, in particular the common occurrence of dissolution enlargement of faults, suggest that fault zone deformation processes in these limestones more commonly enhance rather than reduce permeability. Structural thinning of the aquifer by normal faults does, however, constrict flow/communication pathways (Maclay and Small, 1983). Continuous monitoring of water table elevations in the Edwards Aquifer recharge zone suggests that there is hydraulic communication across some faults (Steve Johnson, Edwards Aquifer Authority, personal communication). This observation warrants further structural and hydrologic investigations.

The Del Rio Formation introduces a very effective barrier to aquifer communication across faults, even in cases where fault displacement is greater than the thickness of the Del Rio Formation (Ferrill et al., 2003b). The mechanically weak character of the clay rich Del Rio Formation may allow it to smear along fault planes, resulting in a barrier to across-fault water movement. In the same way, shale of the Eagle Ford Formation is likely to remain an effective barrier to communication between the limestones of the Austin Group and the Buda Limestone and Edwards Group limestones beneath.

In contrast, across-fault communication between the Edwards Group limestones and underlying limestones of the Trinity Aquifer's Glen Rose Formation is likely. Although argillaceous limestones are present intermittently throughout the Glen Rose Formation, there is no clay-rich shale separating the Edwards Group from the underlying Trinity Aquifer rocks that would retard fault propagation as successfully as the Del Rio Formation. For this reason, the potential for aquifer communication between the Glen Rose Formation (Trinity Aquifer) and Edwards Aquifer warrants further analysis. This is of great importance because the Glen Rose Formation crops out over a very large area adjacent to and north of the Edwards Aquifer recharge zone along the Balcones Fault System. If water from the Glen Rose Formation feeds into the Edwards Aquifer along subsurface flow pathways, then the Edwards Aquifer recharge zone is in effect larger than currently described and modeled. Also, groundwater contamination north of the Edwards Aquifer recharge zone may be a threat to water quality in the Edwards Aquifer.

Additional structural characterization, coupled with water table characterization, pump testing, and natural and induced tracer tests, is needed to further evaluate the potential for subsurface aquifer communication.

3 AQUIFER ARCHITECTURE

We constructed the three-dimensional digital geologic framework model of a portion of the interface between the rocks of the upper and middle Trinity Aquifer and Edwards Aquifer using EarthVision 6.1 (Dynamic Graphics, 2001; Figures 1-3 and 3-1 through 3-8). The model was constructed with goals of producing a three-dimensional representation of the faulted aquifers and confining strata that can be used to determine and illustrate potential structural controls upon recharge and groundwater flow and transmissivity within or between the Edwards and Trinity Aquifers in the Camp Bullis and the southern portion of the Bergheim Quadrangles.

3.1 Methodology

We followed the approach for model construction that we previously developed in producing the three-dimensional geologic framework model of the Castle Hills quadrangle, immediately to the south of the Camp Bullis area of this study (Waiting et al., 2003; Ferrill et al., 2003a). The workflow for model construction is summarized below. For a thorough discussion of the workflow for three-dimensional geologic framework model construction, see Waiting et al. (2003).

3.1.1 Data

Construction of a three-dimensional geologic framework model requires data in sufficient quantity to cover as much of the model area as possible. In the case of the Camp Bullis model, this includes both surface and subsurface data.

Acquisition of surface data for this project began with downloading United States Geological Survey (USGS) 30-meter horizontal resolution Digital Elevation Models (DEMs) from the Texas Natural Resources Information System website. This supplied surface elevations for the area of the model.

The USGS supplied vector coverages of faults digitized from published hydrogeologic maps of the Edwards Aquifer for Bexar, Comal, Hays, and Medina Counties (Small and Hanson, 1994; Hanson and Small, 1995; Stein and Ozuna, 1996; Small and Clark, 2000). The Texas Bureau of Economic Geology made available digital coverages from the 30′ x 60′ New Braunfels, Texas Geologic Quadrangle map, which is comparable in area to thirty-two (32) 7 ½ minute quadrangles (Collins, 2000). This information provided the mapped surface geology, including faults, for comparison with other interpretations. Preliminary results from detailed geologic mapping of the confines of Camp Bullis were provided by Allan Clark (USGS).

Surface data included field observations from exposures of the Edwards Group and Glen Rose Formation in roadcuts and quarries. Exposure locations were fixed using a Global Positioning Satellite (GPS) system and topographic maps. Information recorded included fault strike and dip, slickenline orientation (if measurable), exposure location, and the geologic unit.

Subsurface data provide important constraints for a three-dimensional geologic framework model to correctly represent the bedding thickness and bedding orientation, as well as constrain the geometry of model horizons. Subsurface data also verify surface data and provide fault dips at depth, as well as fault throw. San Antonio Water System (SAWS) and Mr. Alvin Schultz (a consulting geologist with SAWS) provided a database file containing the tops of the stratigraphic units from interpreted geophysical logs for 42 wells located in the Camp Bullis Quadrangle.

3.1.2 Map Projection

In a digital three-dimensional geologic framework model, geologic structures are constructed as a system of geometric elements. In the case of the model of the Camp Bullis Quadrangle, these elements include stratigraphic horizons represented as volumes having upper and lower bounding surfaces that are terminated either by fault surfaces or model boundaries. To reasonably replicate the spatial and angular relationships between the natural geologic features and model elements, it is necessary that the map projection be both equal area and equal angle, and that the horizontal and vertical units are similar. Universal Transverse Mercator meets these requirements, and is widely used in the geologic and hydrologic communities. We used the Universal Transverse Mercator (UTM, NAD27) coordinate system.

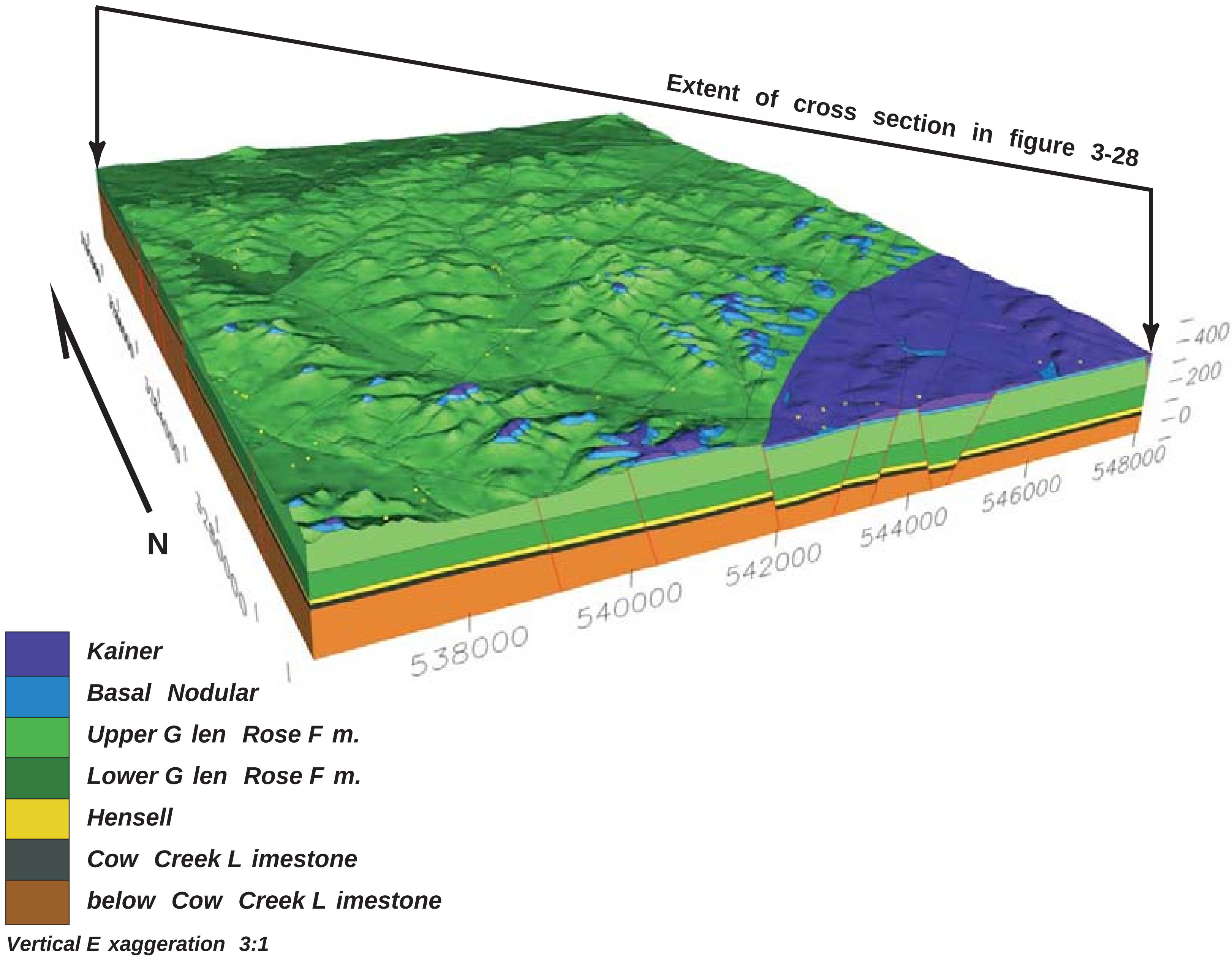

Figure 3-1. Oblique view of geologic framework model. Coordinates are UTM meters, NAD27. View direction is NE. Illumination from SW. Yellow points show well locations.

3.2 Results

The model covers the area outlined by the USGS 7 ½ minute 1:24,000 Camp Bullis Quadrangle and southern portion of the Bergheim Quadrangle including Cibolo Creek (approximately 2.0 $x10^8$ m^2) (Figures 1-3 and 3-1). The model volume is 1.8 $x10^{11}$ m^3, its upper boundary is the topographic surface (maximum elevation 461 m (1512 ft)), and it extends to a depth of 100 m (328 ft) below mean sea level. USGS 30 m (98 ft) digital elevation data in DEM format (Digital Elevation Model) were used to construct the topographic surface.

Seven stratigraphic horizons present in outcrop or in the subsurface are represented in the model volume. The stratigraphic horizons are selected for hydrogeologic associations (Figure 1-2) and for characteristic outcrop or geophysical log signatures, and represent both aquifer and confining strata. Represented in the model are portions of the unconfined Edwards Aquifer, and the upper and middle Trinity Aquifers. Model horizon designations, from oldest to youngest, are 'below Cow Creek' (Figure 3-2), 'Cow Creek' (Figure 3-3), 'Hensell' (Figure 3-4), 'Lower Glen Rose Fm.' (Figure 3-5), 'Upper Glen Rose Fm.' (Figure 3-6), 'Basal Nodular' (Figure 3-7), and 'Kainer' (Figure 3-8). Although designated as model horizon 'Hensell', the stratigraphic association of this horizon may be the downdip equivalent of the Bexar Shale (Barker et al., 1994; Mace et al., 2000).

Structure in the model is constrained using published (Arnow, 1963; Reeves, 1972; Small and Hanson, 1994; Hanson and Small, 1995; Groshen, 1996; Stein and Ozuna 1996; Collins and Hovorka, 1997, Mace et al., 2000, and Collins, 2000) and unpublished (Alvin Schultz, consultant to San Antonio Water System, San Antonio, Texas, 78298; Allan Clark, U.S. Geological Survey) maps, cross-sections and subsurface data, results from field investigations, and unpublished interpreted geophysical well logs (Alvin Schultz, consultant to San Antonio Water System, San Antonio, Texas, 78298). Lithologies exposed in the area consist of a thick sequence of faulted carbonate layers that can be difficult to differentiate. As a result, published geologic and hydrogeologic maps of the Balcones escarpment do not show uniform interpretations of fault traces or surface outcrops. Collaboration between Alvin Schultz, Edwards Aquifer Authority personnel and the authors of this report resulted in the formulation of a set of criteria by which to reconcile the different interpretations. Faults from published maps are generally included in the model where: (i) the fault is included and congruent in all interpretations, (ii) the fault is included on one or more maps and is required to reconcile outcrop or subsurface data, (iii) the fault shows vertical offset greater than 5 m (16 ft), or (iv) the fault is included on one or more maps and is geometrically reasonable relative to the fault system. The selection of 5 m (16 ft) as the threshold vertical displacement for inclusion in the model is based on the ambiguity and inconsistency in regional mapping of faults smaller than this based on uncertain field and wellbore data. Faults from published maps are generally excluded where: (i) maximum vertical displacement is less than 5 m (16 ft), (ii) the fault is clearly in conflict with outcrop or subsurface data, or (iii) the fault is clearly not required to accommodate horizon or fault system geometry. The selection of faults was refined and supported unpublished (Alvin Schultz, consultant to San Antonio Water System, San Antonio, Texas, 78298) interpretations of geophysical well logs.

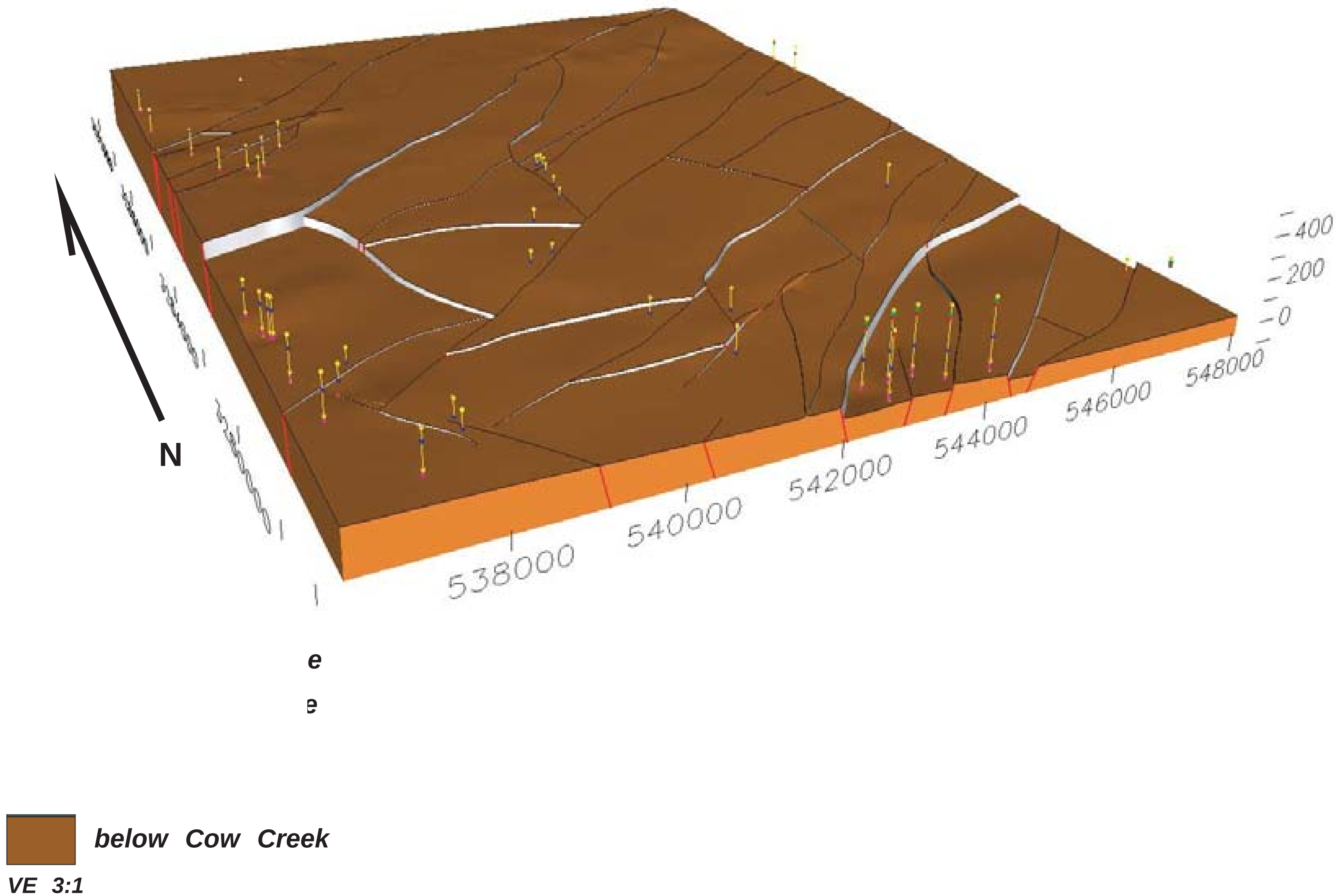

Figure 3-2. Oblique view of model horizon 'below Cow Creek'. Coordinates are UTM meters, NAD27. View direction is NE. Illumination from SW. Yellow points show well locations at land surface.

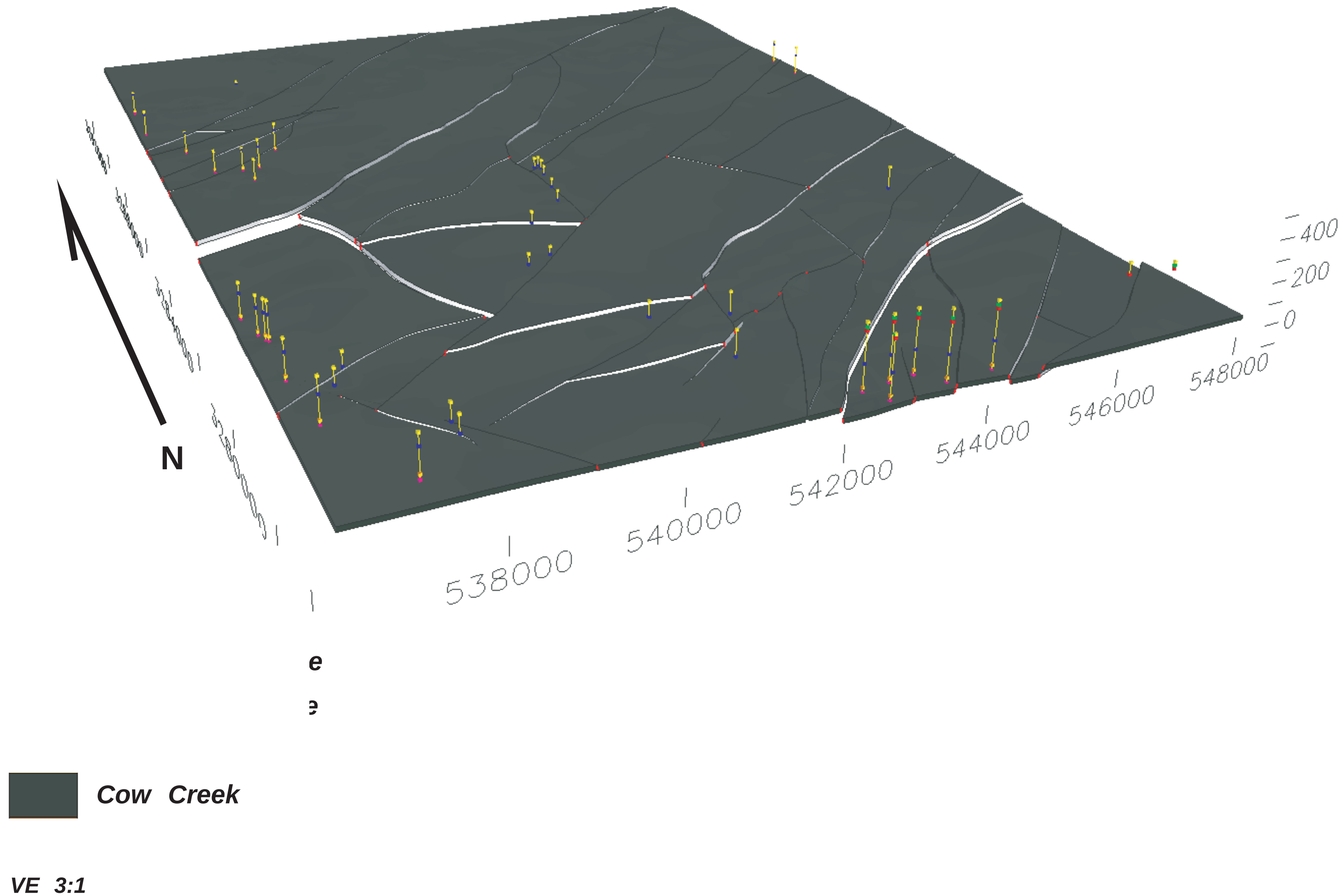

Figure 3-3. Oblique view of model horizon ‘Cow Creek'. Coordinates are UTM meters, NAD27. View direction is NE. Illumination from SW. Yellow points show well locations at land surface.

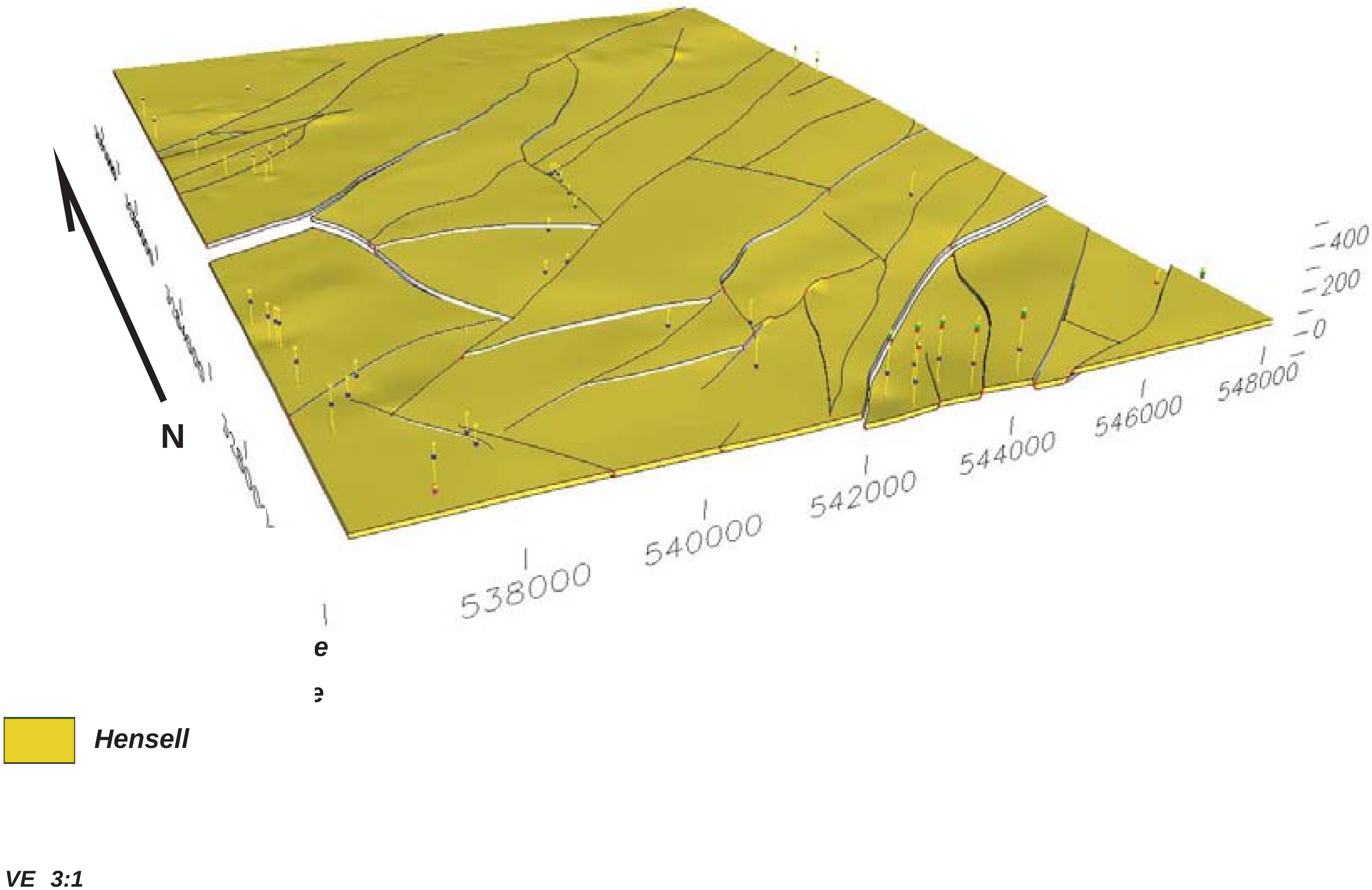

Figure 3-4. Oblique view of model horizon 'Hensell'. Coordinates are UTM meters, NAD27. View direction is NE. Illumination from SW. Yellow points show well locations at land surface.

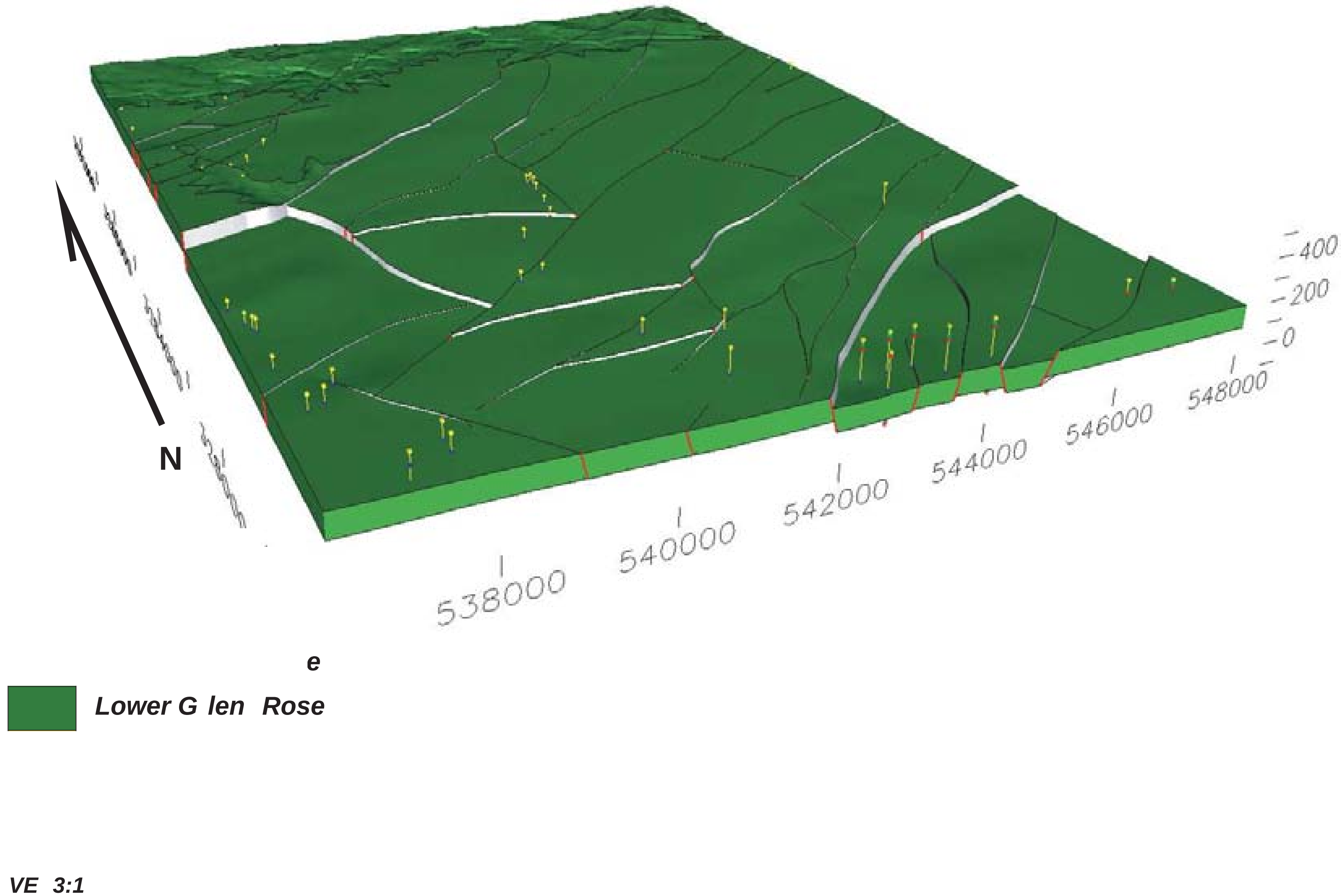

Figure 3-5. Oblique view of model horizon 'Lower Glen Rose Fm.'. Coordinates are UTM meters, NAD27. View direction is NE. Illumination from SW. Yellow points show well locations at land surface.

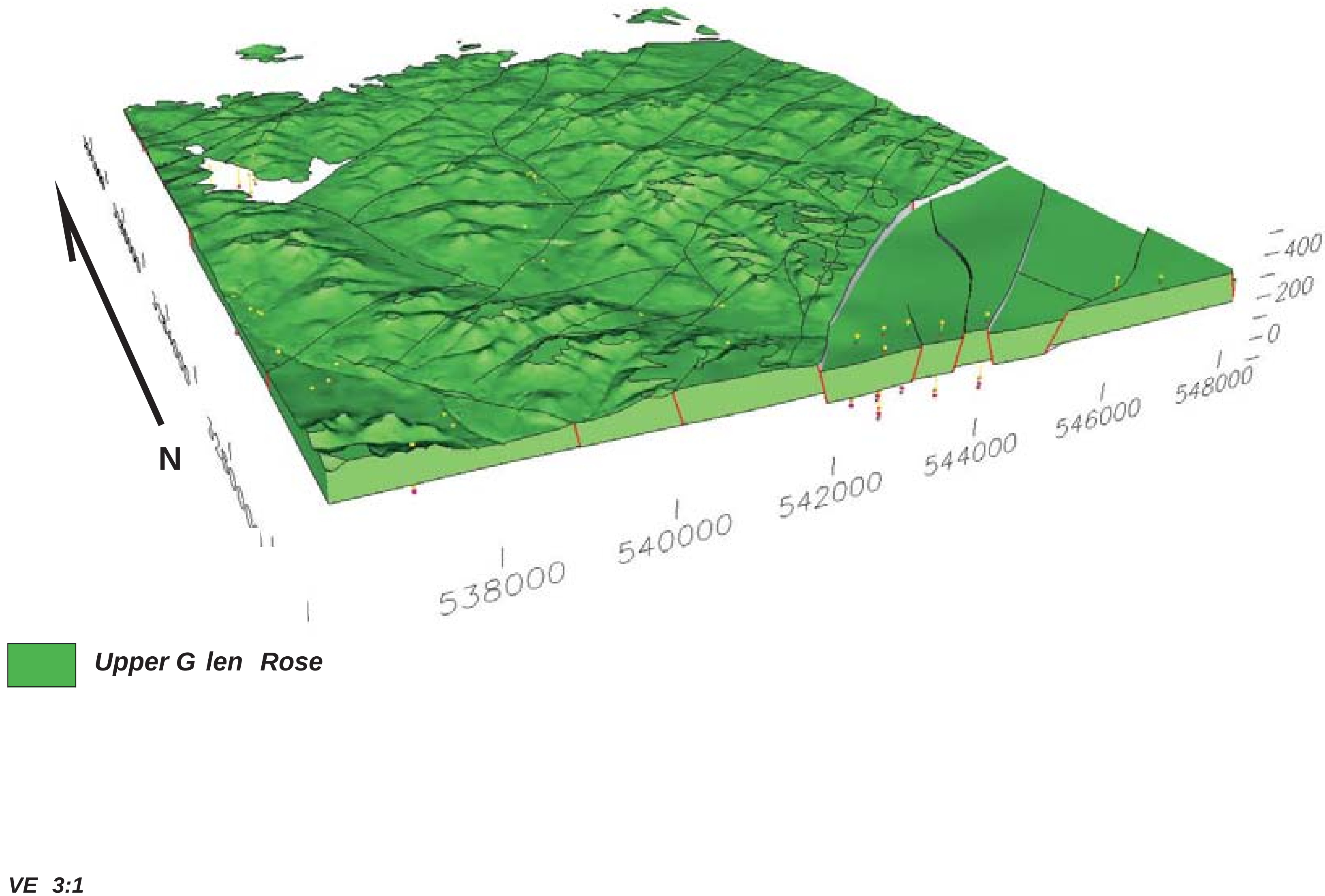

Figure 3-6. Oblique view of model horizon ‘Upper Glen Rose Fm.'. Coordinates are UTM meters, NAD27. View direction is NE. Illumination from SW. Yellow points show well locations at land surface.

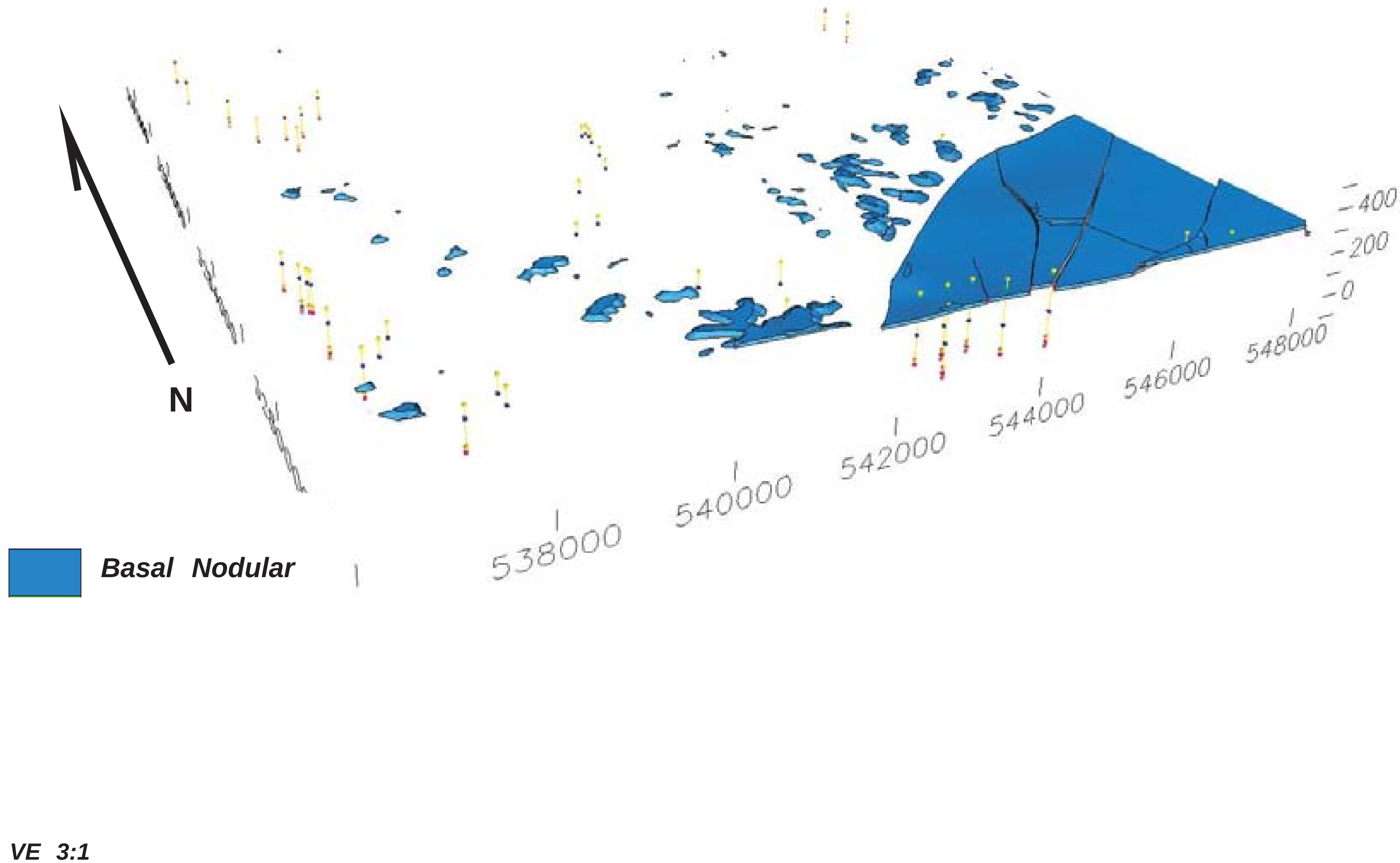

Figure 3-7. Oblique view of model horizon ‘Basal Nodular'. Coordinates are UTM meters, NAD27. View direction is NE. Illumination from SW. Yellow points show well locations at land surface.

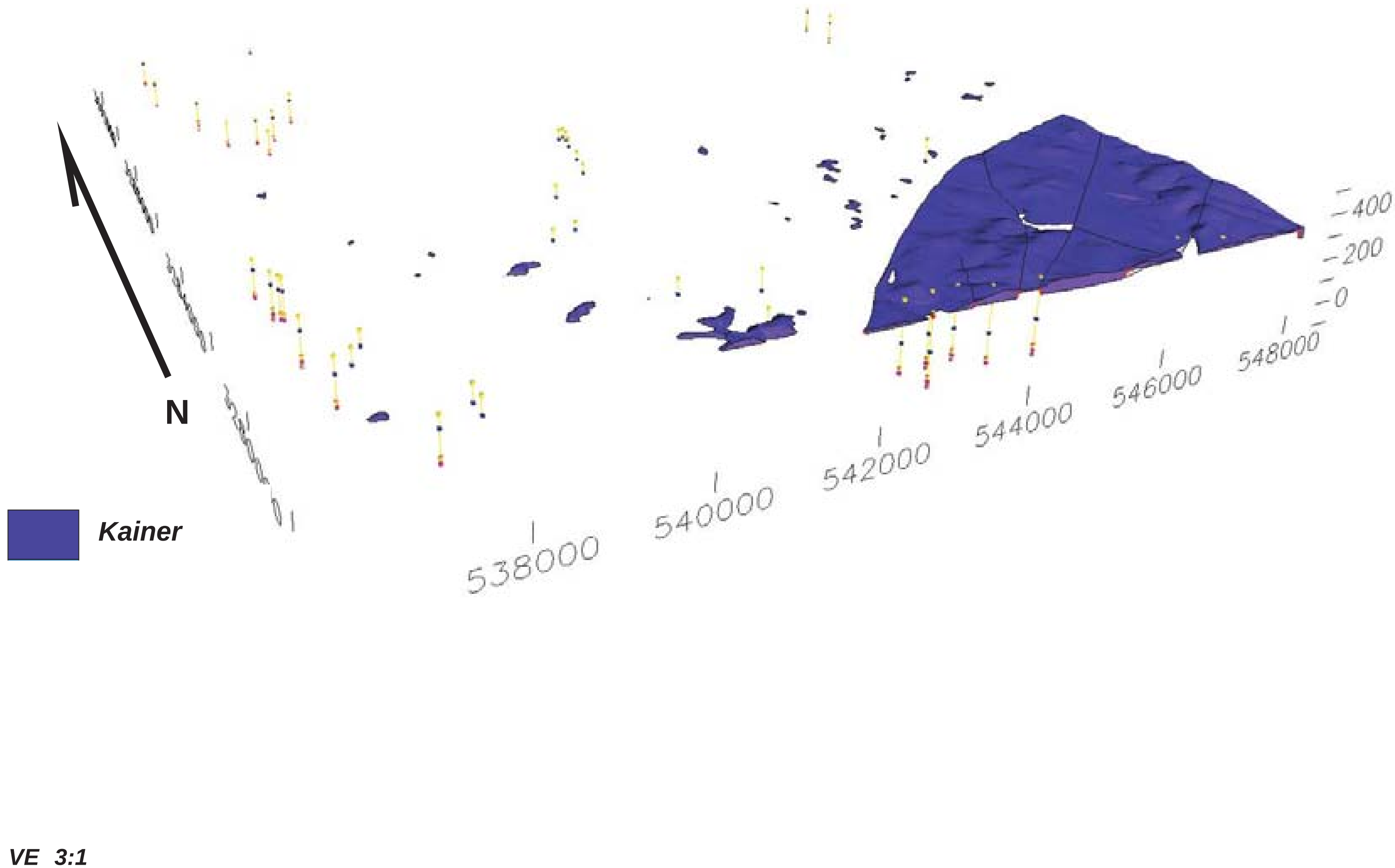

Figure 3-8. Oblique view of model horizon ‘Kainer'. Coordinates are UTM meters, NAD27. View direction is NE. Illumination from SW. Yellow points show well locations at land surface.

and Small, 1976, 1983; Shaw, 1978; Small, 1984, 1985; Waterreus, 1992; Barker et al., 1994; Collins, 2000; Mace et al., 2000; Alvin Schultz, Consultant, San Antonio Water System, San Antonio, Texas, 78298). Sufficient data are available to incorporate local thickness variation into the seven model horizons (Table 3-1, Figures 3-21 through 3-27). In each of these horizons, thickness is calculated from wellbore thickness data using minimum tension gridding. Minimum tension grids such as those produced using EarthVision (Dynamic Graphics, 2001) are formed by calculating a non-linear interpolation between adjacent nodes, where surface curvature is distributed between grid nodes rather than concentrated at grid nodes. The resulting surface gives a reasonable approximation of the geologic layer surfaces commonly observed in nature.

The seven horizons in the geologic framework model are offset by 40 faults (Figure 3-28). Dominant fault trace orientation is NE-SW, and dip is predominantly to the southeast. Faults are distributed across the model. Most faults intersect with other faults at one or both ends, or are cut by the model boundaries. Fault tips are less common, and no fault exists as an isolated structure. Vertical offset (throw) ranges from near zero to an approximate maximum of 110 meters (361 ft). Displacement sense is normal, and commonly down to the southeast. Displacement gradients are generally small, including where faults have isolated tips. In map view, fault blocks are elongate, with the long axis oriented NE-SW. Block tilting is not remarkable, but can be detected in some blocks. Half-graben systems are dominant, but large full-graben systems are also present. Maximum offset is concentrated along three fault systems (Figures 3-2 to 3-5). The southernmost of these systems forms the northern boundary of the aquifer recharge zone, where rocks of the Edwards Group are in faulted juxtaposition with rocks of the Glen Rose Formation. Various juxtapositions by faulting of horizons at depth are shown in Figures 3-28 through 3-46.

TABLE 3-1. MODEL HORIZON THICKNESSES

Model horizon name	Min. thickness (m)	Max. thickness (m)	Mean thickness (m)
Kainer	N.A.	88*	N.A.
Basal Nodular	14.8	17.4	15.6
Upper Glen Rose Fm.	133	149	140.2
Lower Glen Rose Fm.	95.7	108.8	100.3
Hensell	18.3	25.3	20.4
Cow Creek	20.1	22	21.4
Below Cow Creek	N.A.	N.A.	N.A.

*Eroded thickness

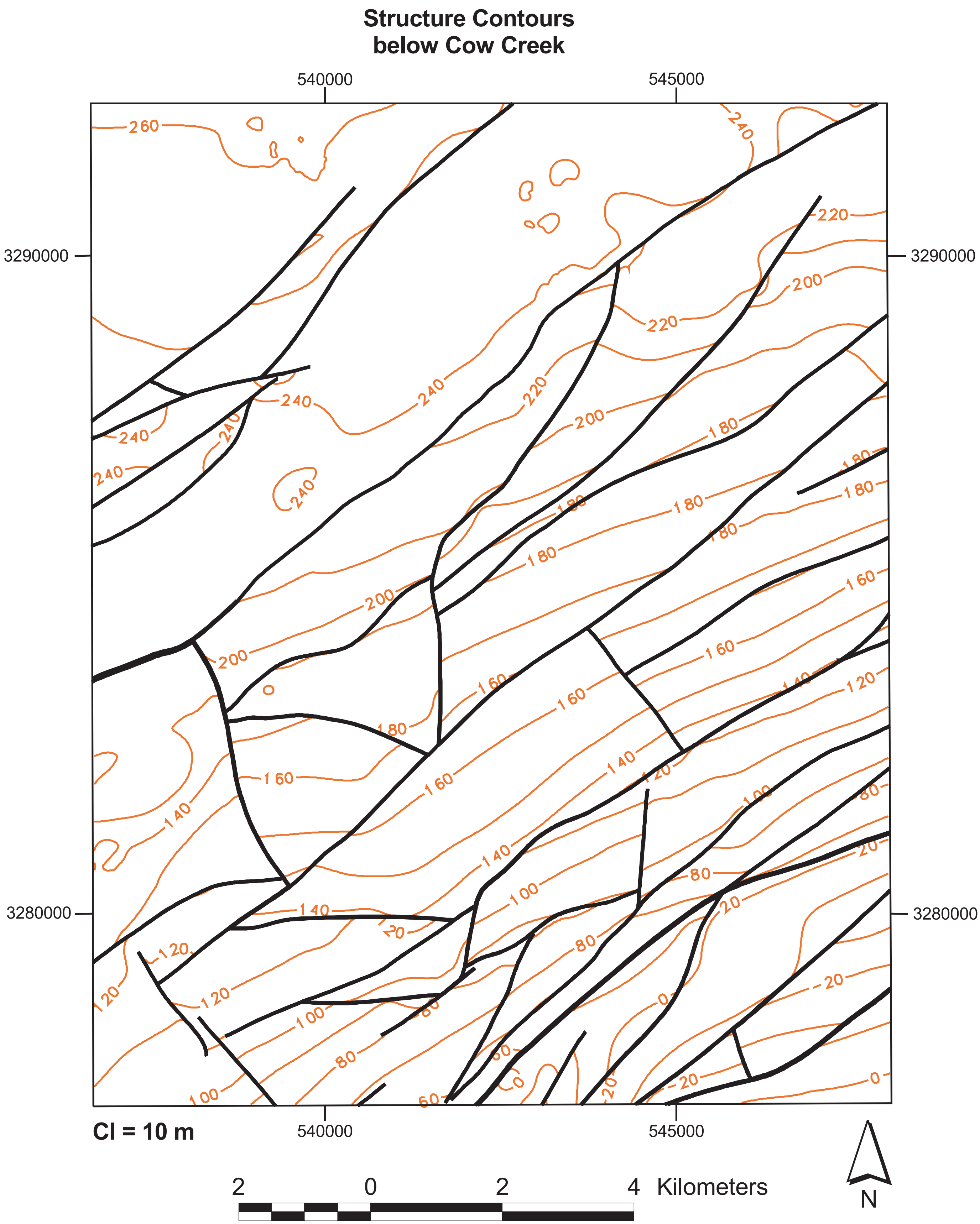

Figure 3-9. Structure contour map drawn on upper surface of model horizon ‘below Cow Creek'. CI = 10 m. Heavy black lines are positions of faults at horizon level. Coordinates are UTM meters, NAD 27.

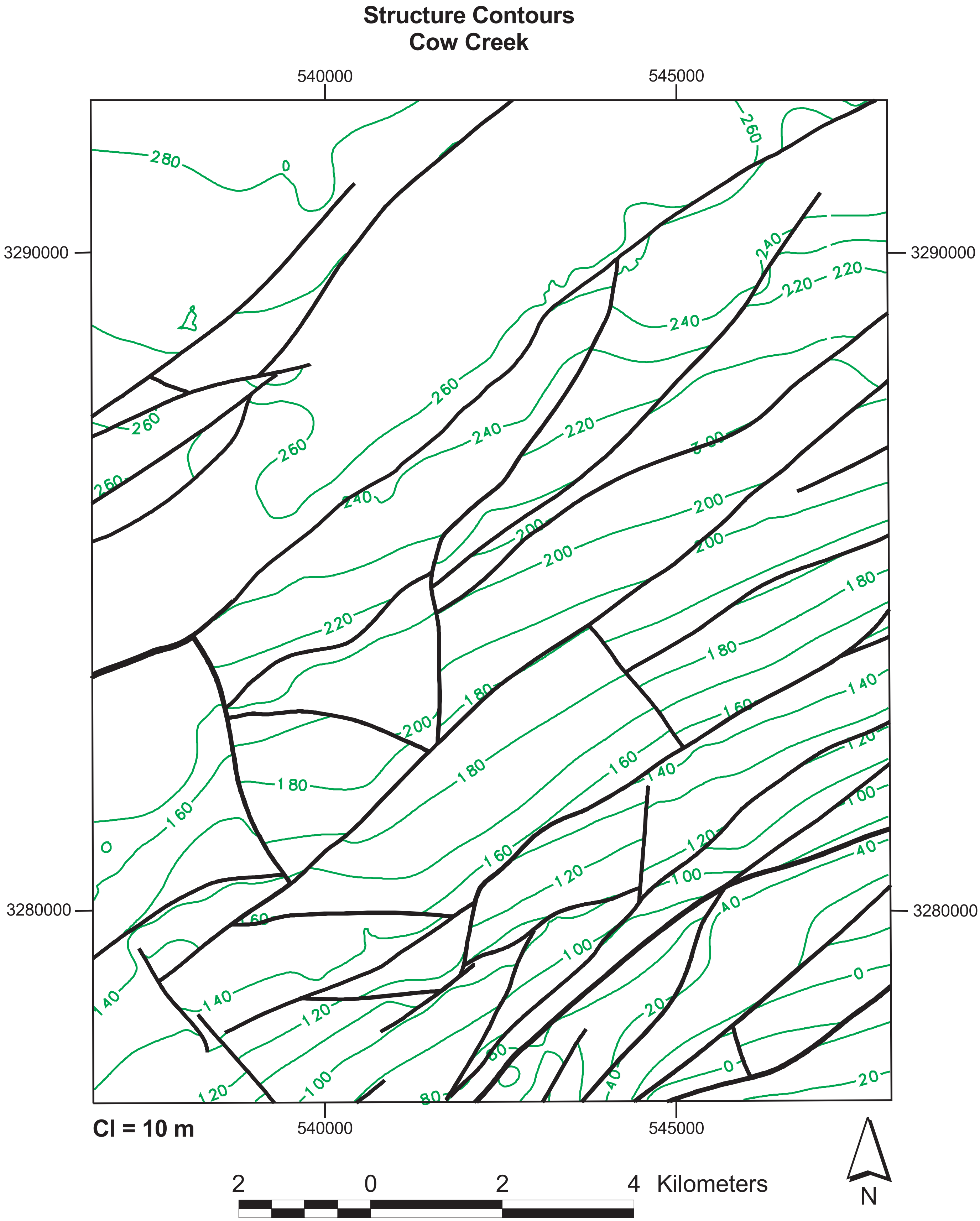

Figure 3-10. Structure contour map drawn on upper surface of model horizon ‘Cow Creek'. CI = 10 m. Heavy black lines are positions of faults at horizon level. Coordinates are UTM meters, NAD 27.

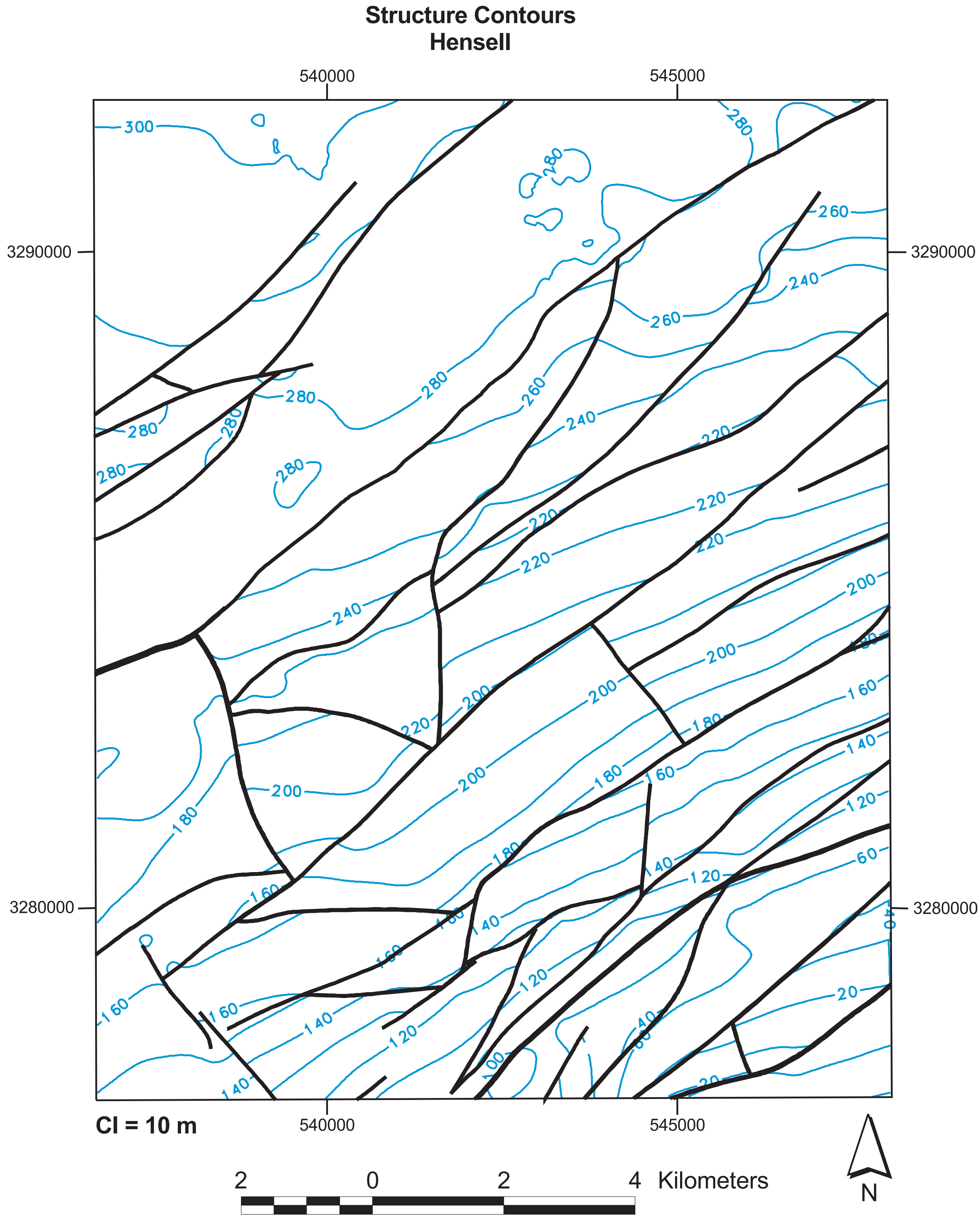

Figure 3-11. Structure contour map drawn on upper surface of model horizon 'Hensell'. CI = 10 m. Heavy black lines are positions of faults at horizon level. Coordinates are UTM meters, NAD 27.

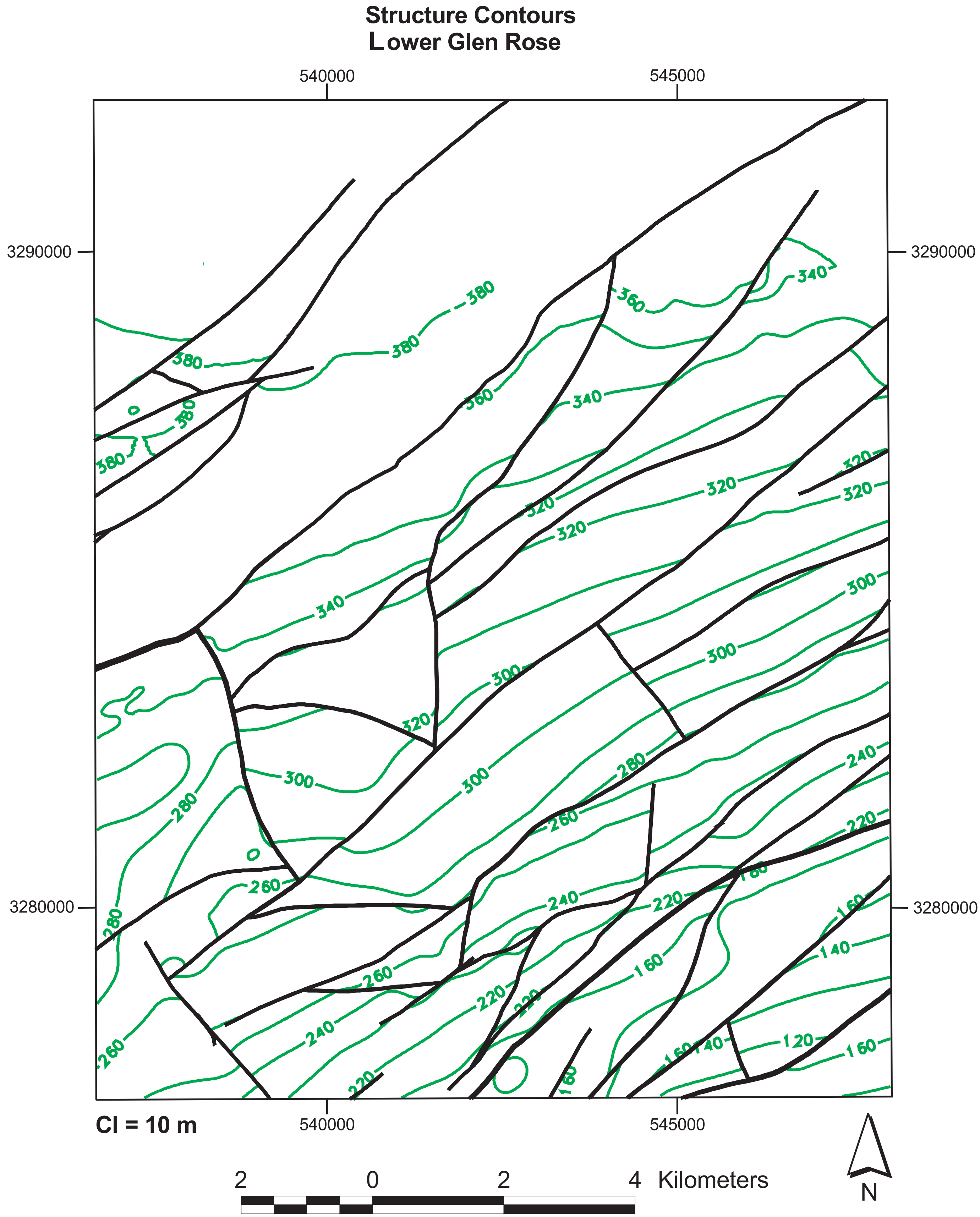

Figure 3-12. Structure contour map drawn on upper surface of model horizon 'Lower Glen Rose Fm.'. CI = 10 m. Heavy black lines are positions of faults at horizon level. Coordinates are UTM meters, NAD 27. Eroded thicknesses are not contoured.

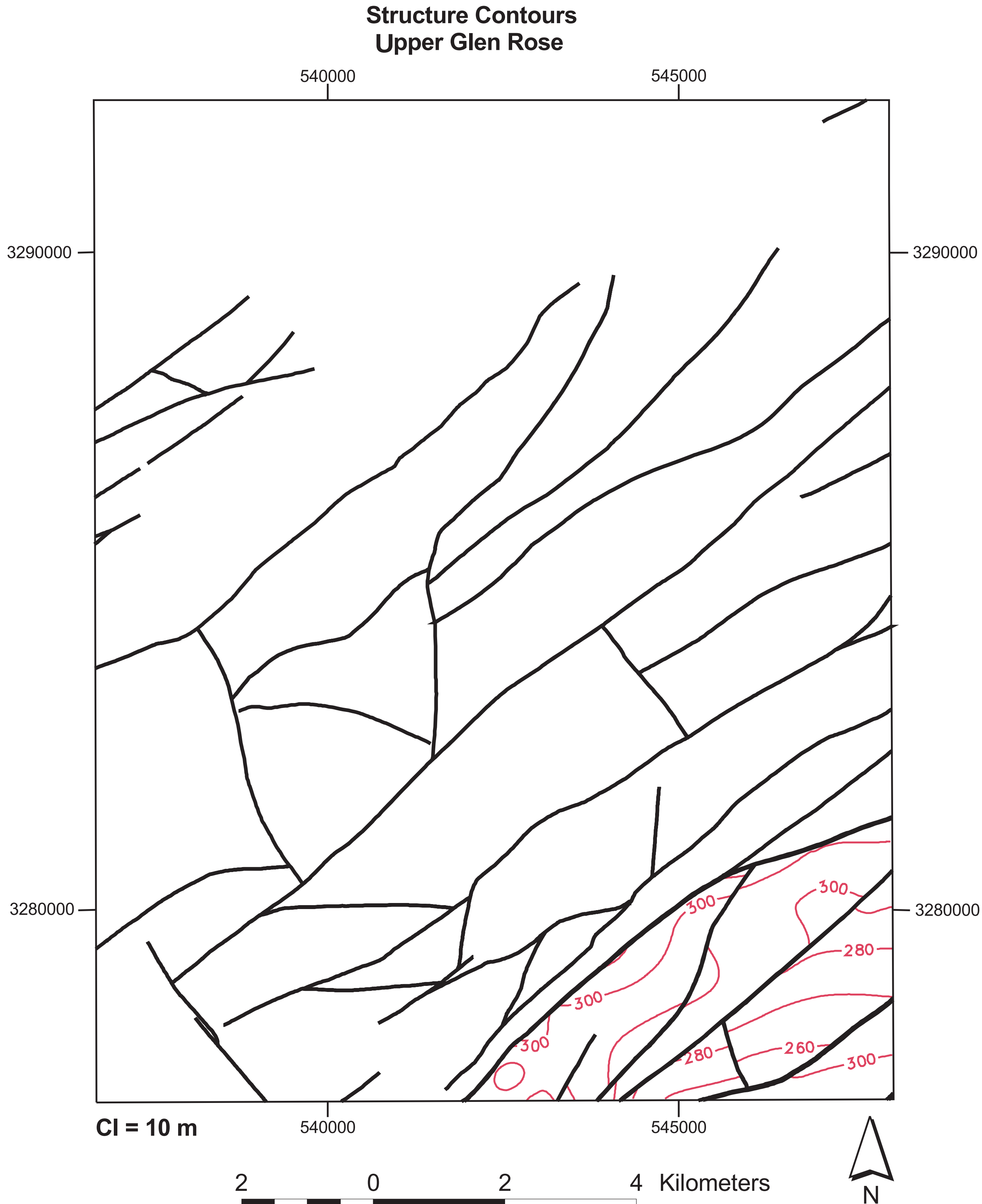

Figure 3-13. Structure contour map drawn on upper surface of model horizon 'Upper Glen Rose Fm.'. CI = 10 m. Heavy black lines are positions of faults at horizon level. Coordinates are UTM meters, NAD 27. Eroded thicknesses are not contoured.

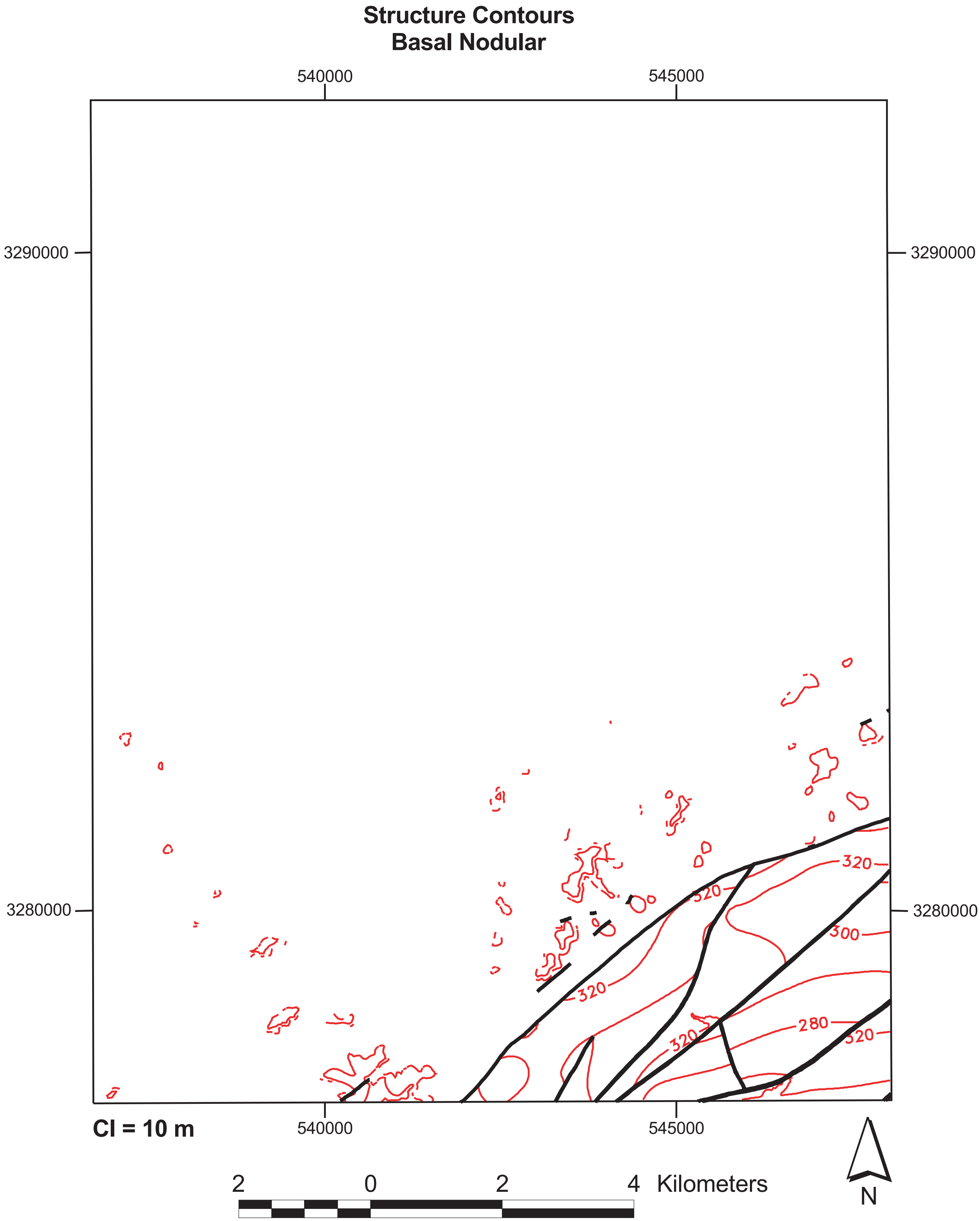

Figure 3-14. Structure contour map drawn on upper surface of model horizon 'Basal Nodular'. CI = 10 m. Heavy black lines are positions of faults at horizon level. Coordinates are UTM meters, NAD 27. Eroded thicknesses are not contoured.

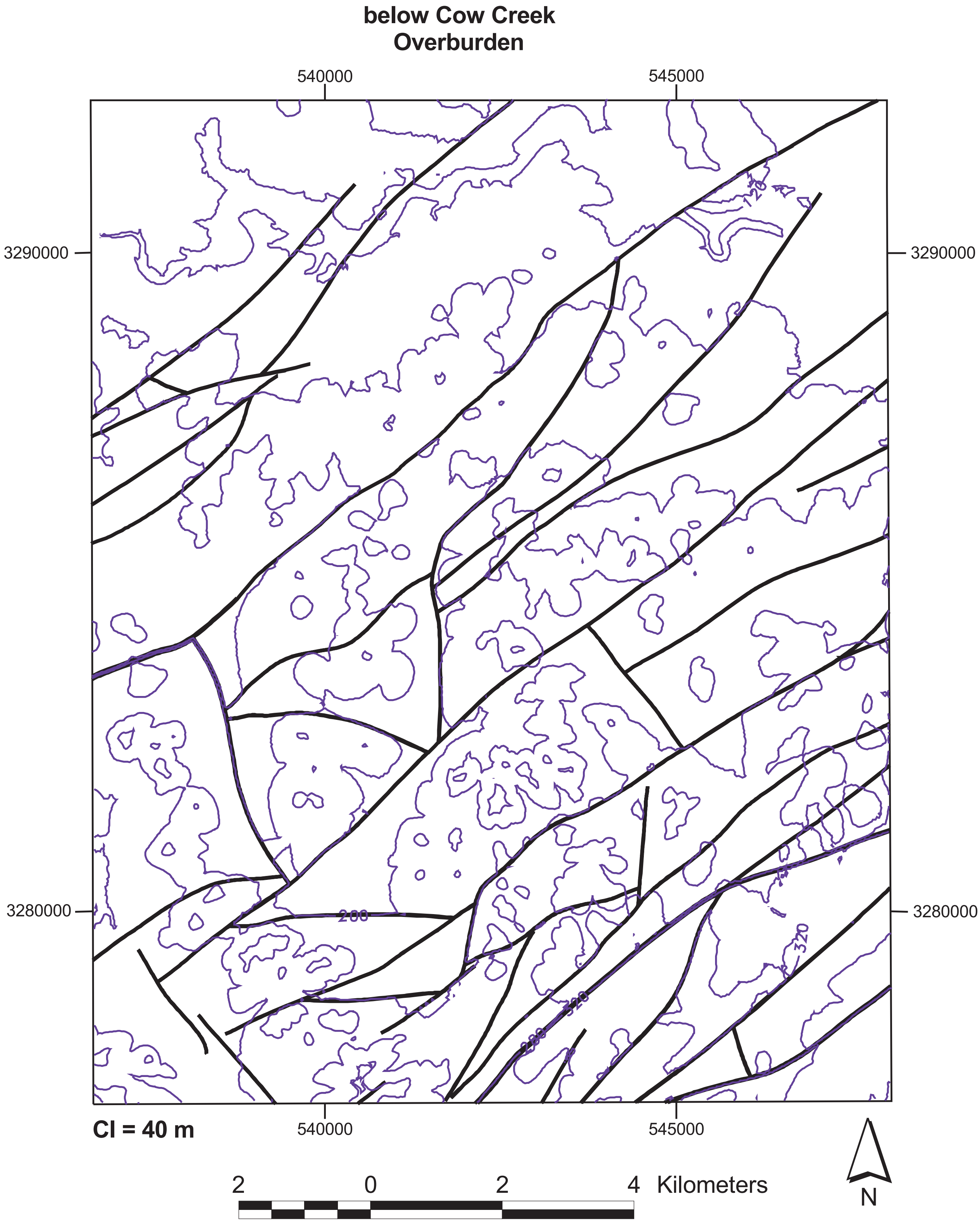

Figure 3-15. Overburden thickness (or depth-to-top) map drawn for upper surface of model horizon 'below Cow Creek'. CI = 40 m. Heavy black lines are positions of faults at horizon level. Coordinates are UTM meters, NAD 27.

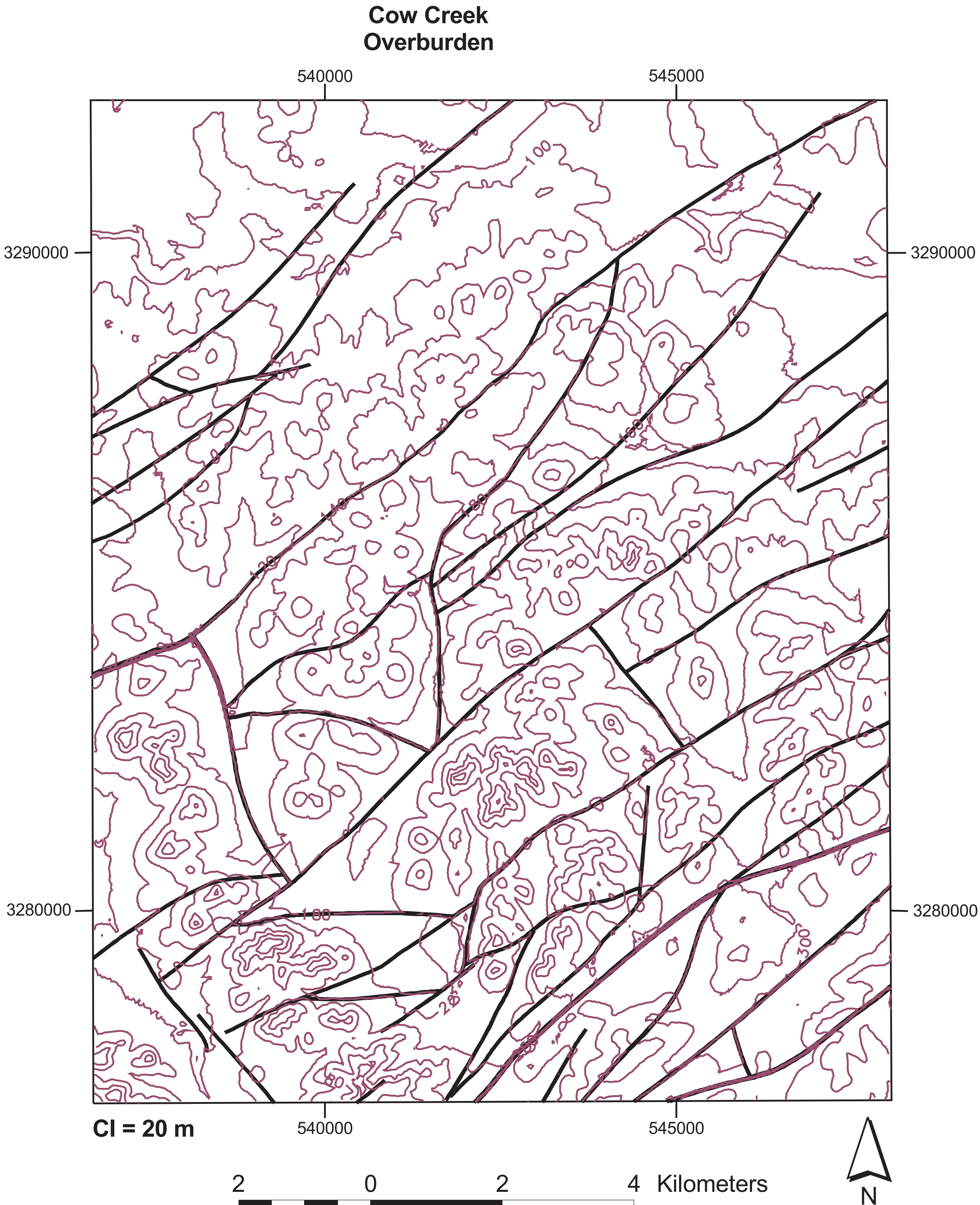

Figure 3-16. Overburden thickness (or depth-to-top) map drawn for upper surface of model horizon 'Cow Creek'. CI = 20 m. Heavy black lines are positions of faults at horizon level. Coordinates are UTM meters, NAD 27.

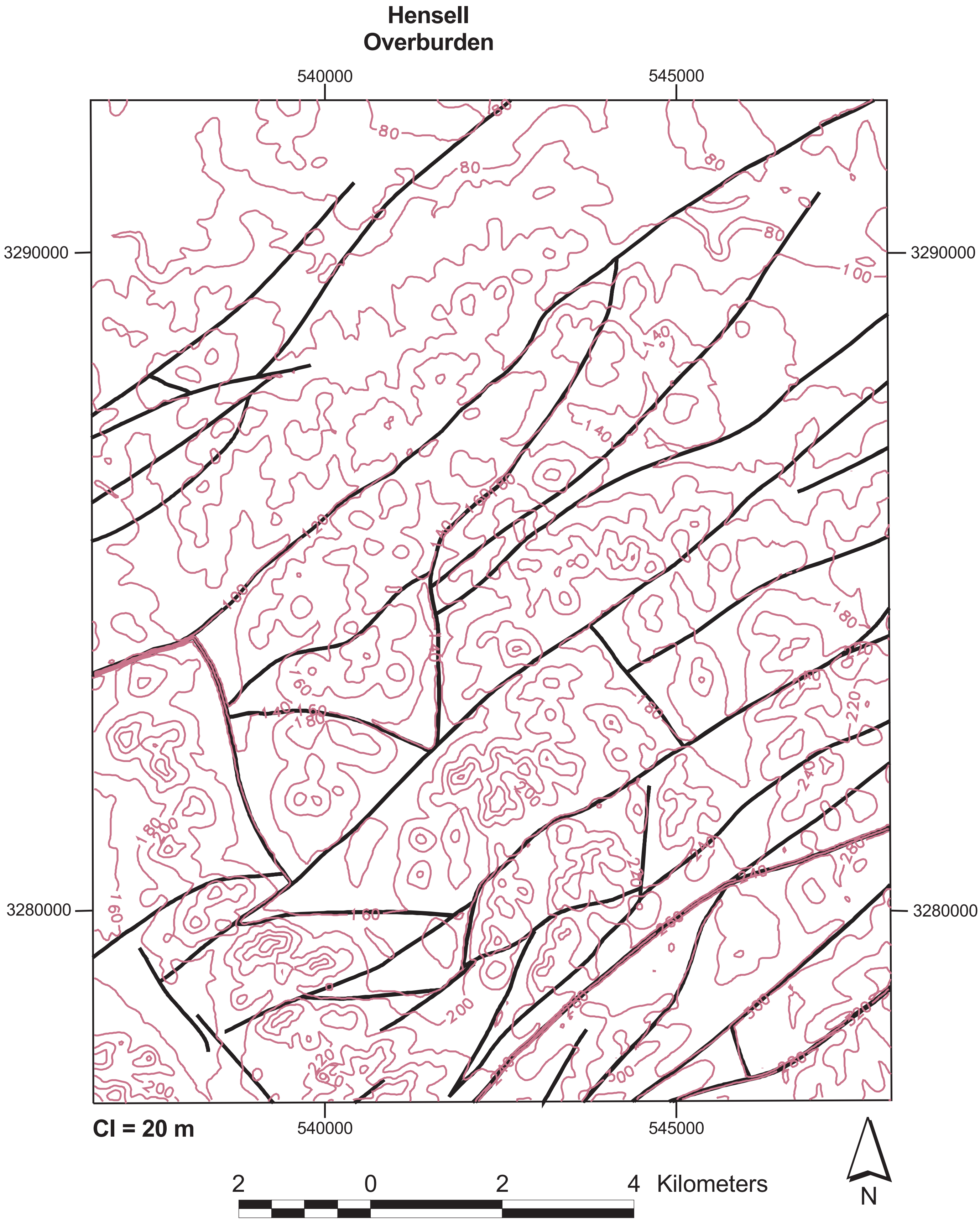

Figure 3-17. Overburden thickness (or depth-to-top) map drawn for upper surface of model horizon ‘Hensell'. CI = 20 m. Heavy black lines are positions of faults at horizon level. Coordinates are UTM meters, NAD 27.

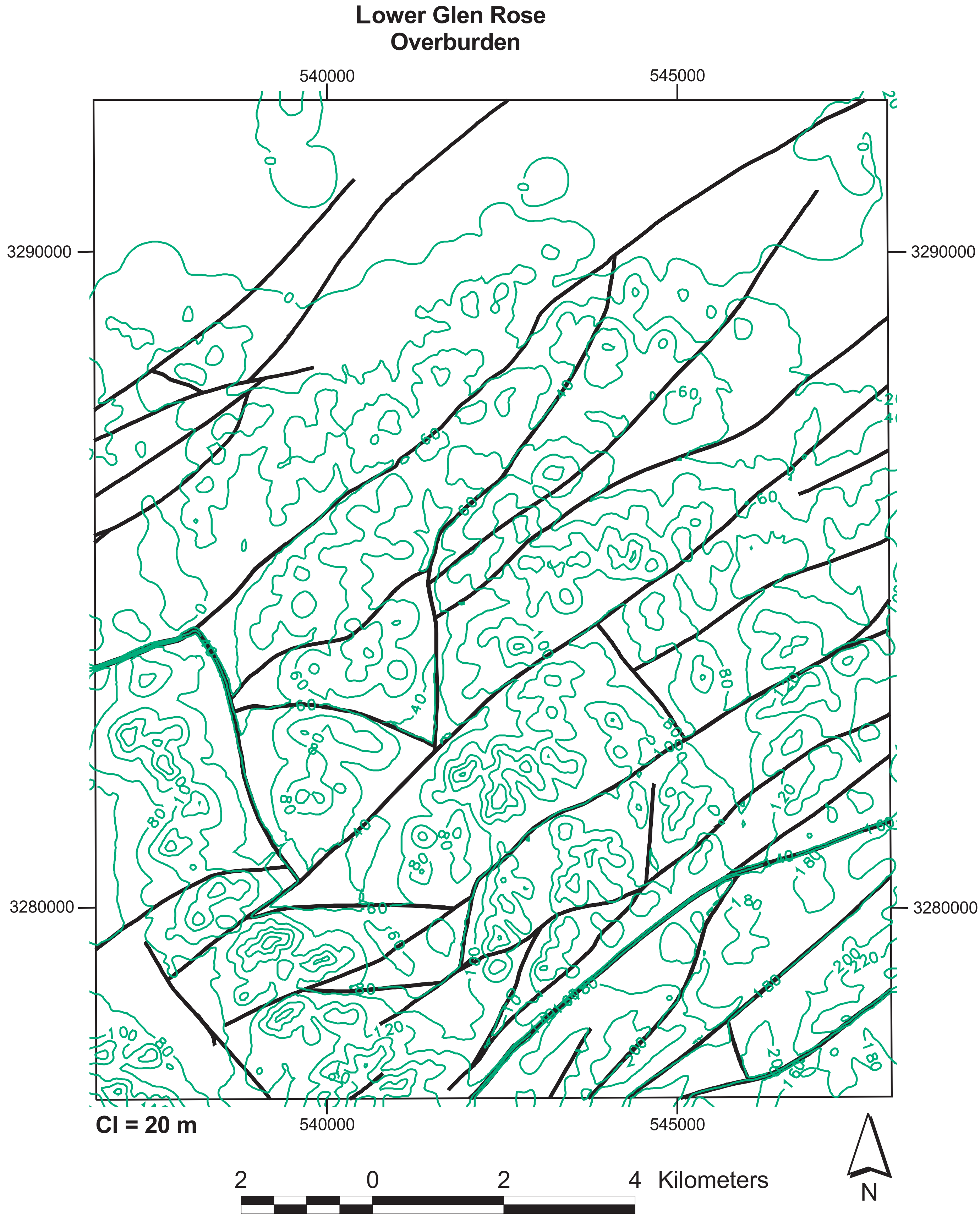

Figure 3-18. Overburden thickness (or depth-to-top) map drawn for upper surface of model horizon 'Lower Glen Rose Fm.'. CI = 20 m. Heavy black lines are positions of faults at horizon level. Coordinates are UTM meters, NAD 27.

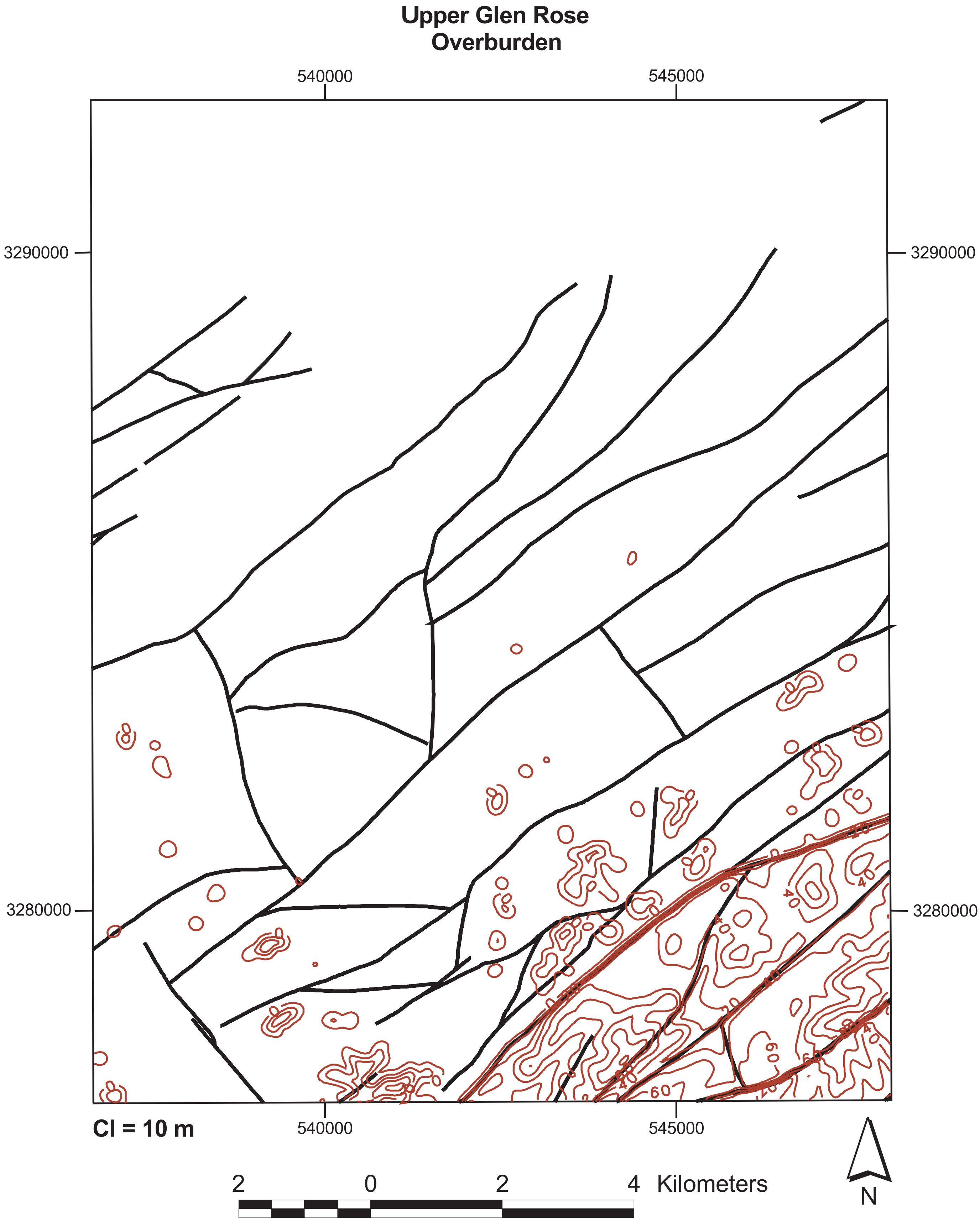

Figure 3-19. Overburden thickness (or depth-to-top) map drawn for upper surface of model horizon 'Upper Glen Rose Fm.'. CI = 10 m. Heavy black lines are positions of faults at horizon level. Coordinates are UTM meters, NAD 27.

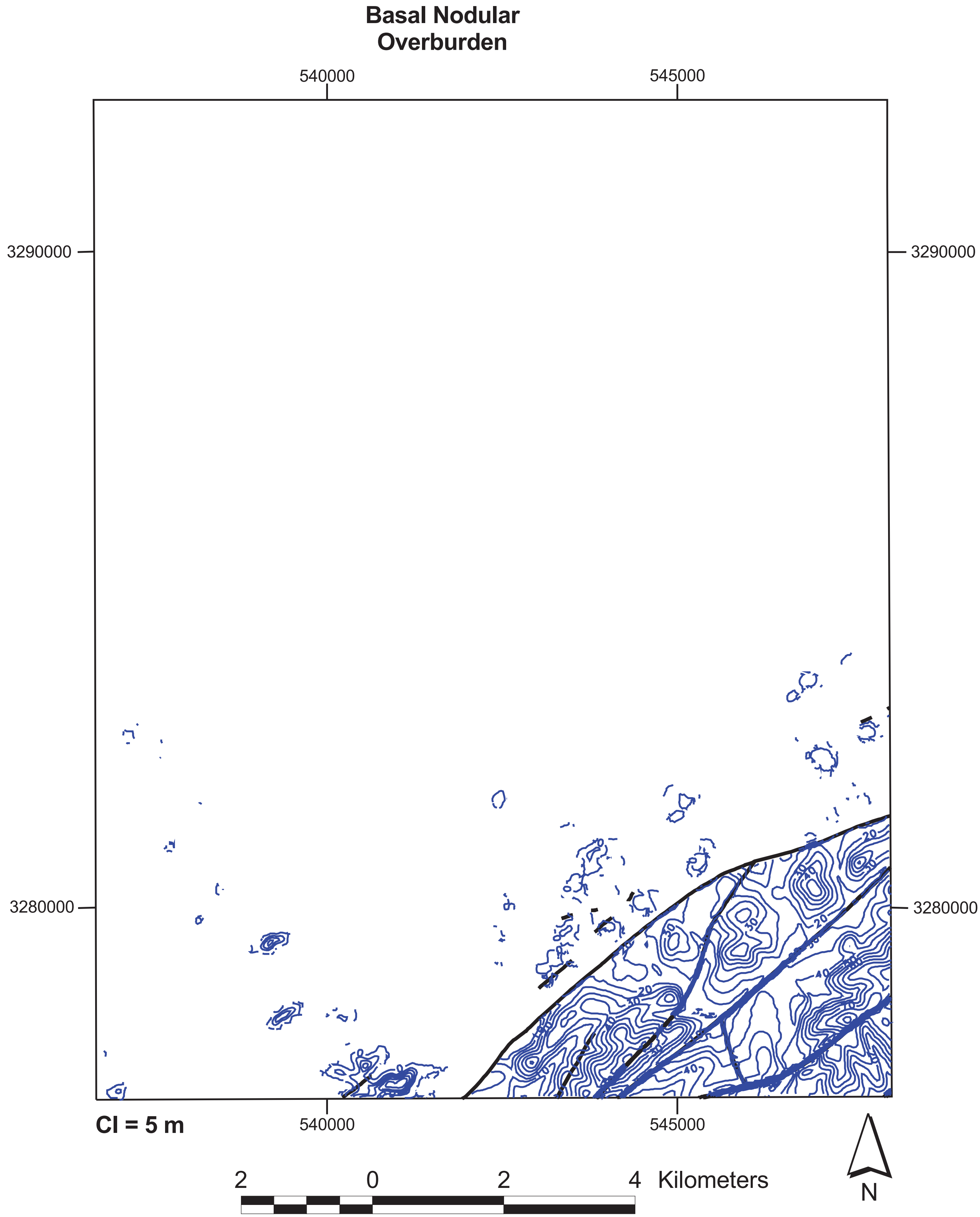

Figure 3-20. Overburden thickness (or depth-to-top) map drawn for model horizon 'Basal Nodular'. CI = 5 m. Heavy black lines are positions of faults at horizon level. Coordinates are UTM meters, NAD 27.

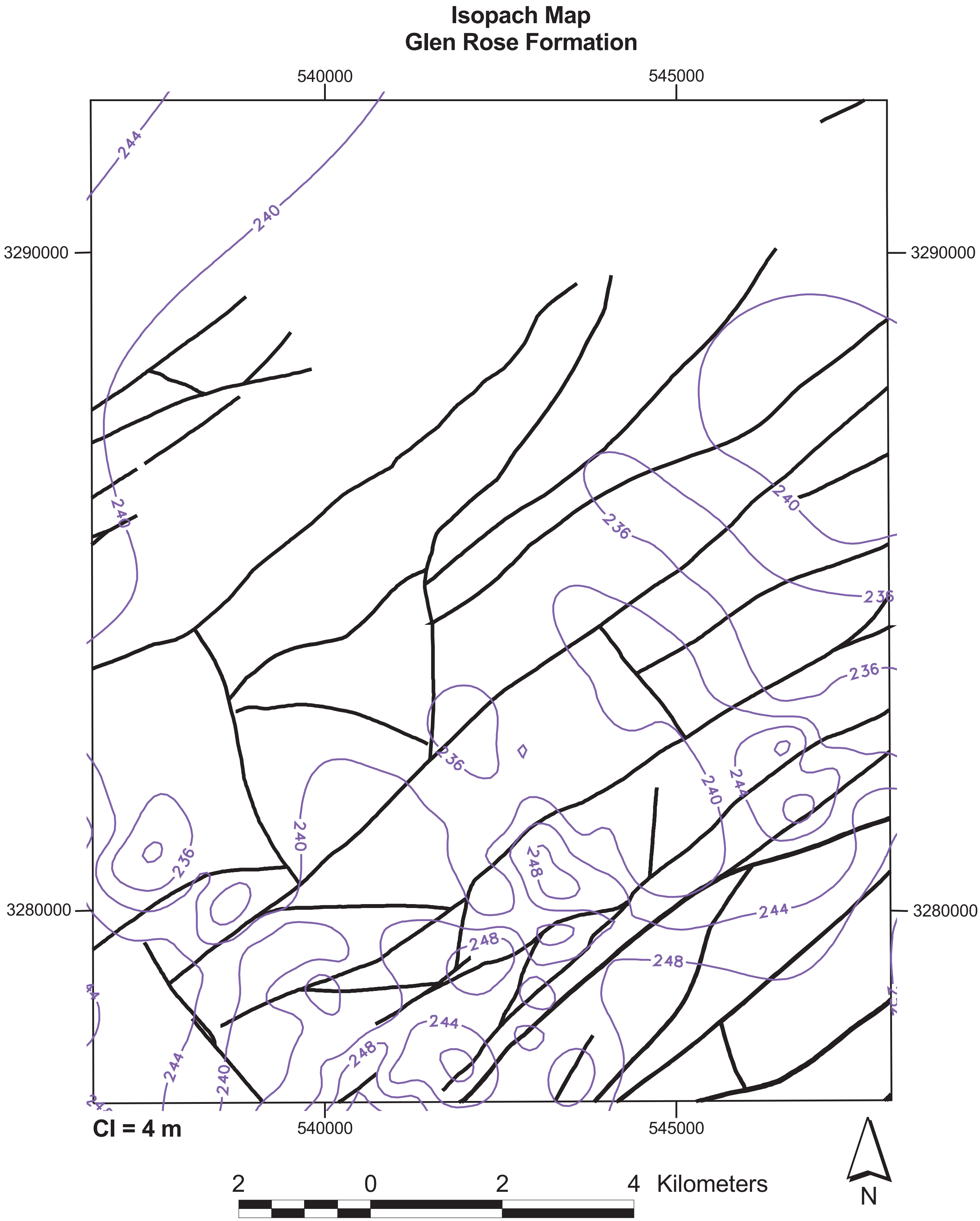

Figure 3-21. Isopach map showing model thickness of the Glen Rose formation. CI = 4 m. Heavy black lines are positions of faults at horizon level. Thickness inferred where horizon is eroded. Coordinates are UTM meters, NAD 27.

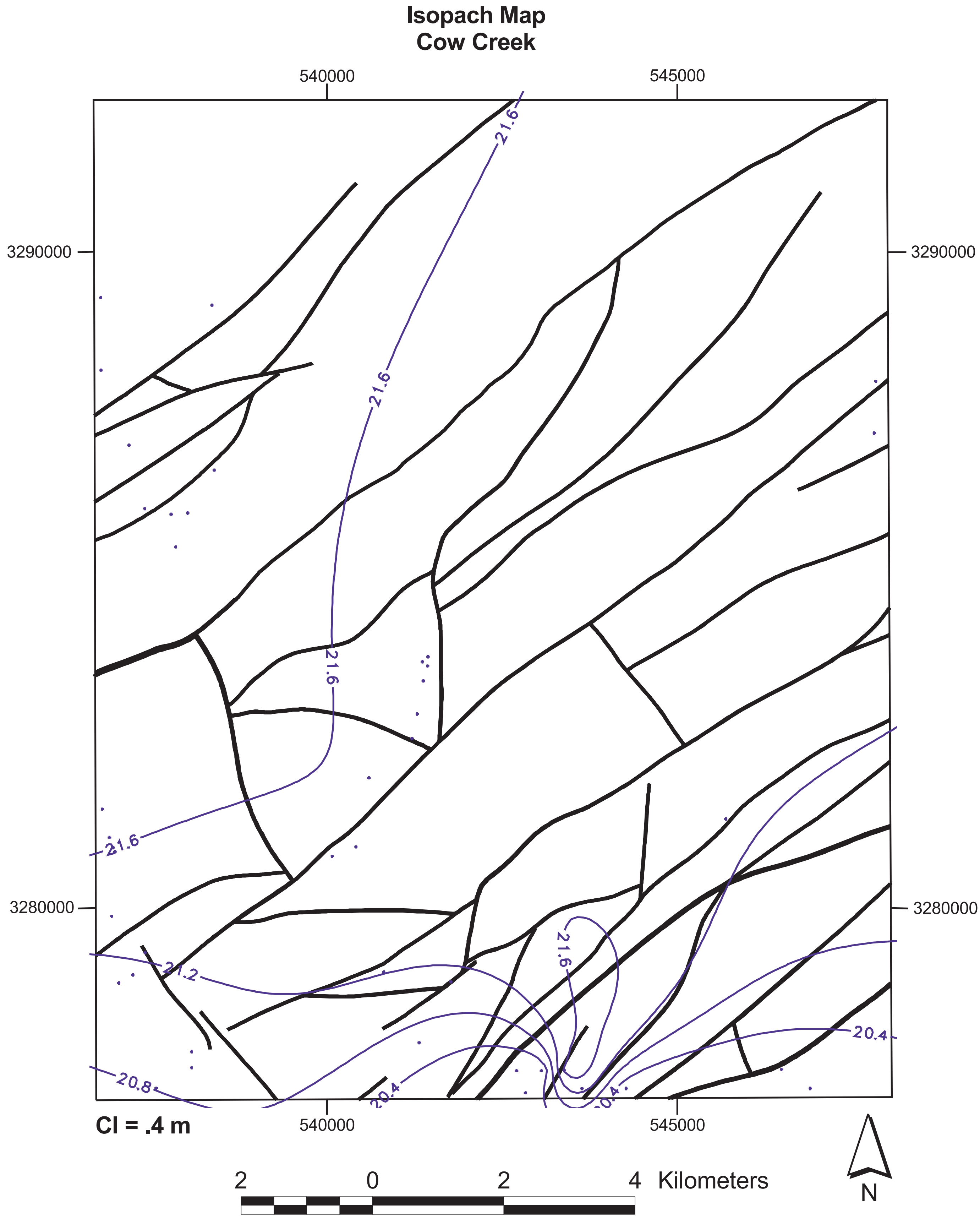

Figure 3-22. Isopach map showing thickness of model horizon ‘Cow Creek'. CI = 0.4 m. Heavy black lines are positions of faults at horizon level. Coordinates are UTM meters, NAD 27.

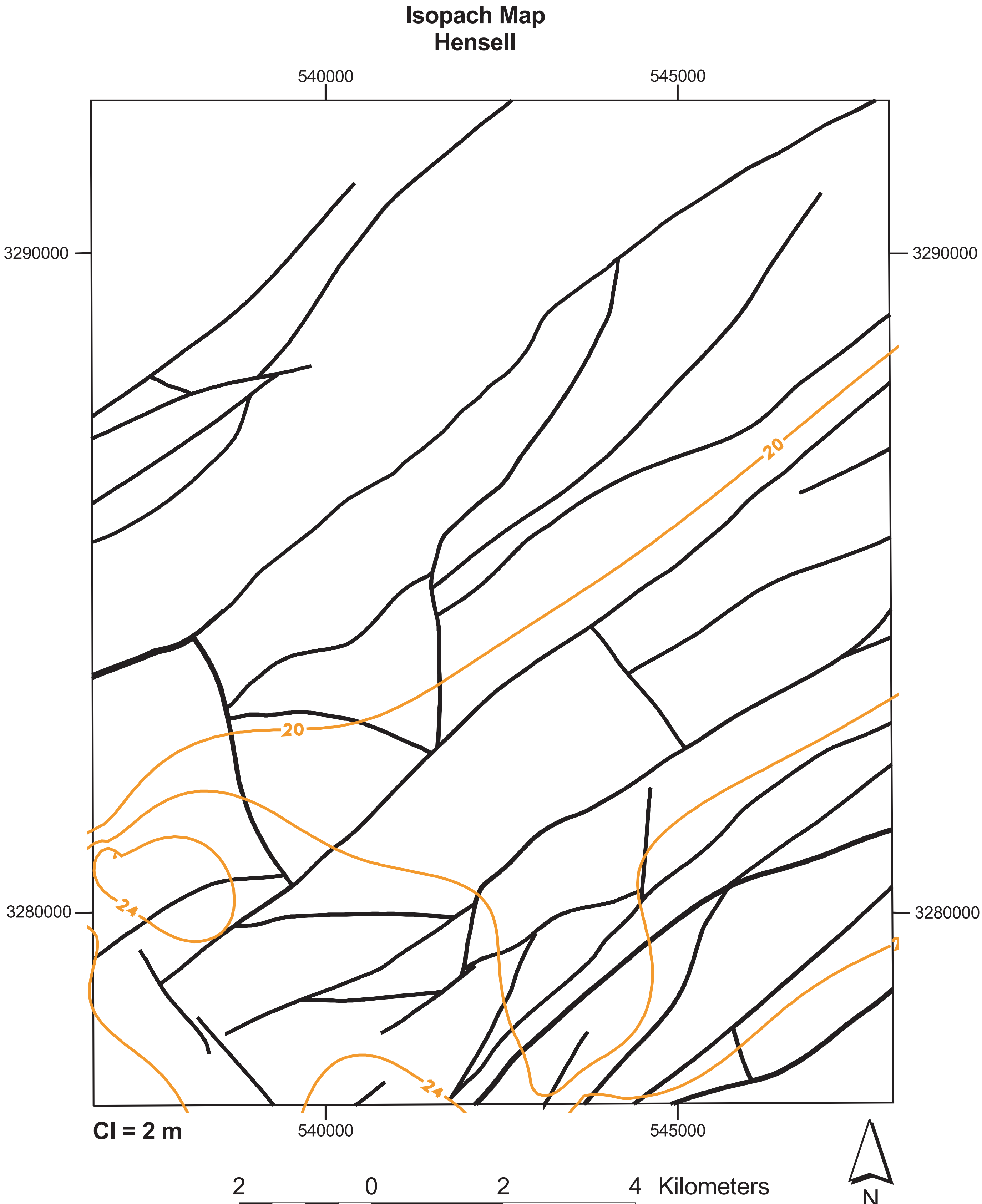

Figure 3-23. Isopach map showing thickness of model horizon 'Hensell'. CI = 2 m. Heavy black lines are positions of faults at horizon level. Coordinates are UTM meters, NAD 27.

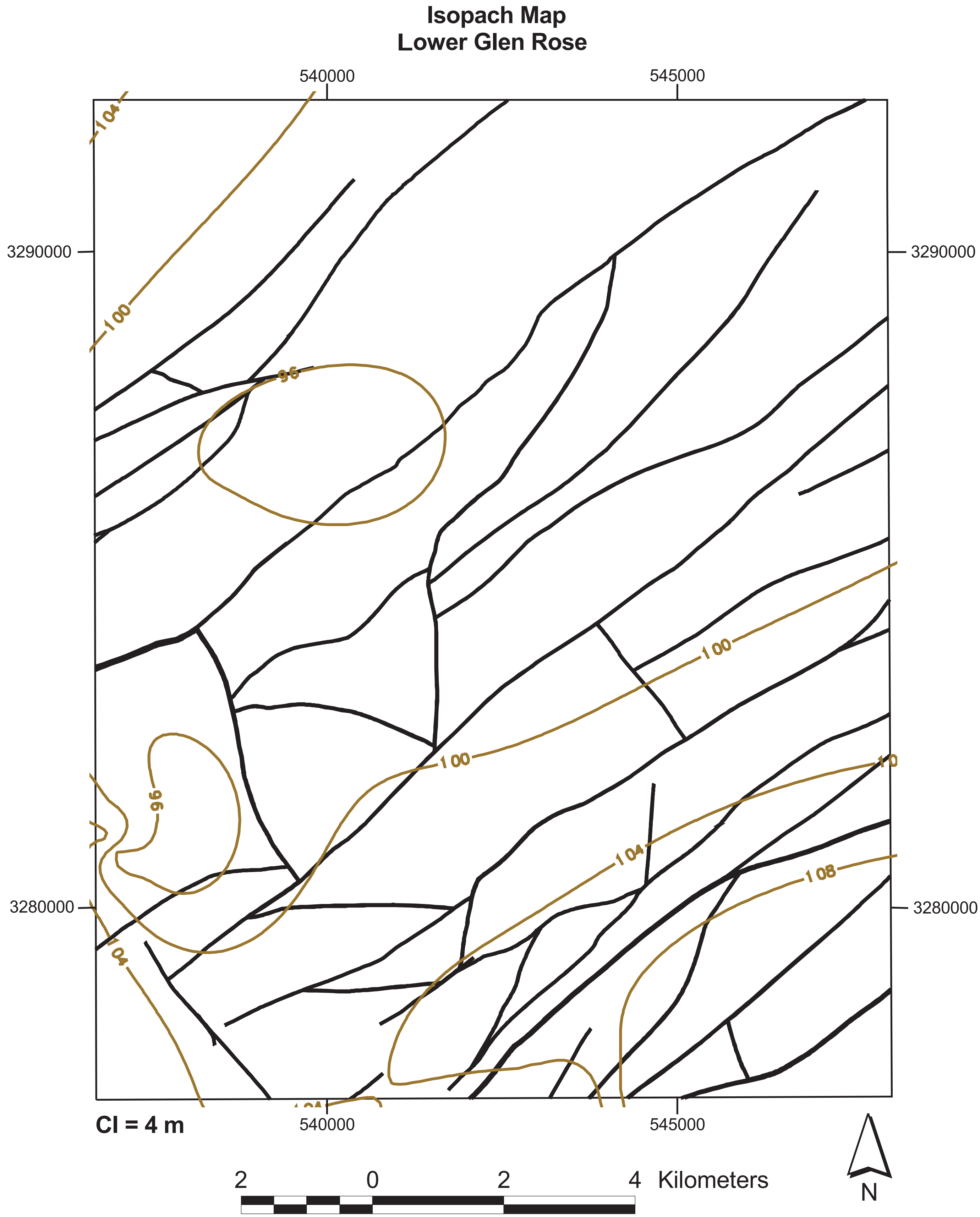

Figure 3-24. Isopach map showing thickness of model horizon ‘Lower Glen Rose Fm.'. CI = 4 m. Heavy black lines are positions of faults at horizon level. Coordinates are UTM meters, NAD 27.

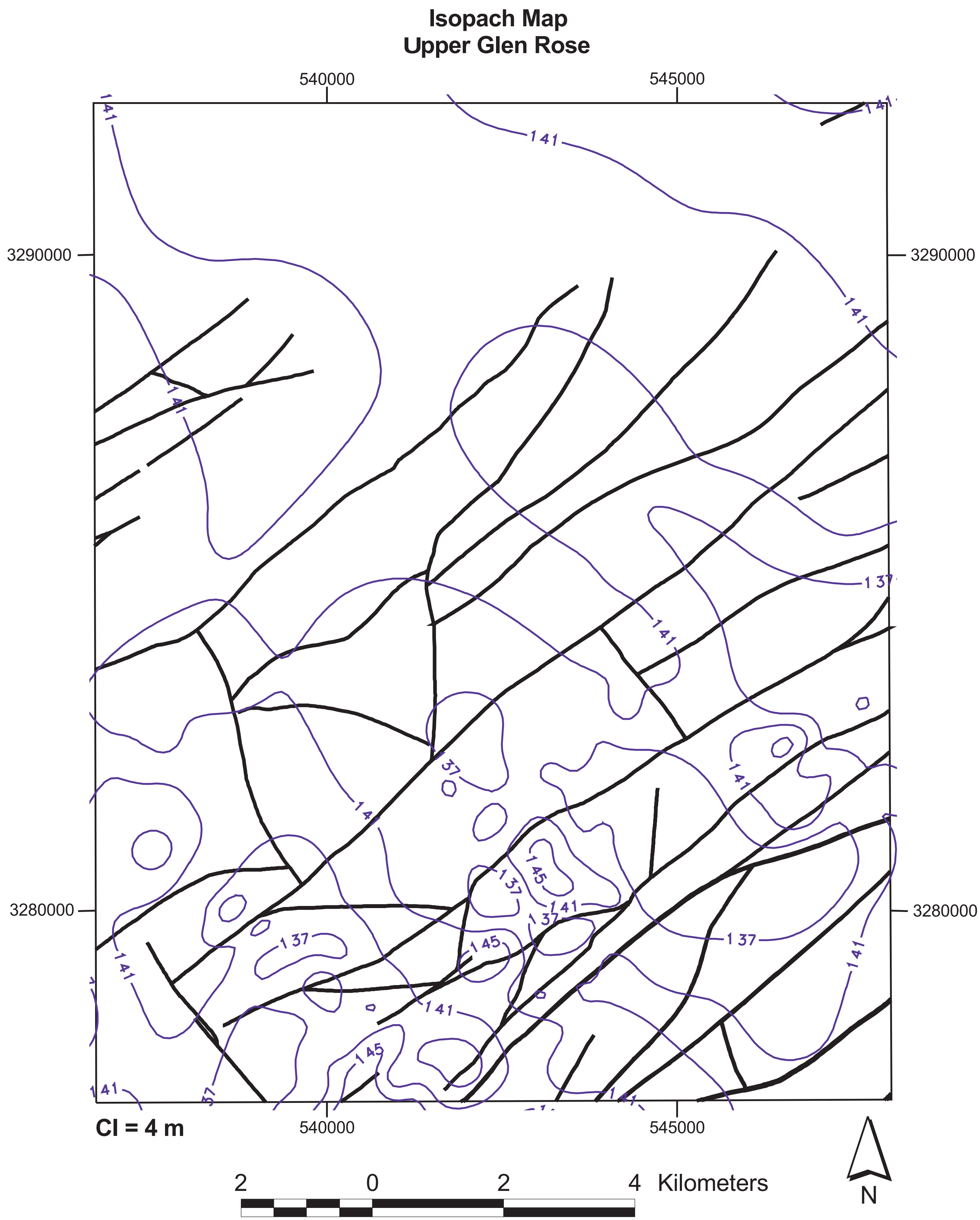

Figure 3-25. Isopach map showing thickness of model horizon ‘Upper Glen Rose Fm.'. CI = 4 m. Heavy black lines are positions of faults at horizon level. Thickness inferred where horizon is eroded. Coordinates are UTM meters, NAD 27.

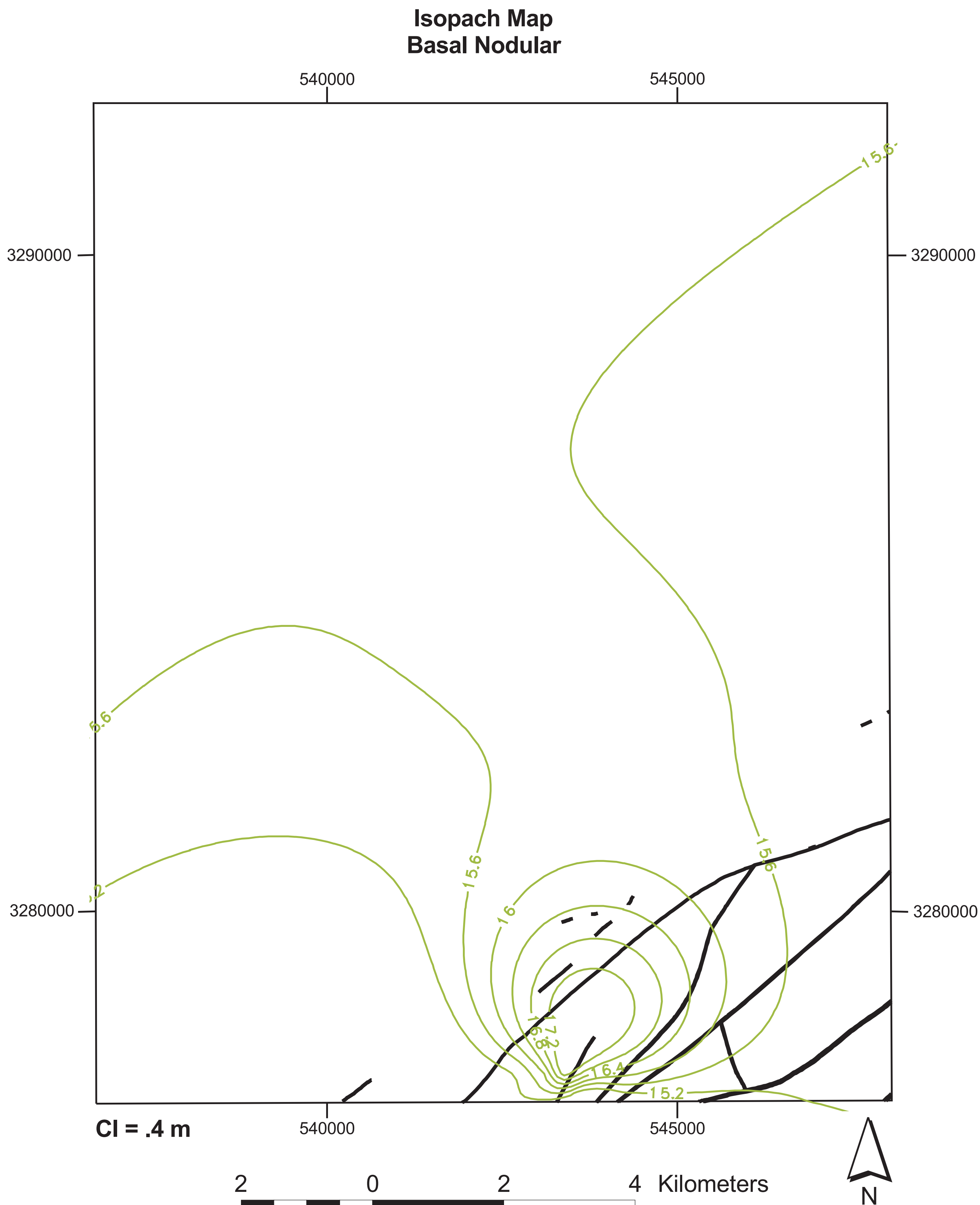

Figure 3-26 Isopach map showing thickness of model horizon 'Basal Nodular'. CI = 0.4 m. Heavy black lines are positions of faults at horizon level. Thickness inferred where horizon is eroded. Coordinates are UTM meters, NAD 27.

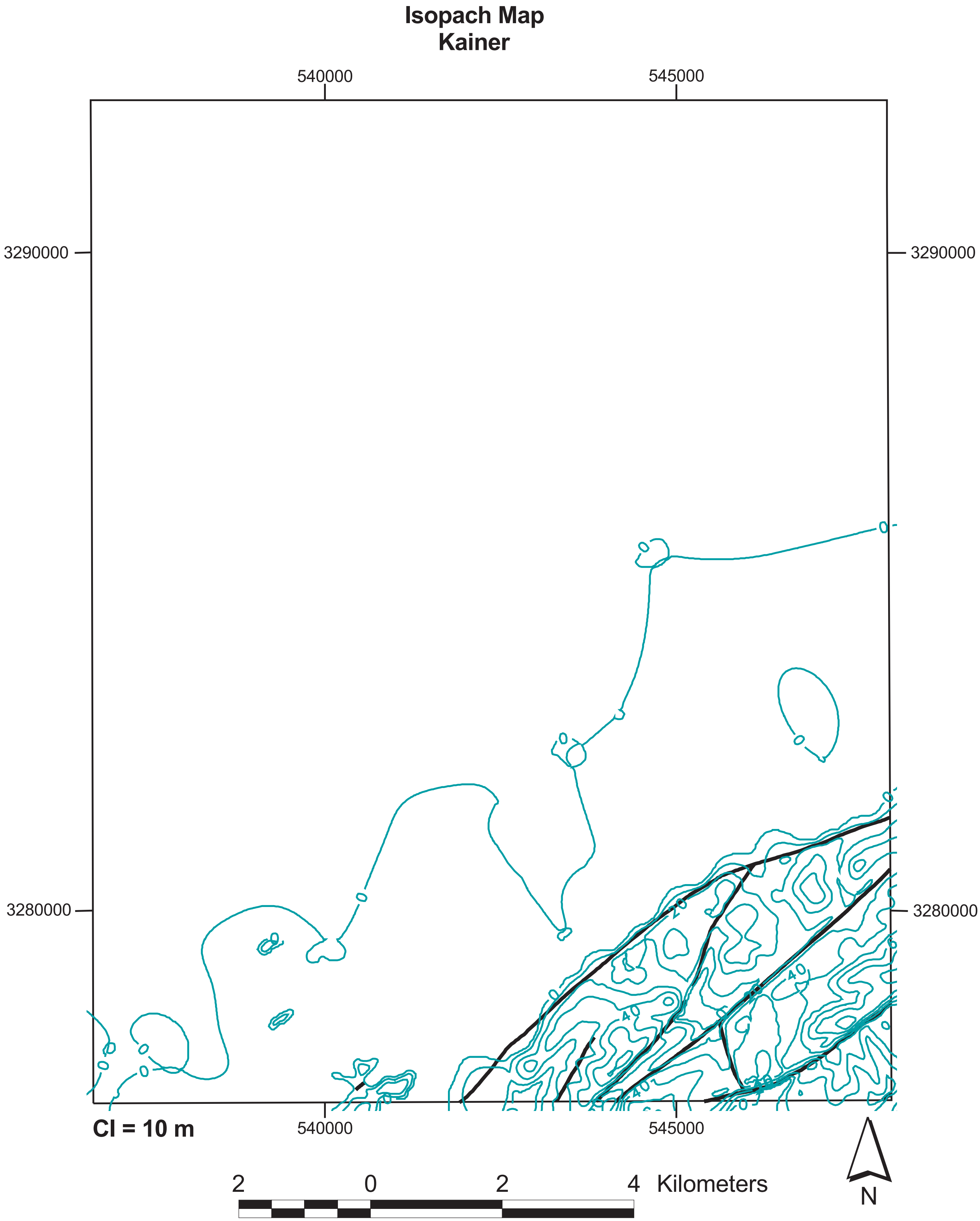

Figure 3-27. Isopach map showing thickness of model horizon 'Kainer'. CI = 10 m. Heavy black lines are positions of faults at horizon level. Coordinates are UTM meters, NAD 27.

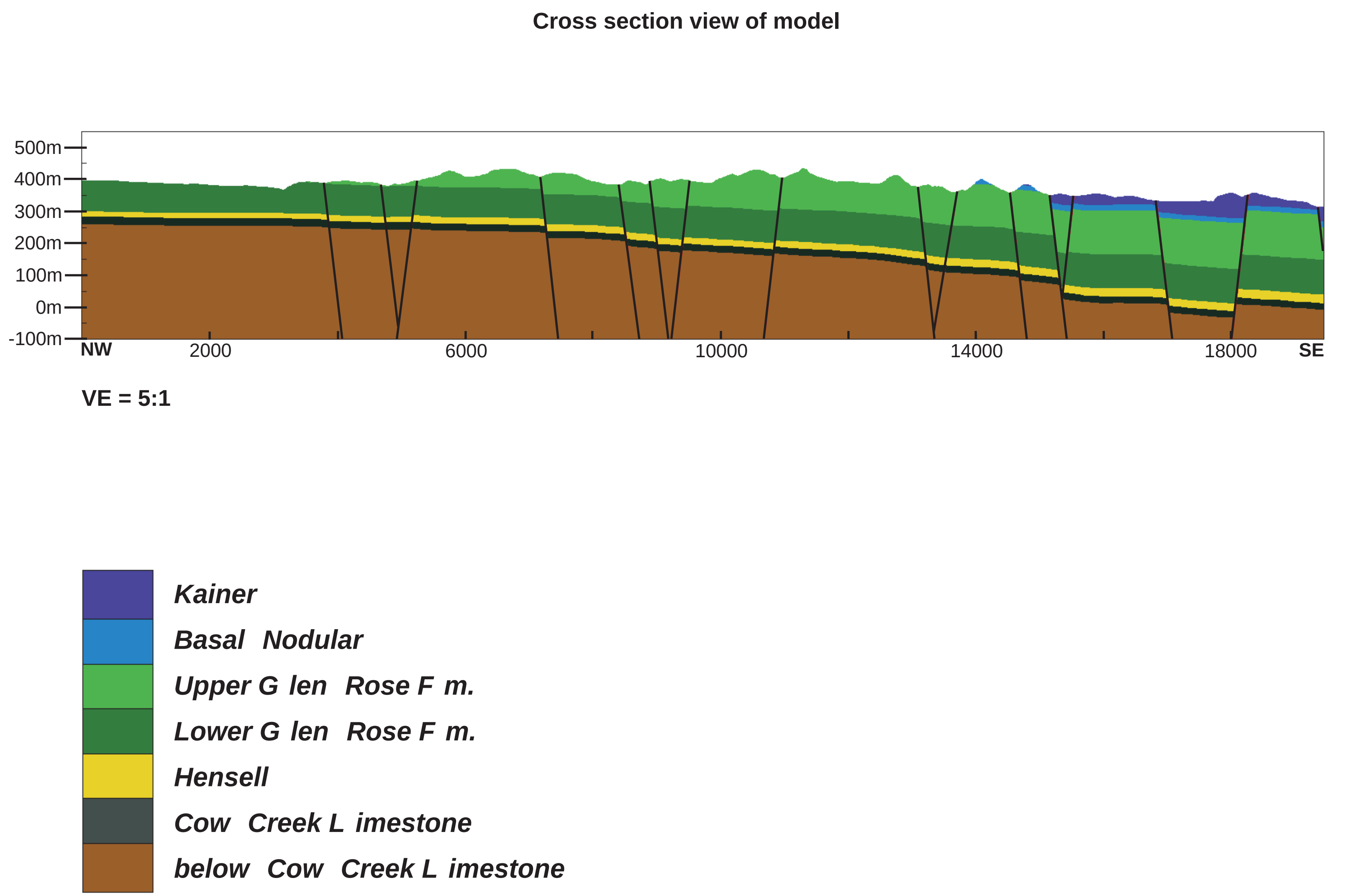

Figure 3-28. Cross section view of model. Section is oriented NW-SE and extends corner to corner across the model area (see Fig. 3-1), with left end starting at NW model corner. Vertical Exaggeration = 5:1. Horizontal units are meters distance from left end.

Constant E levation S lice
Elevation = -50m

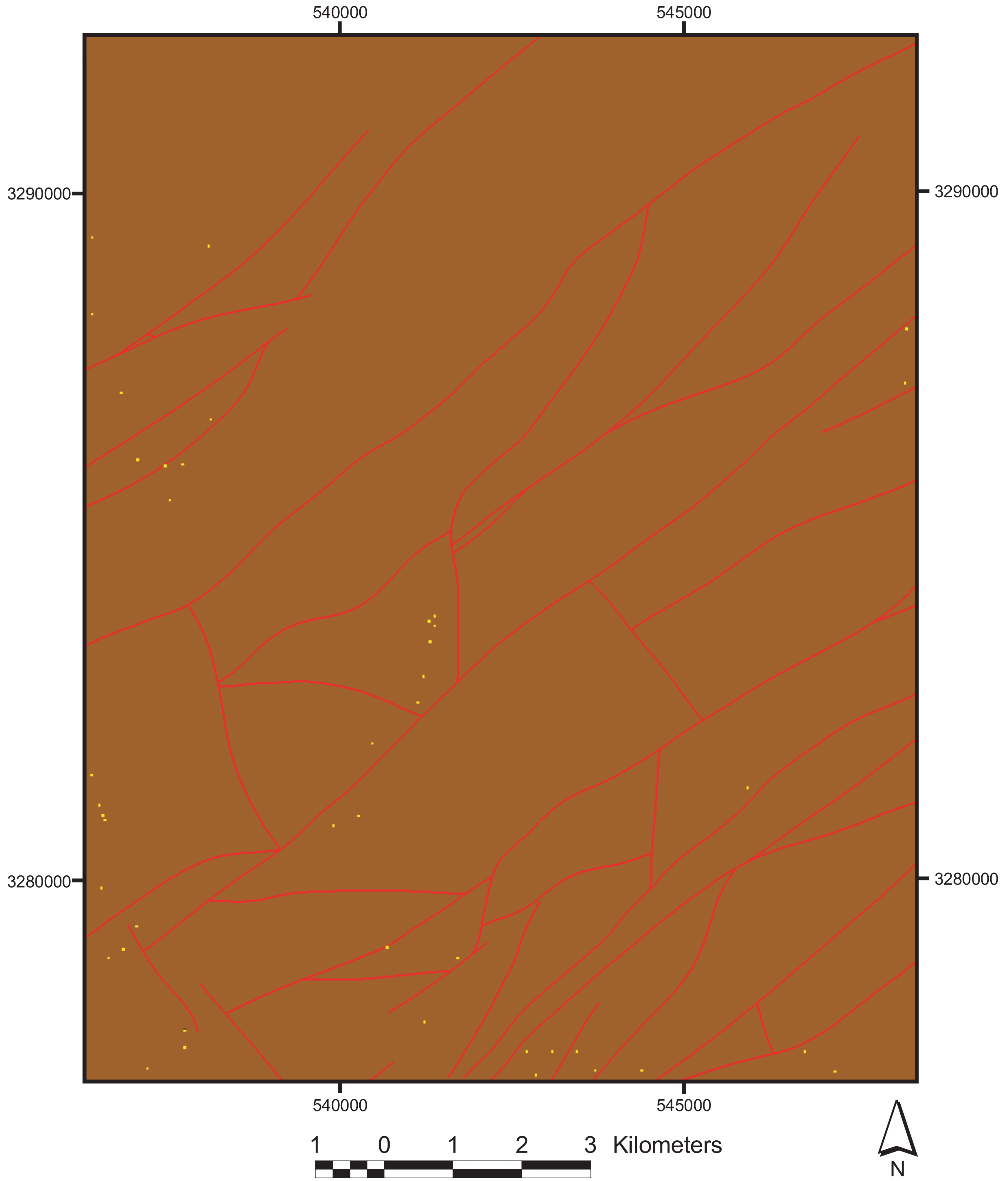

Figure 3-29. Map view of constant elevation (horizontal) slice through model. Elevation = -50 m. Units are UTM meters, NAD27. Red lines show fault traces, and yellow points show well locations. See Figure 3-1 for complete color key.

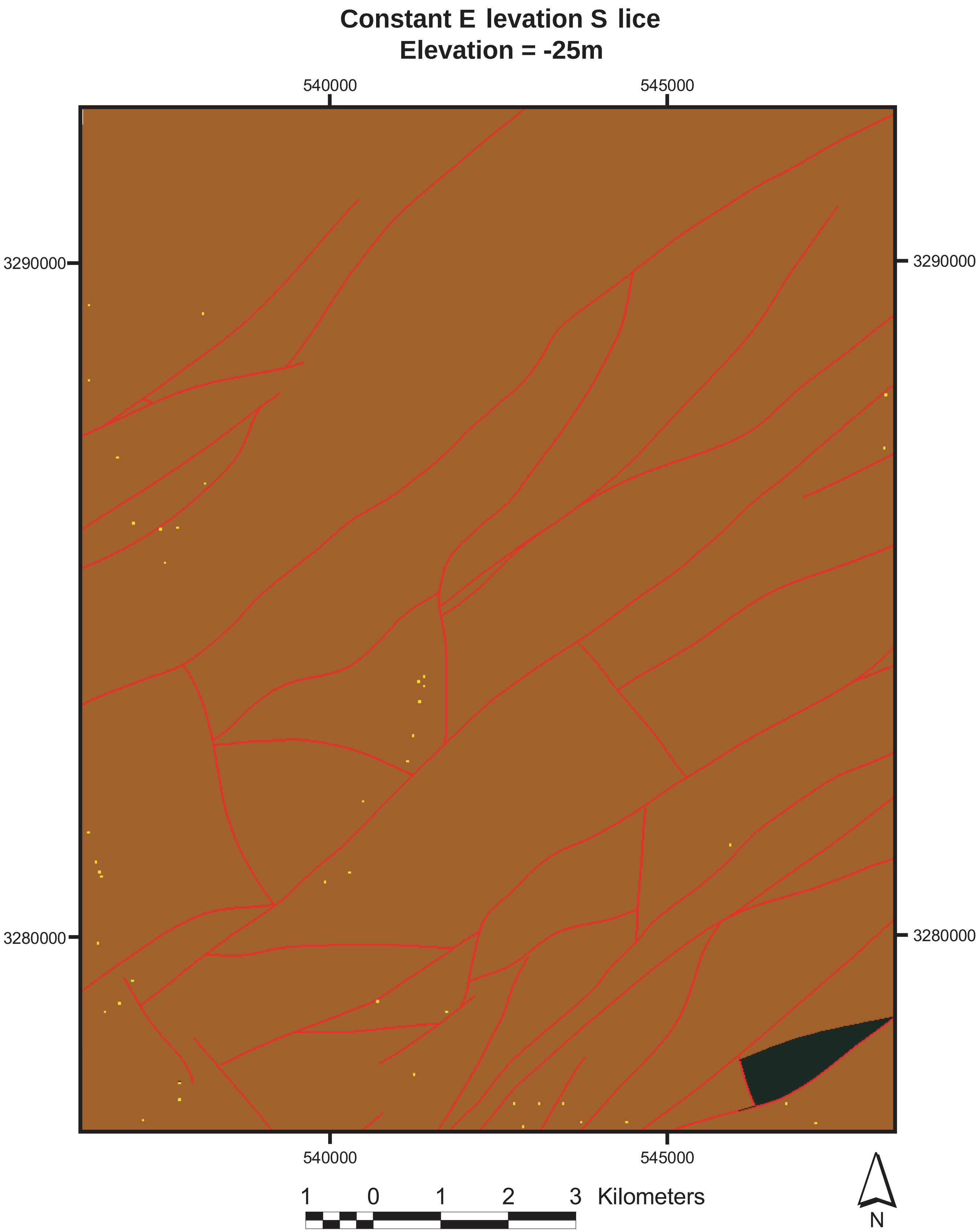

Figure 3-30. Map view of constant elevation (horizontal) slice through model. Elevation = -25 m. Units are UTM meters, NAD27. Red lines show fault traces, and yellow points show well locations. See Figure 3-1 for complete color key.

Figure 3-31. Map view of constant elevation (horizontal) slice through model. Elevation = 0 m. Units are UTM meters, NAD27. Red lines show fault traces, and yellow points show well locations. See Figure 3-1 for complete color key.

Figure 3-32. Map view of constant elevation (horizontal) slice through model. Elevation = 25 m. Units are UTM meters, NAD27. Red lines show fault traces, and yellow points show well locations. See Figure 3-1 for complete color key.

Figure 3-33. Map view of constant elevation (horizontal) slice through model. Elevation = 50 m. Units are UTM meters, NAD27. Red lines show fault traces, and yellow points show well locations. See Figure 3-1 for complete color key.

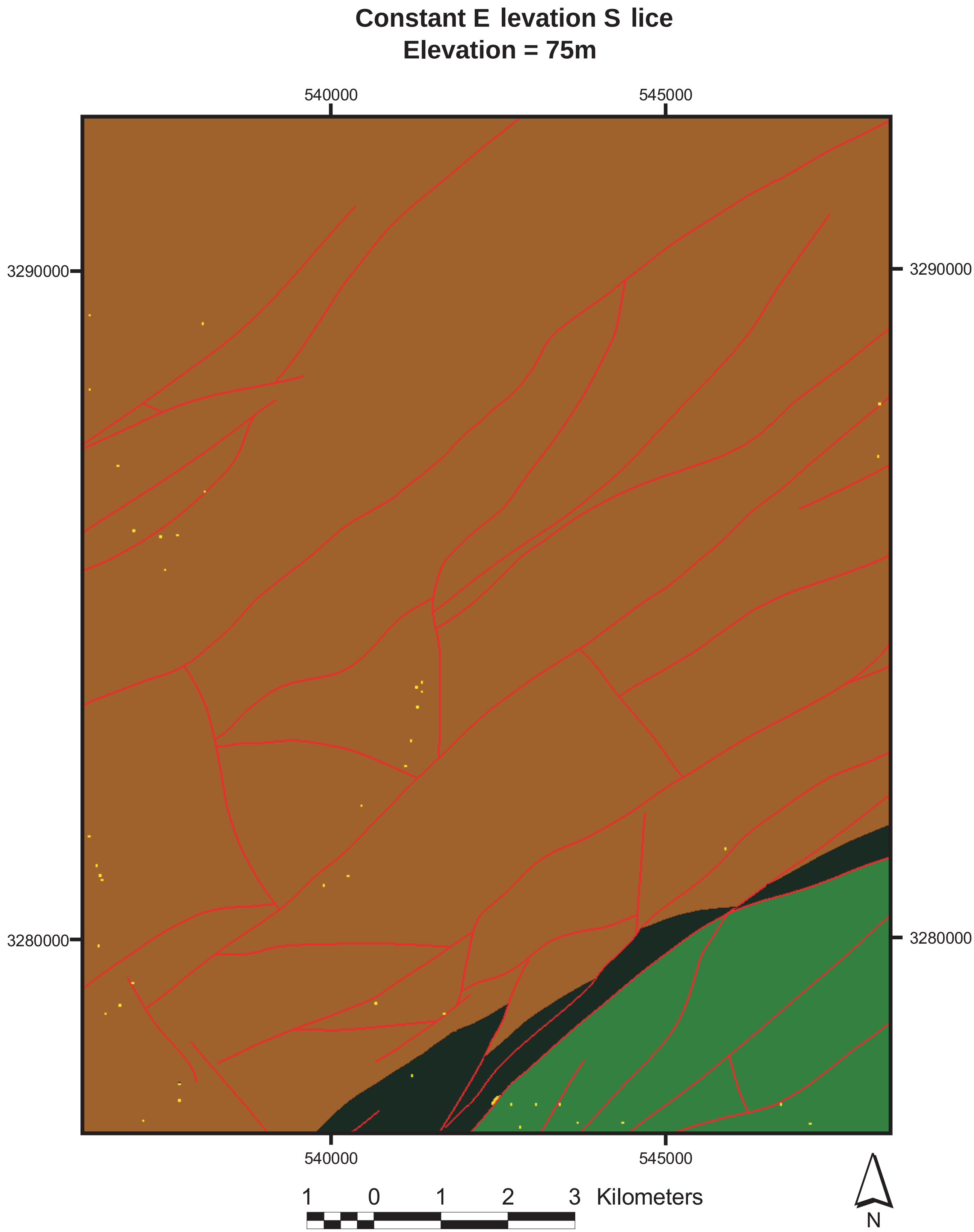

Figure 3-34. Map view of constant elevation (horizontal) slice through model. Elevation = 75 m. Units are UTM meters, NAD27. Red lines show fault traces, and yellow points show well locations. See Figure 3-1 for complete color key.

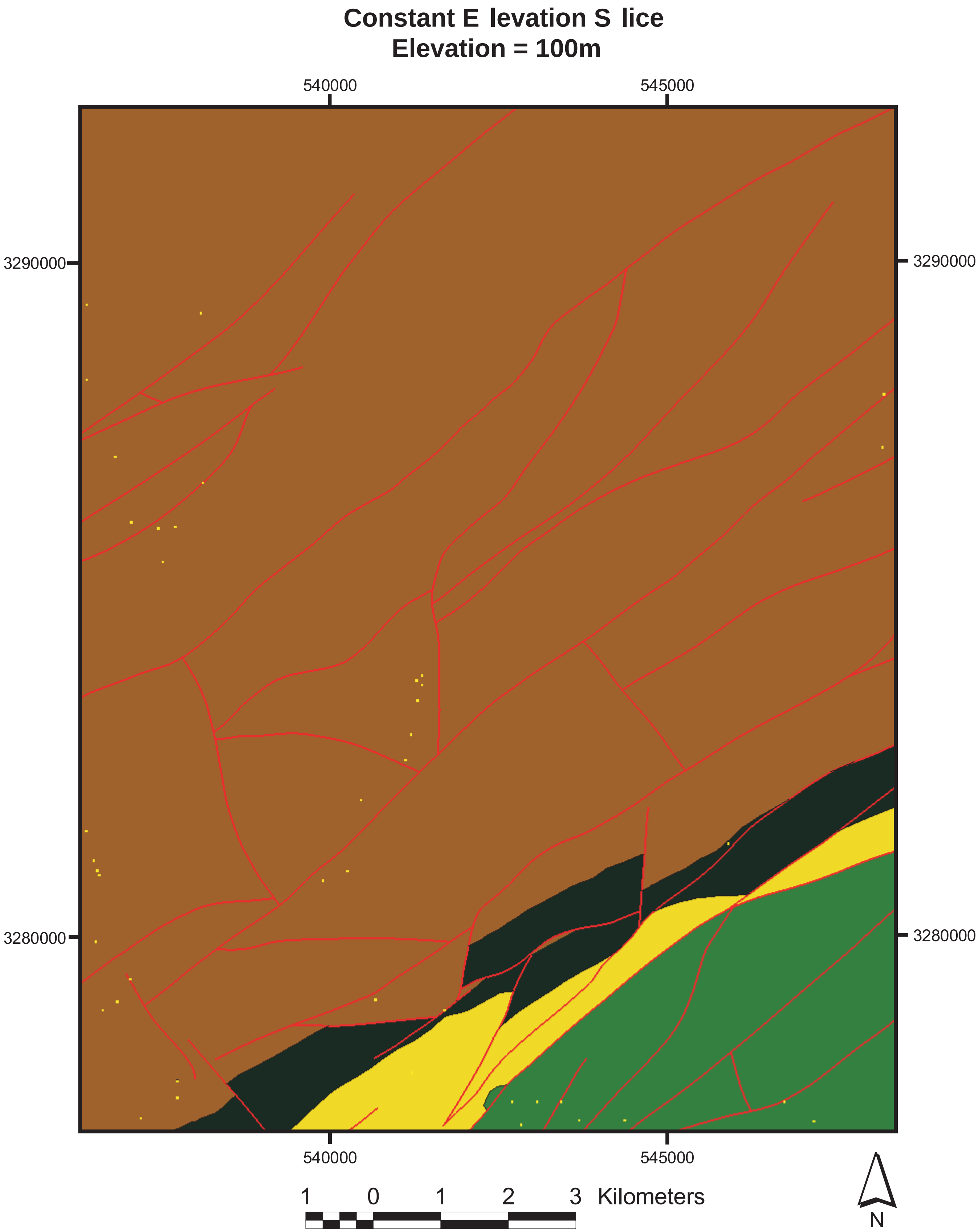

Figure 3-35. Map view of constant elevation (horizontal) slice through model. Elevation = 100 m. Units are UTM meters, NAD27. Red lines show fault traces, and yellow points show well locations. See Figure 3-1 for complete color key.

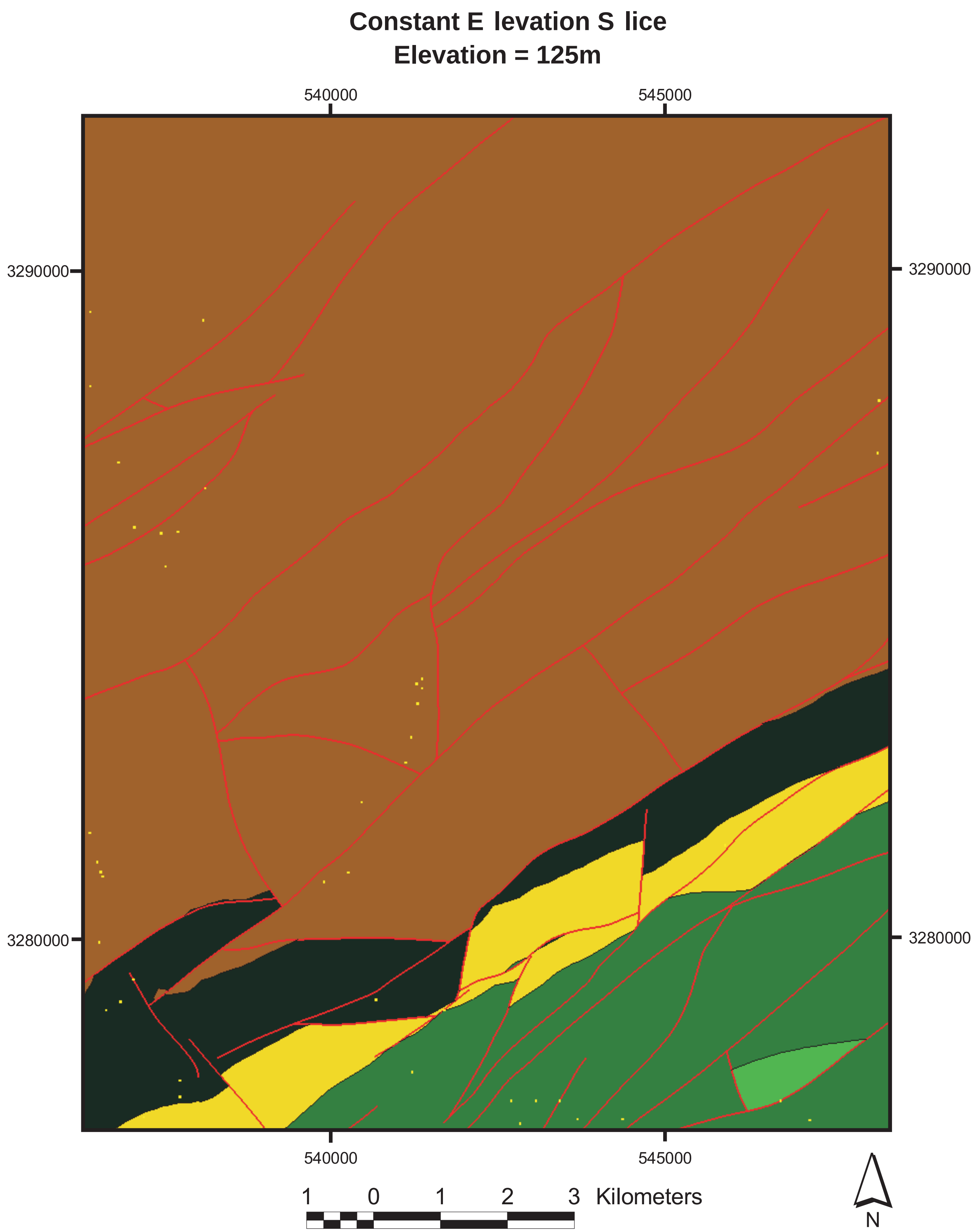

Figure 3-36. Map view of constant elevation (horizontal) slice through model. Elevation = 125 m. Units are UTM meters, NAD27. Red lines show fault traces, and yellow points show well locations. See Figure 3-1 for complete color key.

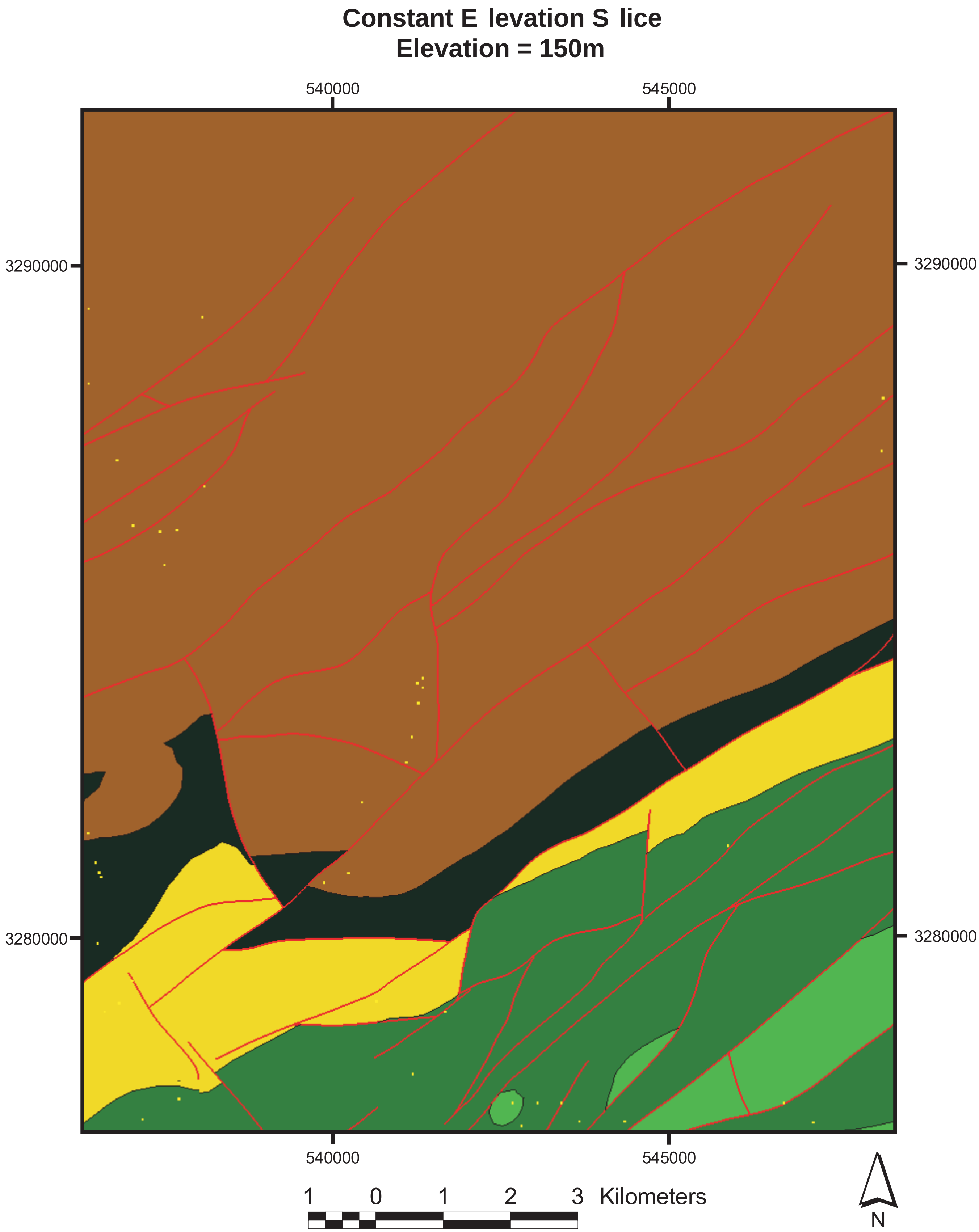

Figure 3-37. Map view of constant elevation (horizontal) slice through model. Elevation = 150 m. Units are UTM meters, NAD27. Red lines show fault traces, and yellow points show well locations. See Figure 3-1 for complete color key.

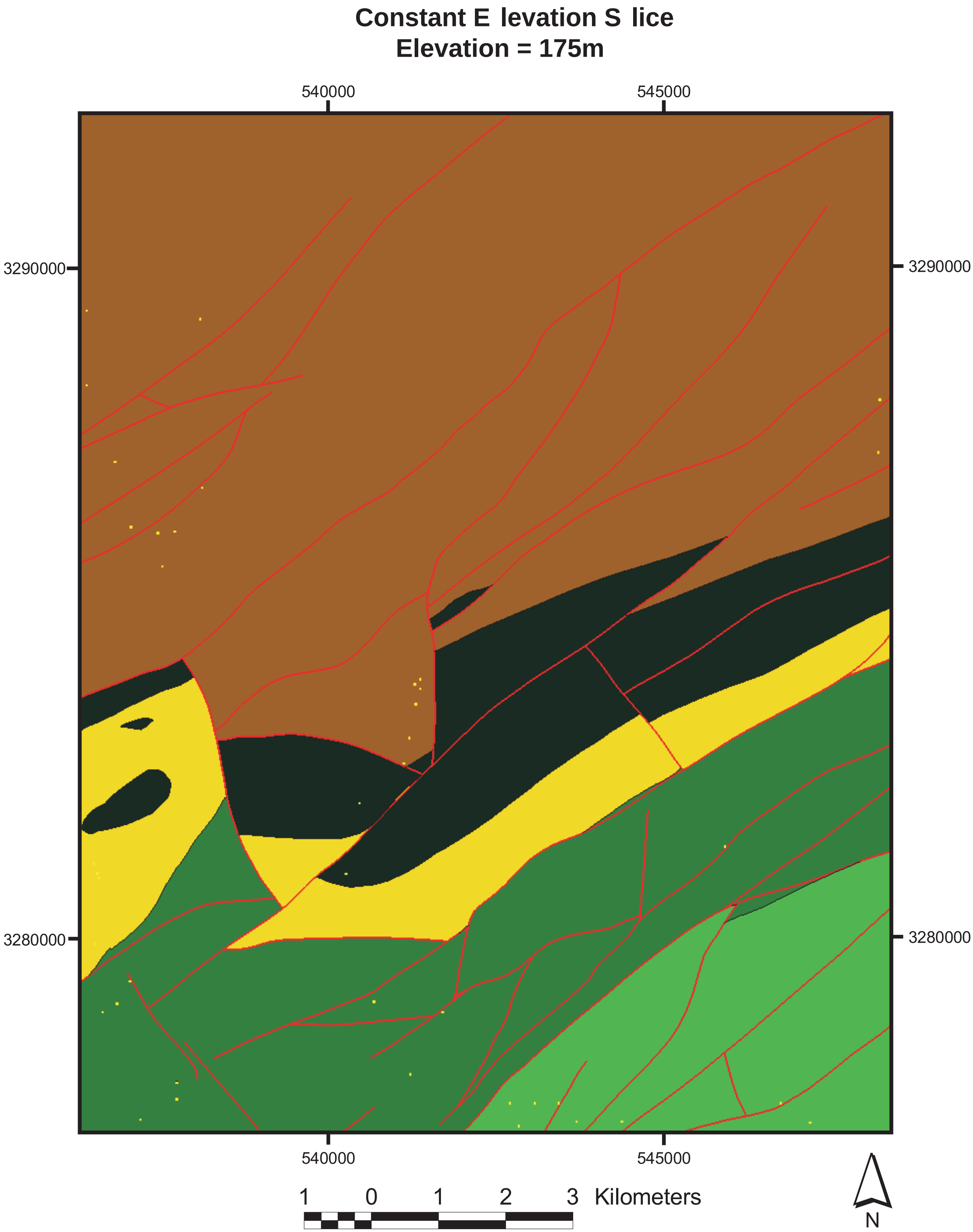

Figure 3-38. Map view of constant elevation (horizontal) slice through model. Elevation = 175 m. Units are UTM meters, NAD27. Red lines show fault traces, and yellow points show well locations. See Figure 3-1 for complete color key.

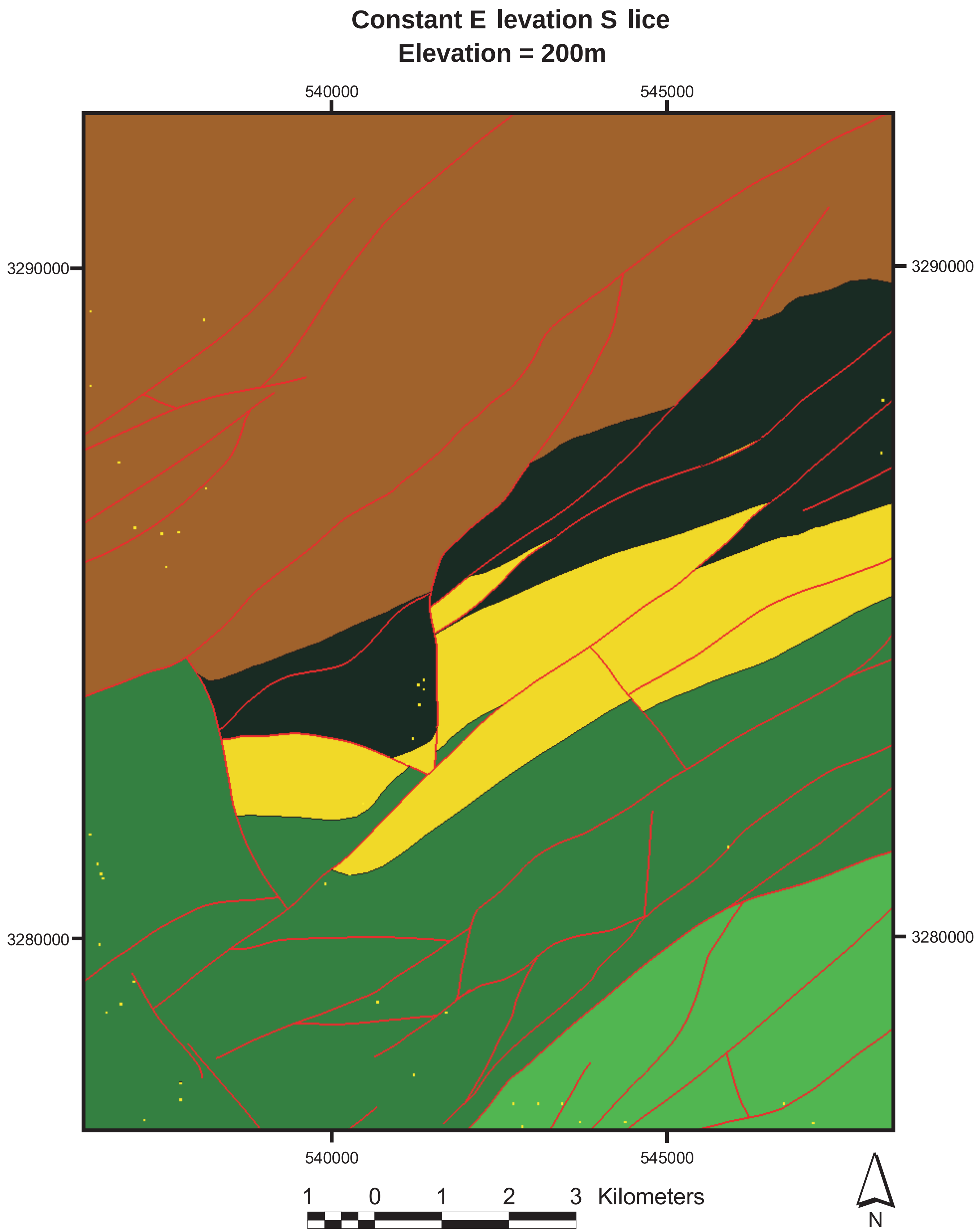

Figure 3-39. Map view of constant elevation (horizontal) slice through model. Elevation = 200 m. Units are UTM meters, NAD27. Red lines show fault traces, and yellow points show well locations. See Figure 3-1 for complete color key.

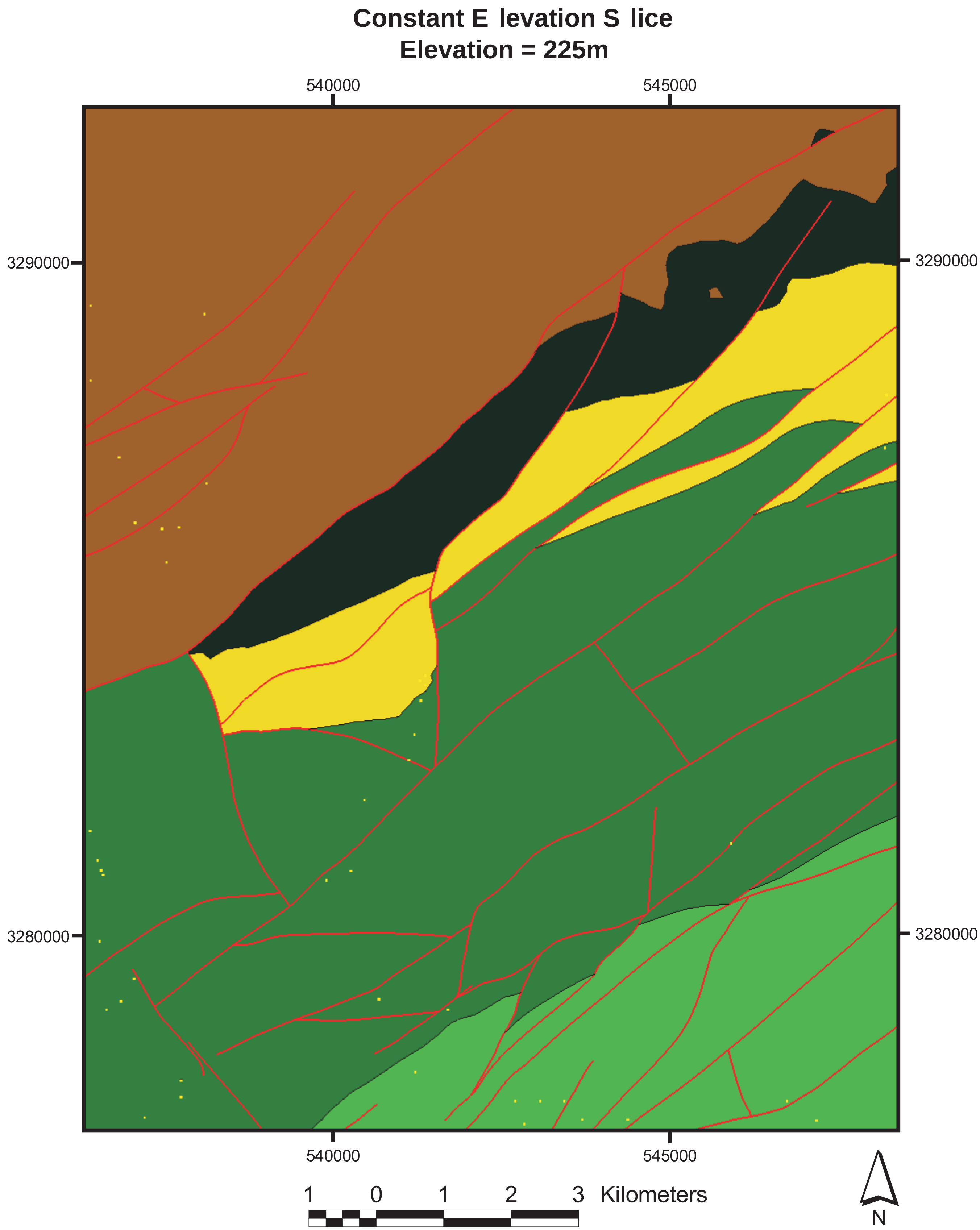

Figure 3-40. Map view of constant elevation (horizontal) slice through model. Elevation = 225 m. Units are UTM meters, NAD27. Red lines show fault traces, and yellow points show well locations. See Figure 3-1 for complete color key.

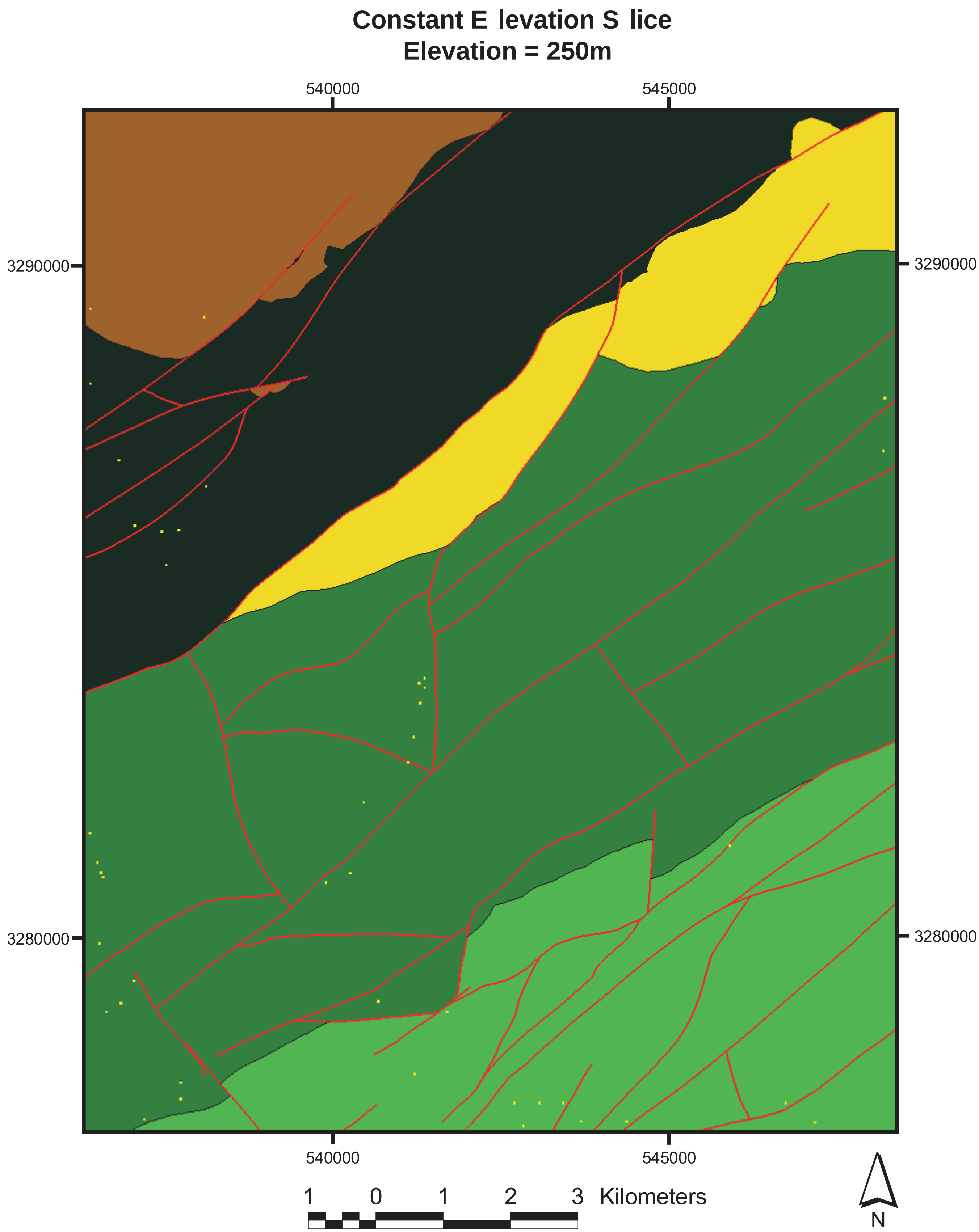

Figure 3-41. Map view of constant elevation (horizontal) slice through model. Elevation = 250 m. Units are UTM meters, NAD27. Red lines show fault traces, and yellow points show well locations. See Figure 3-1 for complete color key.

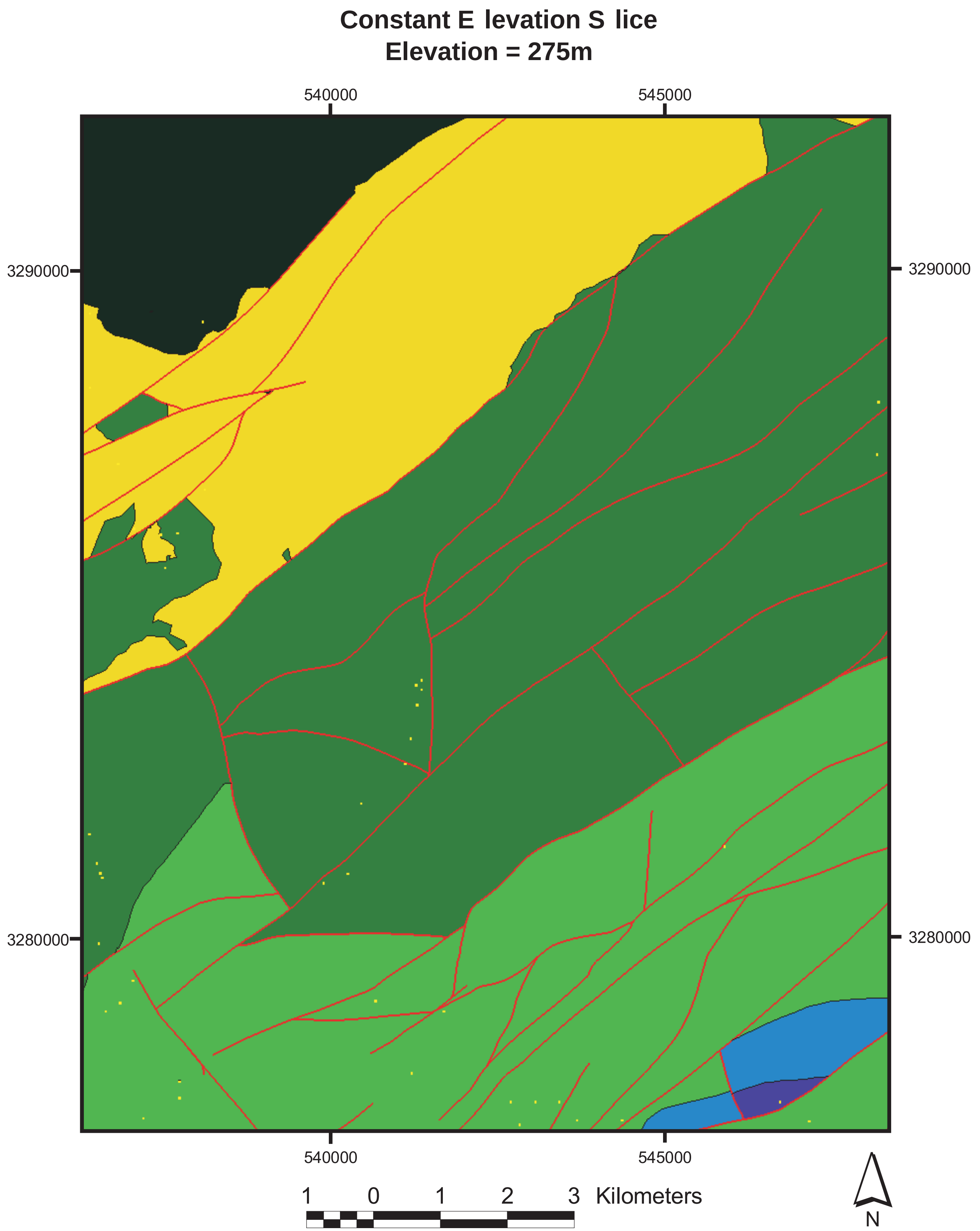

Figure 3-42. Map view of constant elevation (horizontal) slice through model. Elevation = 275 m. Units are UTM meters, NAD27. Red lines show fault traces, and yellow points show well locations. See Figure 3-1 for complete color key.

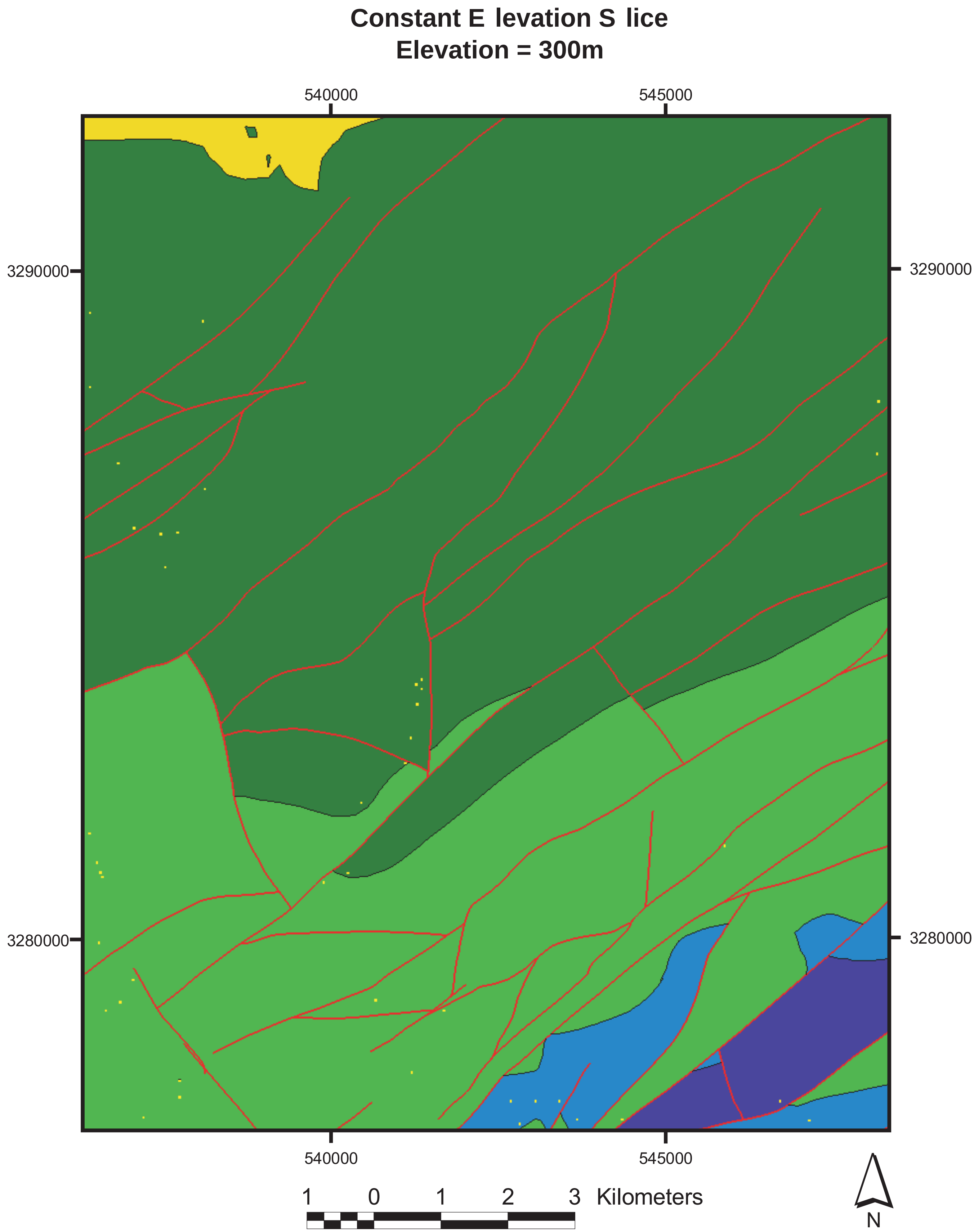

Figure 3-43. Map view of constant elevation (horizontal) slice through model. Elevation = 300 m. Units are UTM meters, NAD27. Red lines show fault traces, and yellow points show well locations. See Figure 3-1 for complete color key.

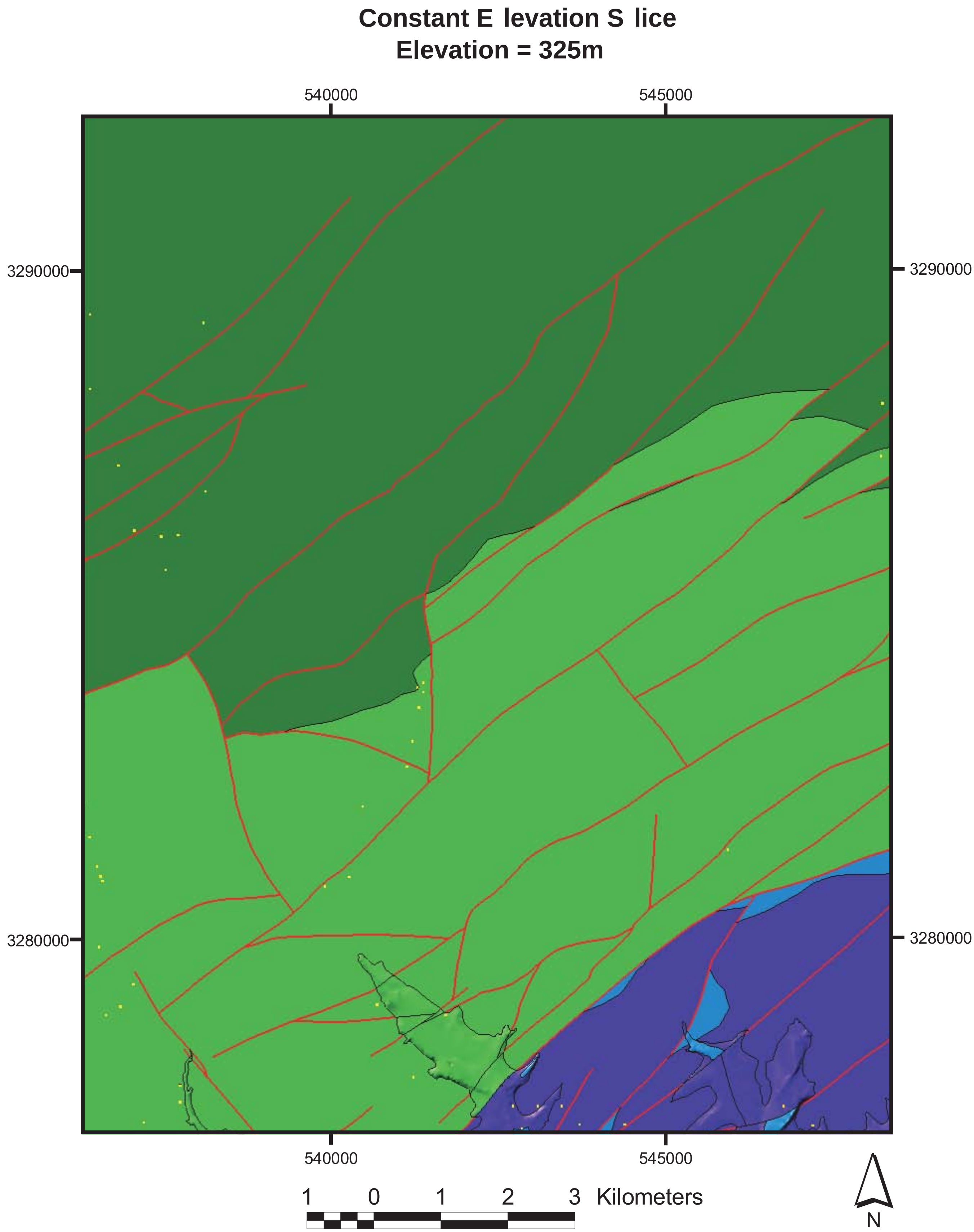

Figure 3-44. Map view of constant elevation (horizontal) slice through model. Elevation = 325 m. Units are UTM meters, NAD27. Red lines show fault traces, and yellow points show well locations. See Figure 3-1 for complete color key.

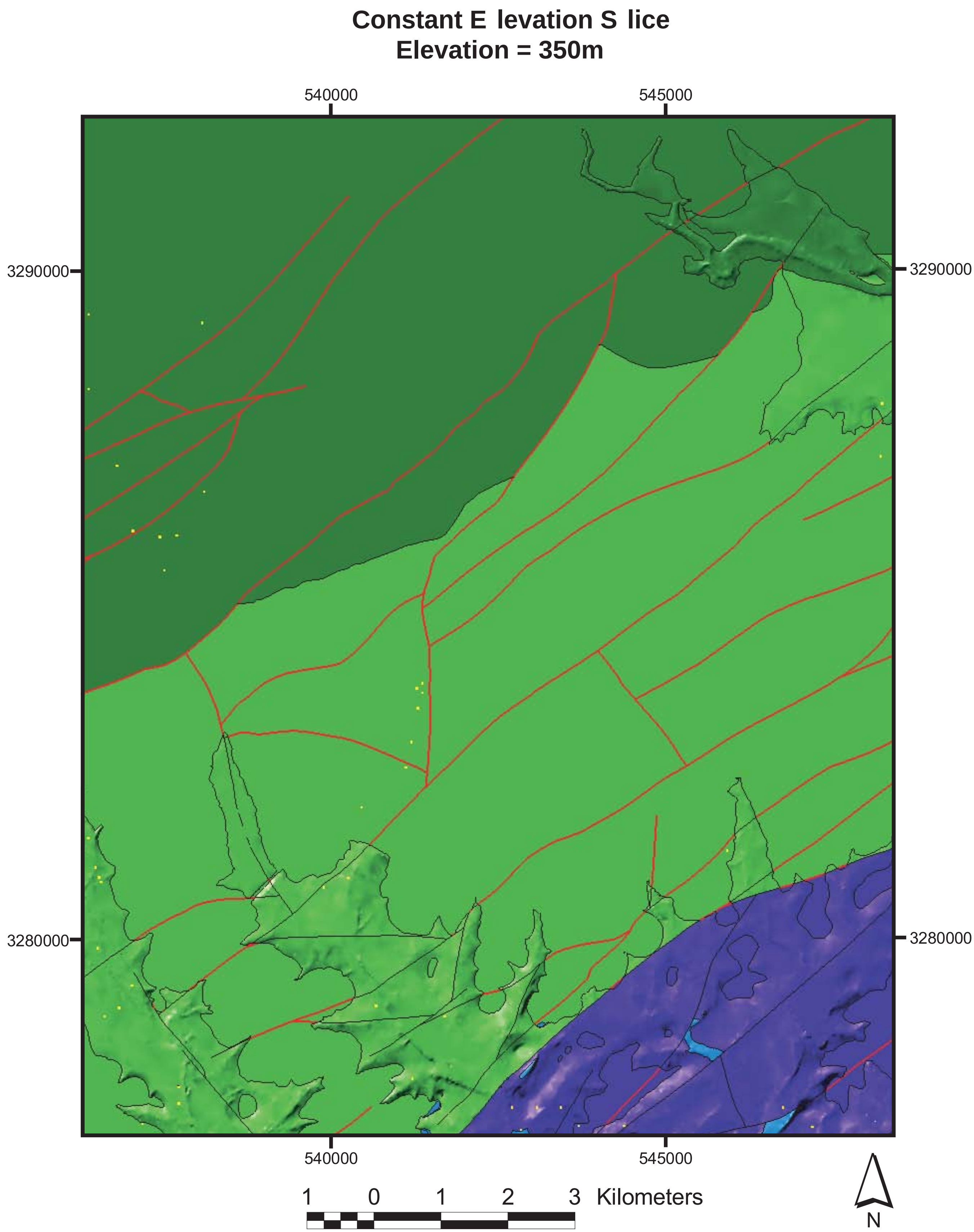

Figure 3-45. Map view of constant elevation (horizontal) slice through model. Elevation = 350 m. Units are UTM meters, NAD27. Red lines show fault traces, and yellow points show well locations. See Figure 3-1 for complete color key.

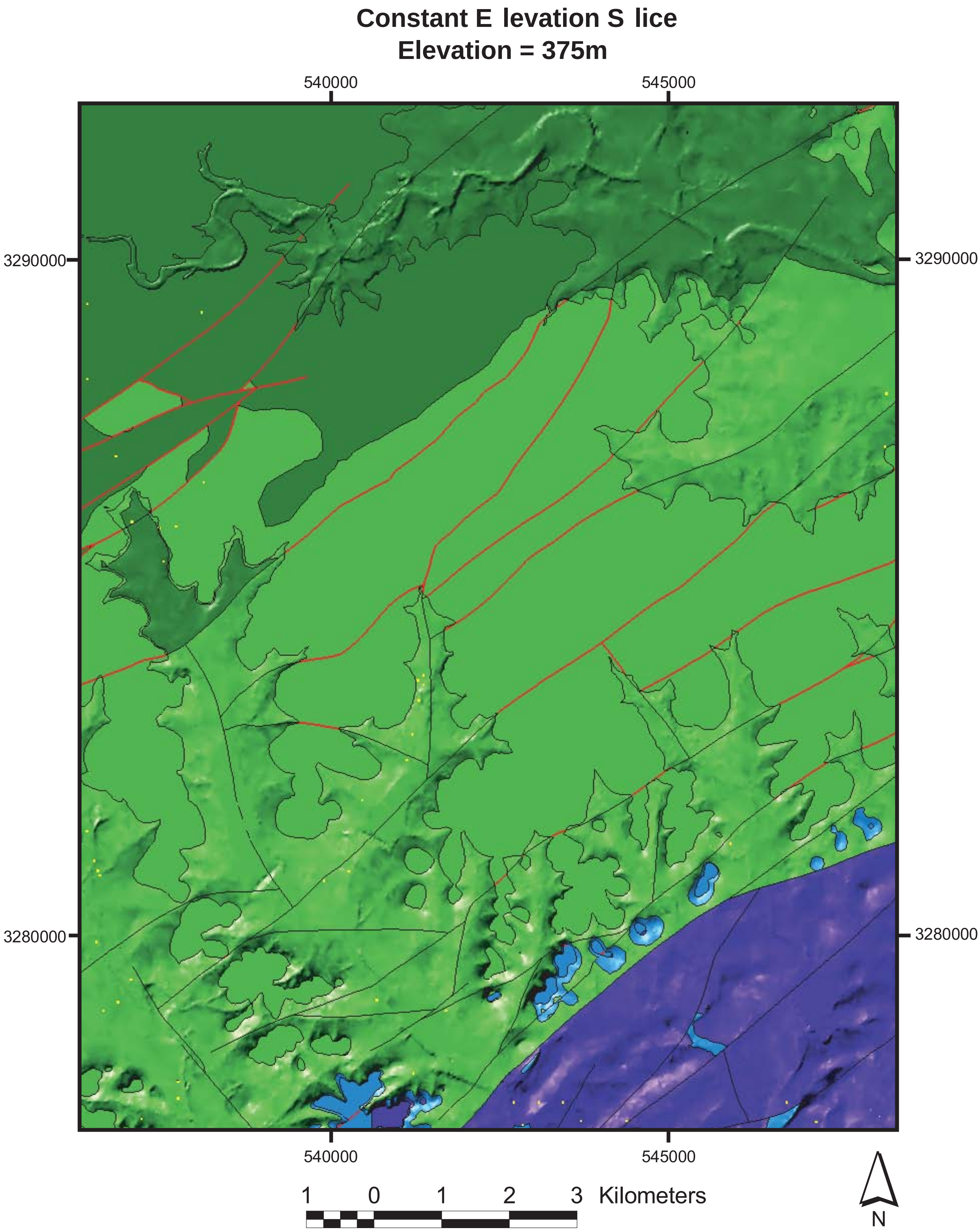

Figure 3-46. Map view of constant elevation (horizontal) slice through model. Elevation = 375 m. Units are UTM meters, NAD27. Red lines show fault traces, and yellow points show well locations. See Figure 3-1 for complete color key.

4 FAULT SYSTEM ARCHITECTURE

In the San Antonio region the Balcones Fault System changes trend by 30° from 080° west of San Antonio to 050° northeast of San Antonio. In contrast, individual fault strikes are relatively consistent through the region with an average strike of about 055° (Figure 4-1; Ferrill et al., 2003a). The pattern of faulting in the Balcones Fault System is compatible with having formed in a relatively uniform normal faulting stress field, controlled by vertical maximum principal compressive stress, and horizontal minimum principal compressive stress in the direction 145° (Figure 4-1). Slip tendency is the ratio of resolved shear stress to resolved normal stress on a surface (Morris et al., 1996). At the time of sliding, slip tendency exceeds the frictional resistance to sliding on a fault surface. Slip tendency analysis of the Balcones Fault System indicates that most of the major faults have orientations compatible with southeasterly directed extension (see rose diagram in Figure 4-1; details of analysis are described in Ferrill et al., 2003a). Thus the difference between individual fault strikes the trend of the fault system reflects an *en echelon* fault system. In the early stages of the development of *en echelon* normal fault systems, fault block connectivity tends to remain high, and fault connectivity remains low. With progressive extension, faults link by intersection of curved fault tips or the formation of connecting faults and fault block connectivity declines as fault connectivity increases (Ferrill et al., 1999a; Ferrill and Morris, 2001).

Northeast and west of San Antonio, a large portion of the displacement associated with the Balcones Fault System is along one primary fault surface or a narrow fault zone associated with the Balcones Escarpment. Through the San Antonio segment, no single fault dominates the displacement of the fault system. Instead, displacement is distributed across a 12 km wide system of faults. Collins and Hovorka (1997) noted this fault displacement pattern, and that the San Antonio area represents a stepover between two large-displacement faults, resulting in a broad displacement transfer system or relay ramp (Collins and Hovorka, 1997). The detailed investigation of the Camp Bullis quadrangle study area is on the northern margin of this zone of distributed faulting. Faults in this area have relatively small displacements compared with the total displacement across the Balcones Fault System.

Our analysis uses a combination of field data and results from the geologic framework modeling to characterize fault system architecture. The predominant stratigraphic units that crop out in this area are the Glen Rose Formation with isolated outcrops of younger Edwards Group rocks (Collins, 2000). Rocks of the Glen Rose Formation are not well exposed within the study area and in order to fully characterize the nature of faulting in this formation we extended the field analysis to adjacent areas where these lithologies can be studied in surface exposures. The following sites were identified for possible detailed investigation (Figure 1-3): (i) Recently exhumed bedrock pavements in the Canyon Lake Spillway, (ii) roadcuts along Highway 281 in the vicinity of the Route 46 intersection and a new exposure on the property of H.L. Chapman Pipeline Construction, Inc. adjacent to Highway 281, (iii) a roadcut exposure along Route 46 west of Highway 281, and (iv) FM 3351 (Ralph Fair Road) along the west side of Camp Stanley. These exposures include faults with displacements ranging from <1 m (3 ft) to tens of meters in the Upper and Lower Glen Rose Formations. The most spectacular exposure is in the spillway of Canyon Lake where bedrock of the Upper Glen Rose Formation was exhumed by flooding in July 2002. One fault in the spillway exposure has displacement of at least tens of meters and is exposed laterally for a distance of >500 m (1640 ft). This fault zone both discharges and recharges groundwater along its exposed length and is an excellent example for detailed investigation of fault zone characteristics and relevance for groundwater movement. Several other faults with smaller displacements (<1 m (3 ft)) are exposed for tens of meters along strike in the spillway. In several places these faults have evidence of dissolution and precipitation of calcite associated with the fault zone. At several locations, these small-displacement faults were flowing water.

Project staff conducted field work to study fault orientations, fault zone materials and deformation mechanisms in road cut exposures along FM 3351 (Ralph Fair Road), State Route 46, Highway 281, and a new exposure on the property of H.L. Chapman Pipeline Construction, Inc. adjacent to Highway 281. Staff also conducted field work in the Canyon Lake Spillway gorge to analyze fault-related deformation and associated springs and recharge features in the Upper Glen Rose limestone.

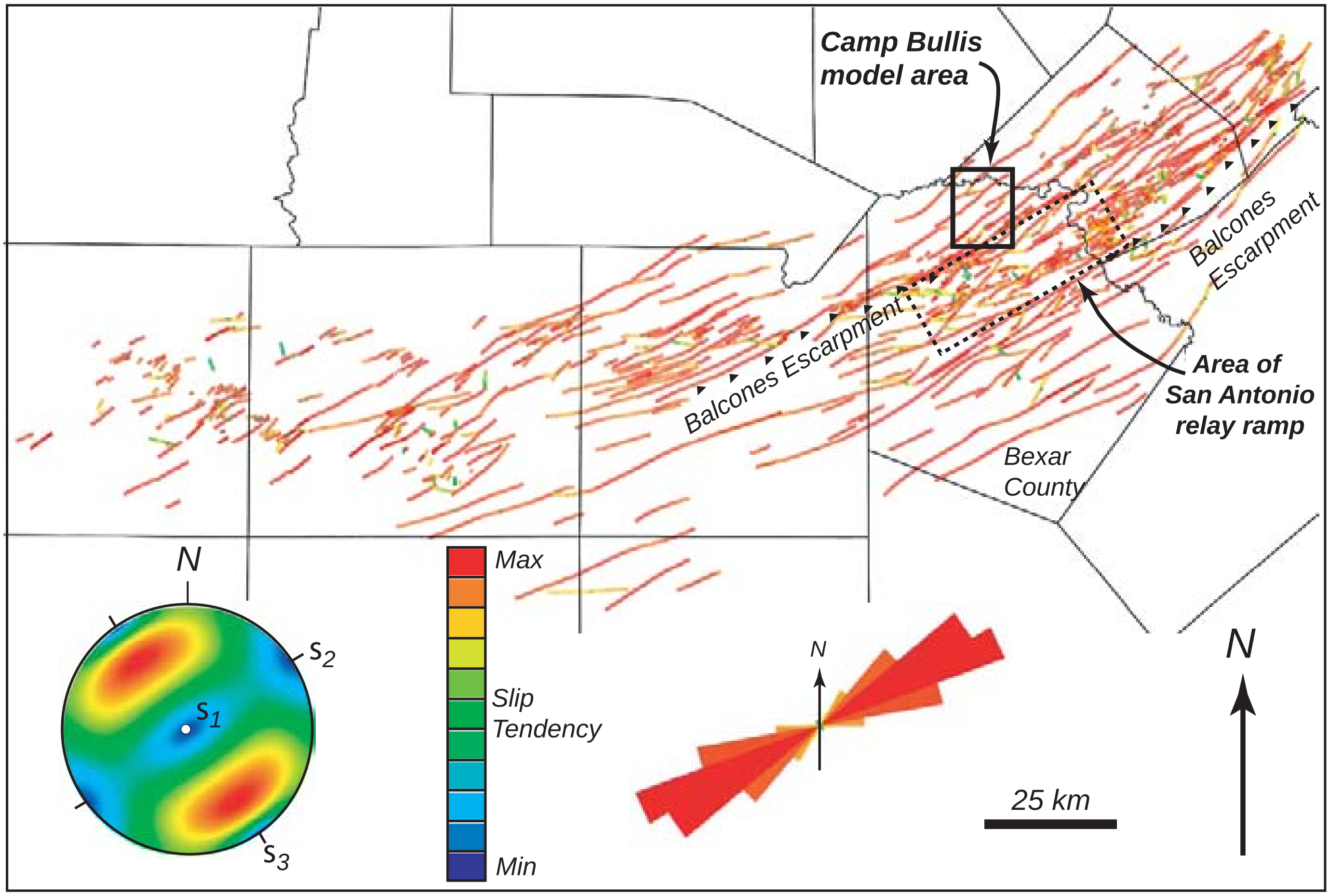

Figure 4-1. Map of the Balcones fault system in the San Antonio area with fault traces colored according to their slip tendencies. Slip tendency analysis was performed using 3DStress™ v. 1.3.2 (see Ferrill et al., 2003a) based on mapped faults of Collins and Hovorka (1994).

4.1 Fault Juxtaposition of Stratigraphy

Faulting can juxtapose layers of different permeability characteristics. Displacement gradients on faults can produce complicated juxtaposition relationships so that originally continuous layers are partially or completely separated across faults, and layers that were originally vertically separated from one another can be juxtaposed by fault displacement. This means that with increasing fault displacement, original hydraulic communication pathways are diminished or broken and new pathways may be formed. Simple geometric juxtaposition analysis as described by Allan (1989) assumes that the fault zone has no particular properties that cause it to differ from unfaulted host rock. Maclay and Small (1983; also Maclay, 1989) used a similar approach to analyze juxtaposition of permeable zones and relatively impermeable zones in the Edwards Aquifer and coined the term "barrier fault" for faults across which hydraulic connection is partially or completely lost due to fault displacement (aquifer thinning). The effects of faulting of the Trinity and Edwards Aquifers' stratigraphic section are illustrated in Figure 4-2.

Viewing the Upper Glen Rose Formation model layer in 3-dimensions reveals that fault displacements within the area of this study are too small to place the base of the Edwards Aquifer (basal nodular layer) against the permeable Lower Glen Rose Formation layer (Figure 4-3). Note that each fault thins the strata that are cut by the fault, causing thinning of both aquifer and aquitard layers. Structural thinning of aquifer layers can cause flow constrictions, and areas of such flow constrictions can be identified using a map of fault throw (vertical component of fault displacement) distribution as described in the next section.

4.2 Fault Throw Distribution

The vertical component of displacement (throw) on faults in both the Camp Bullis (based on the model discussed in Section 3) and the Castle Hills study areas (Ferrill et al., 2003a) was measured using the fault gaps on top of the Lower Glen Rose Formation model layer in the Camp Bullis area and the top of the Upper Glen Rose Formation in the Castle Hills area. Throw values range from 0 m at fault tips to approximately 110 m (361 ft) at the point of maximum throw in the Camp Bullis area and up to 127 m (417 ft) in the Castle Hills area (Figure 4-4).

In the Castle Hills area several faults offset the Kainer-Walnut layer (Edwards Aquifer) by distances equal to or greater than its full thickness (Figures 4-2 and 4-4). Consequently, these faults locally thin the aquifer by 67%. The effect of this faulting is to constrict flow paths by structural thinning of the aquifer, causing flow to be diverted and the local water table to fluctuate from fault block to fault block. In addition, the full thickness of the Kainer in the fault hanging wall is juxtaposed against the Upper Glen Rose Formation, and in one case the top of the Lower Glen Rose Formation, in the footwall. Smaller fault displacements in the Camp Bullis area and the northern part of the Castle Hills quadrangle reduce the amount of direct juxtaposition of Kainer against Lower Glen Rose Formation in these areas to a minimum (Figure 4-2).

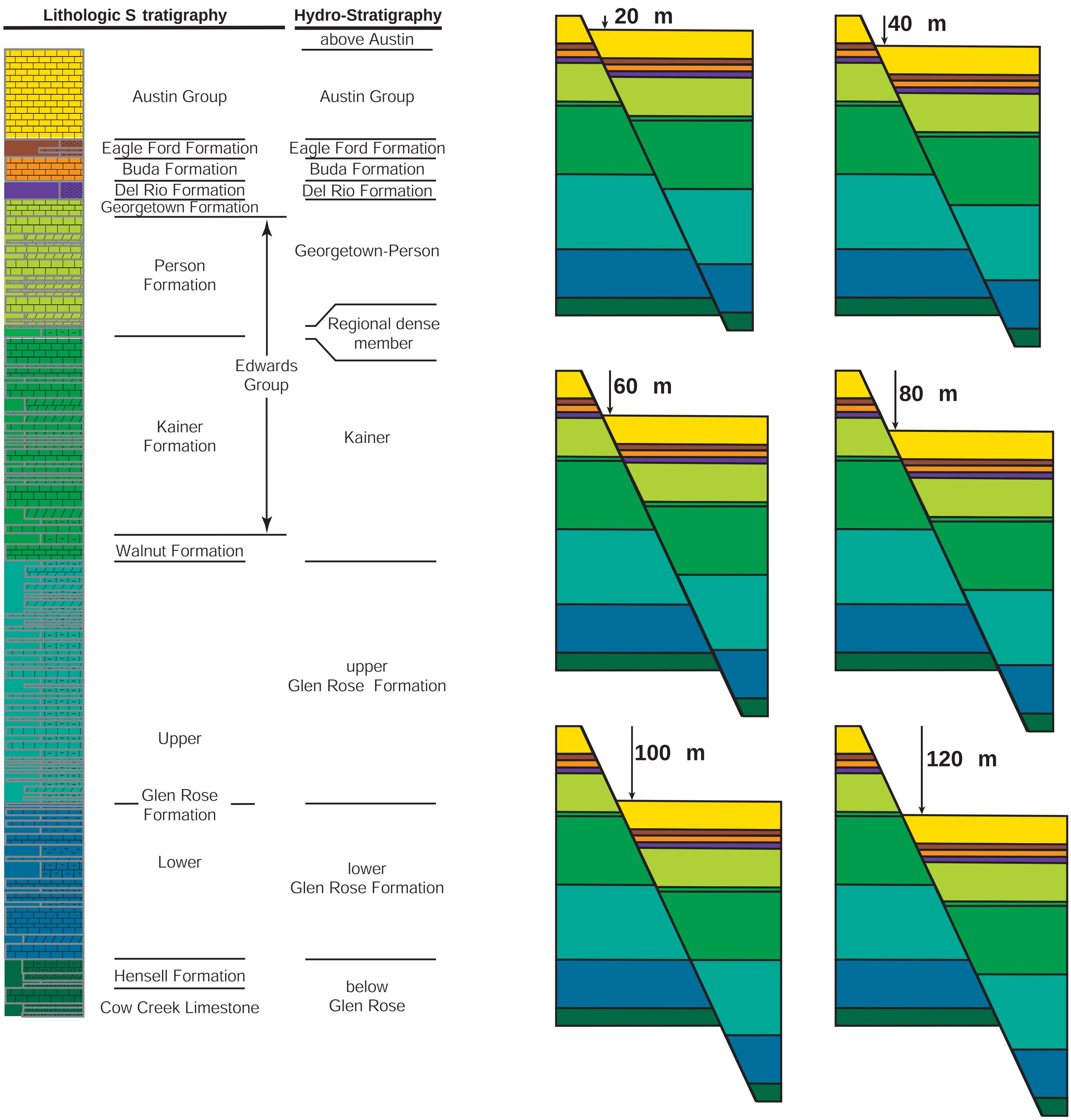

Figure 4-2. The effects of faulting on the Trinity and Edwards Aquifers. Different stratigraphic layers are juxtaposed across faults with different displacements; pattern of juxtaposition is related to the amount of displacement on the fault. Faults with 20 m (66 ft), 40 m (131 ft), 60 m (198 ft), 80 m (262 ft), 100 m (328 ft), and 120 m (394 ft) throw are illustrated. In this generalized model, a fault with 40 m (131 ft) of throw could juxtapose the Trinity Aquifer with the lower portion of the Edwards Aquifer. A fault with greater than 100 m (328 ft) of throw would juxtapose the Trinity Aquifer with the upper portion of the Edwards Aquifer.

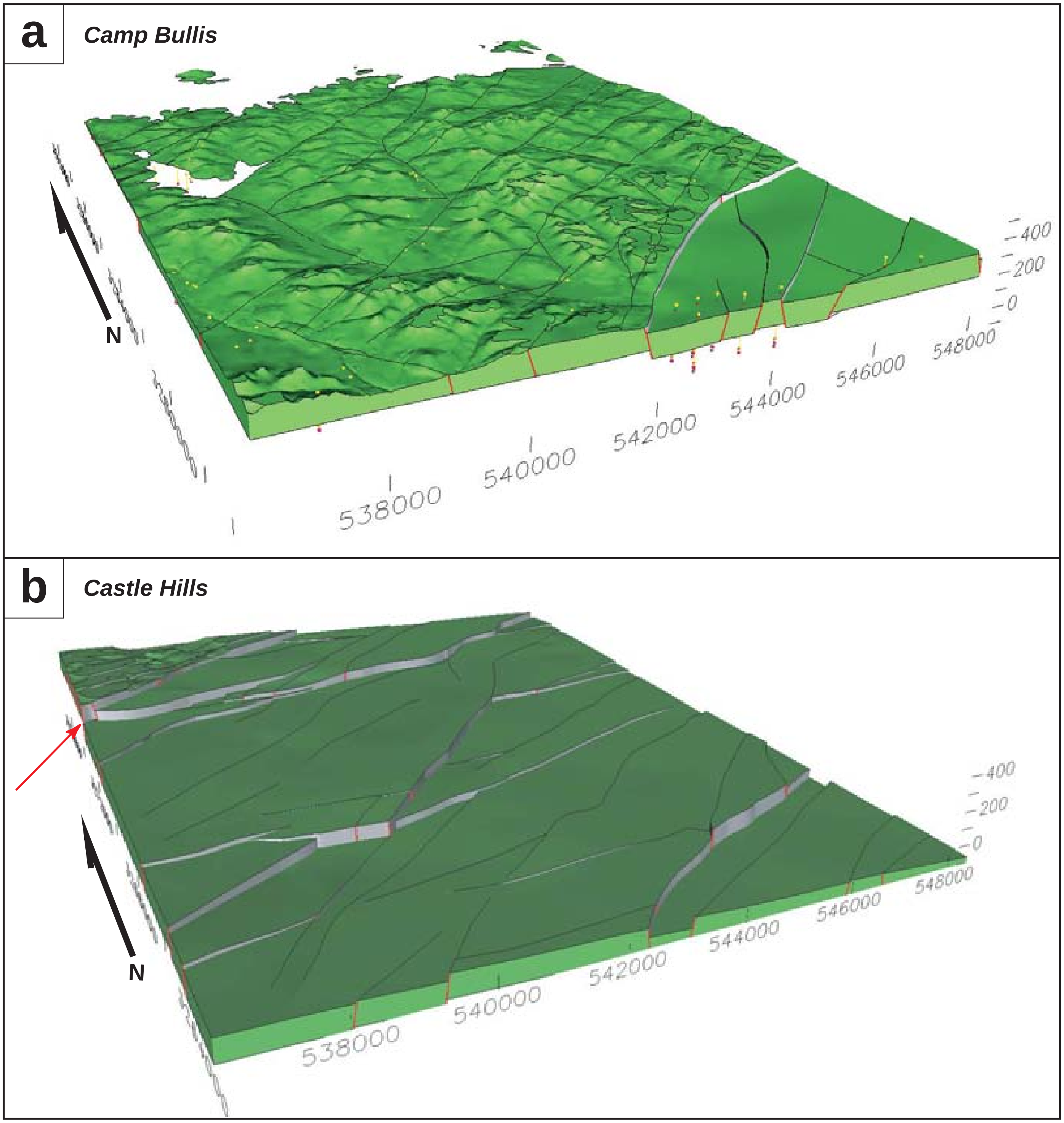

Figure 4-3. Oblique views of Upper Glen Rose Fm. model layer in (a) Camp Bullis geologic framework model, and (b) Castle Hills geologic framework model. Note that fault displacement is insufficient to completely offset Upper Glen Rose Fm. from itself except in one very localized area as indicated by the arrow in b. Therefore, the overlying Edwards Aquifer and underlying Middle Trinity Aquifer are not in fault juxtaposition in the Camp Bullis and Castle Hills (Ferrill et al., 2003a) study areas except near the NW corner of the Castle Hills quadrangle.

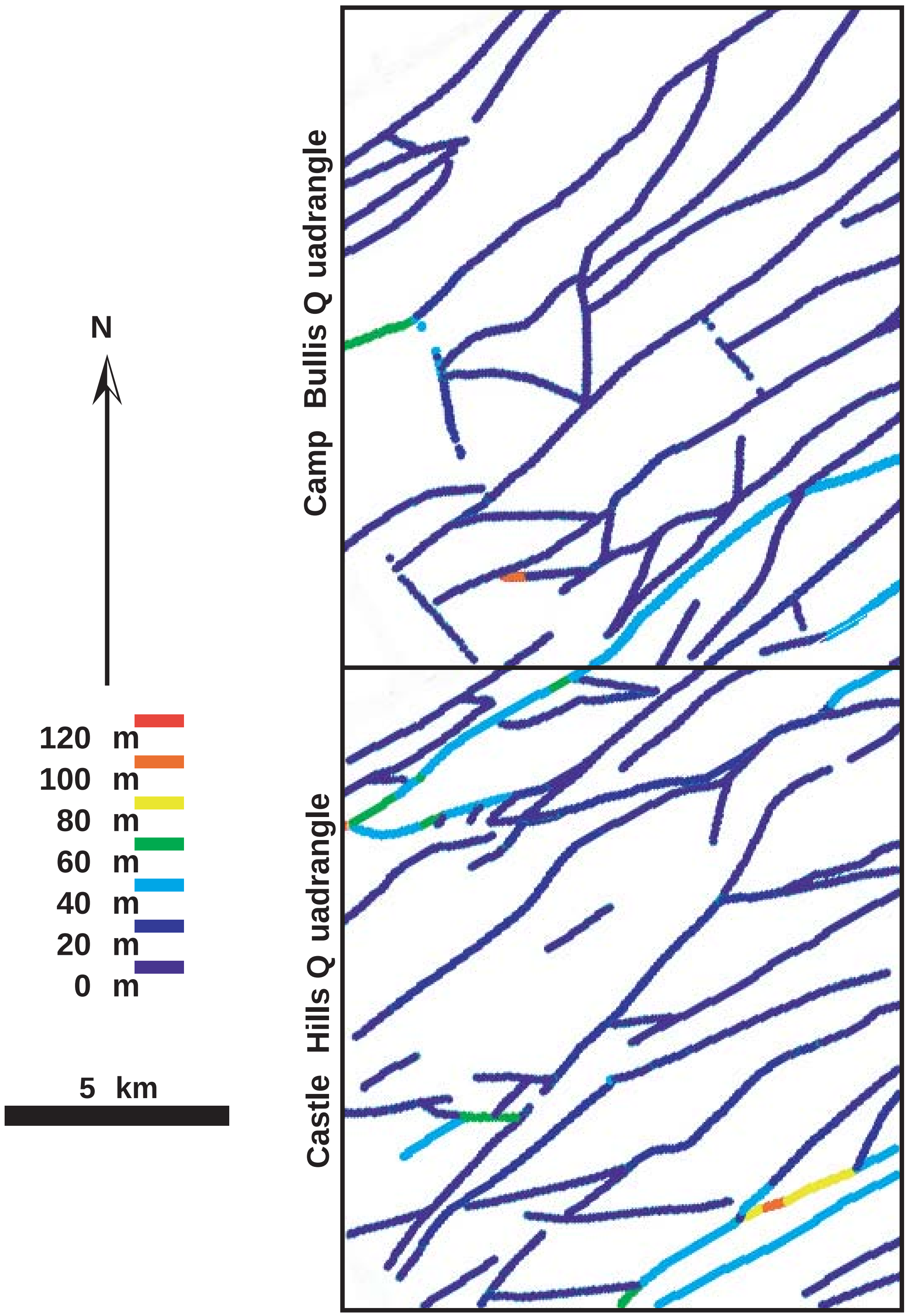

Figure 4-4. Throw map at the top of the Lower Glen Rose Fm. in the Camp Bullis study area (see Section 3) combined with the throw map at the top of the Upper Glen Rose Fm. in the Castle Hills quadrangle (after Ferrill et al., 2003a).

4.3 3DStress^{TM} Analysis

Slip tendency analysis (e.g., Morris et al., 1996; Ferrill et al., 1999b) of the Camp Bullis Quadrangle fault system is based upon two principal assumptions and field observations of faults exposed in the Glen Rose Formation in the vicinity of the study area. First, we assume that the rocks of the Glen Rose Formation were deformed during the middle to late Tertiary (Murray, 1961; Young, 1972) beneath an overburden that included the younger Cretaceous rocks of the region and the middle to lower Tertiary formations. The total overburden thickness was likely of the order of 0.9 km (0.3 mile) (e.g., Collins, 2000). Second, the rock column above the Glen Rose Formation was essentially water-saturated at the time of deformation. Approximate magnitudes of the principal stresses can be obtained from these assumptions. Normal faults predominate those observed in the field in this study and by other workers throughout the Balcones Fault zone, therefore the vertical stress at the time of faulting would have been the maximum principal effective stress (σ_1'). Using the assumptions of overburden thickness and rock column saturation (above), σ_1'would have been equal to the lithostatic stress (here based on an average rock density of 2.7 gm/cm^3) minus the hydrostatic pore water pressure, yielding a vertical effective stress of 15 MPa. In order for faulting to have occurred, the differential stress must have been sufficient to generate a maximum slip tendency of about 0.7 (Morris et al., 1996). We estimate the minimum horizontal effective stress (σ_3') to have been 4 MPa. Field observations of slickenlines indicate that rakes of slip vectors were steep (Table 4-1), in other words, faults of almost all strikes experienced near dip-slip displacement. In order to accomplish this we chose a σ_2' value of 9.5 MPa. Azimuths of the two principal horizontal stresses were established by visually fitting the slip tendency data to poles to measured fault surfaces (Figures 4-5 and 4-6a) in the Glen Rose Formation in and around the study area. This analysis yields an extension azimuth of 150° (Figure 4-6).

Applying this inferred stress system to the fault surfaces exported from the three-dimensional model (Figure 4-7) indicates that the large, ENE-WSW striking faults were favorably oriented to have accommodated regional strains by normal fault movement. A few NW-SE trending faults experience low slip tendencies and probably formed in response to local stress perturbations. The fault system within the Camp Bullis study area is dominated by faults that are consistent with the regional trend of the Balcones Fault zone, and these faults probably formed in response to the stress tensor inferred from the 3DStress™ analysis. Faults with anomalous orientations (i.e., NW-SE strikes) are rare at the scale of resolution of the three-dimensional model, indicating that local perturbations resulting from such effects as displacement-gradient-driven fault block deformation were not widely developed in this area. In addition to experiencing high slip tendencies in the inferred stress system, the predominant faults are also subject to high dilation tendencies (Figures 4-6b and 4-7b; Ferrill et al., 1999b). Dilation tendency is the likelihood that a fracture or fault will be open (dilate) and thus be more transmissive to fluid flow. This combination of high slip and dilation tendencies implies that the major faults would have been effective fluid transmission pathways, subject to the constraints of fault zone architecture, at the time of faulting (Finkbeiner et al., 1997; Ferrill et al., 1999b). If a similar stress system were extant today, the faults would be in favorable orientations for fluid transmissivity.

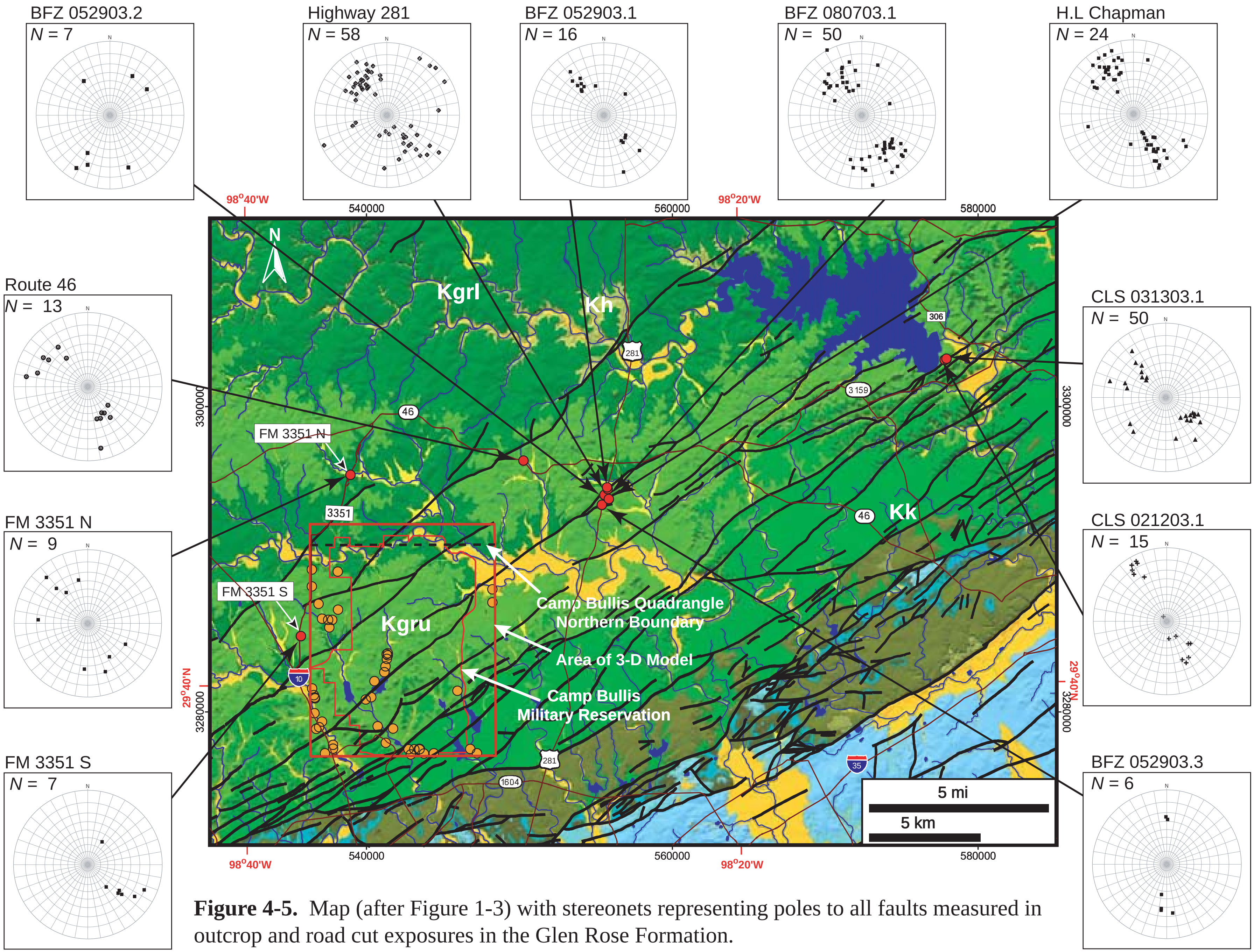

Figure 4-5. Map (after Figure 1-3) with stereonets representing poles to all faults measured in outcrop and road cut exposures in the Glen Rose Formation.

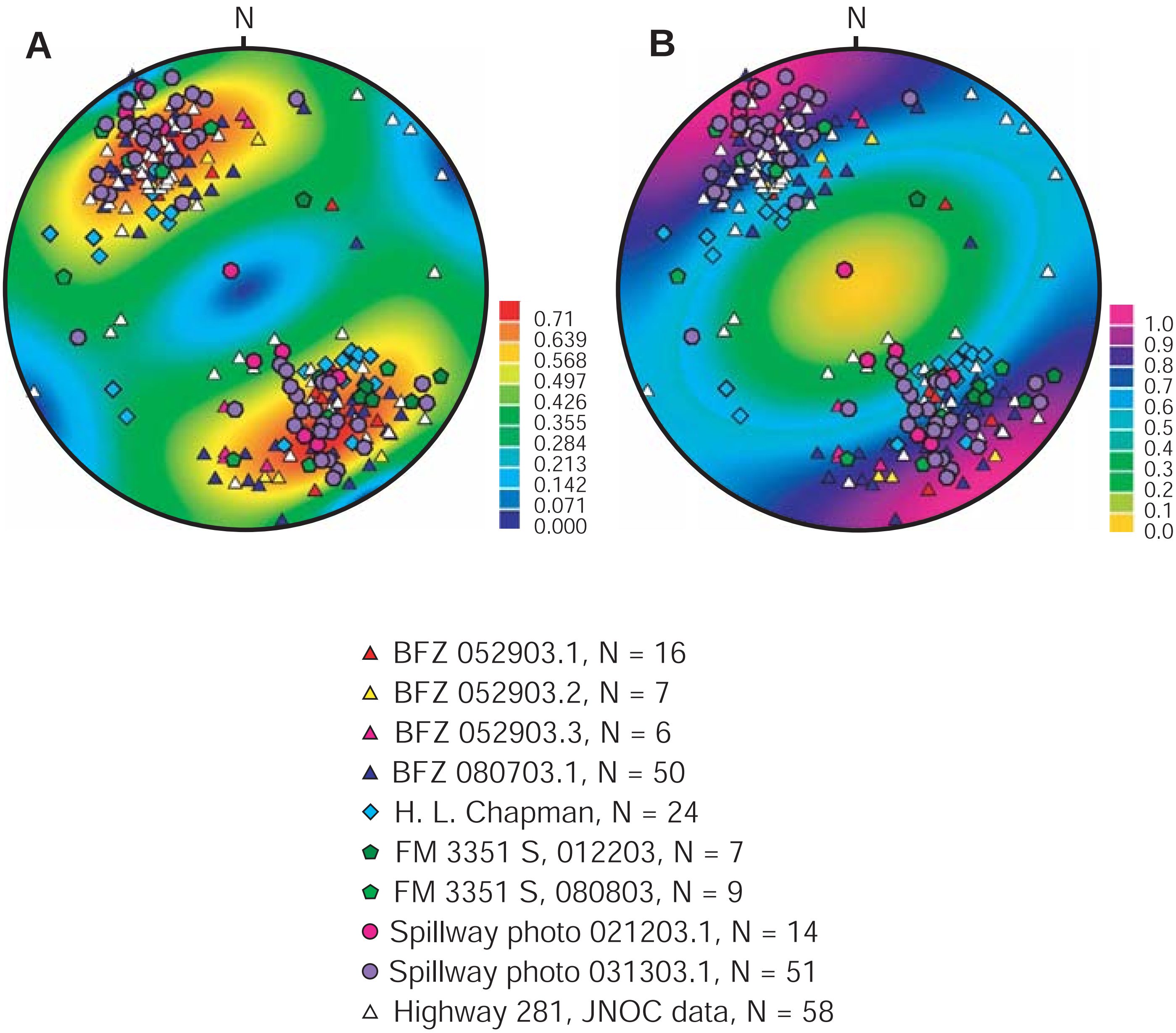

Figure 4-6. (a) Slip tendency plot and (b) dilation tendency plot with poles to all faults measured in the field with different colors and symbols for each field locality.

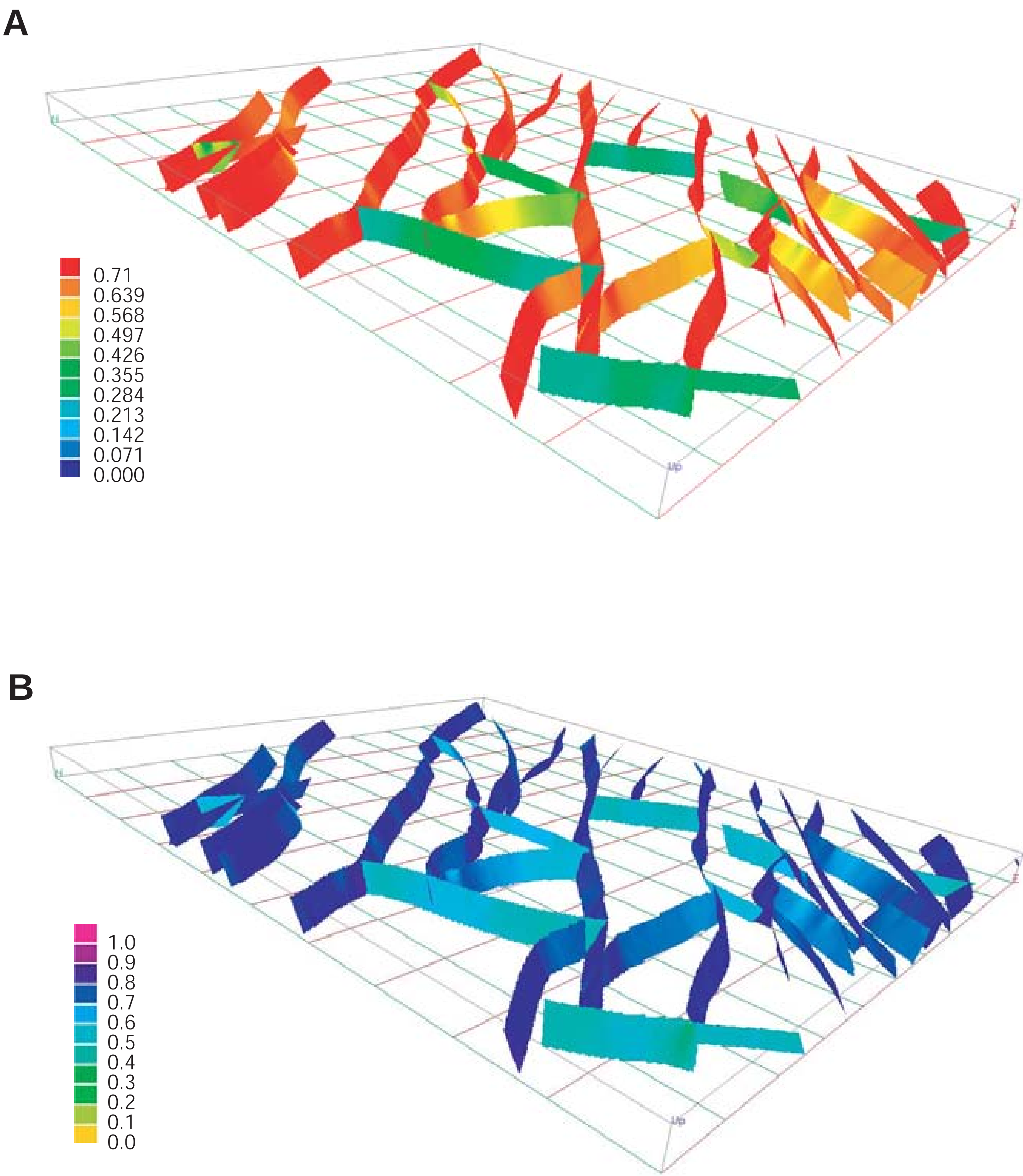

Figure 4-7. Three-dimensional fault surfaces from geologic framework model color coded according to (a) slip tendency and (b) dilation tendency (s_1 = 15 MPa, vertical; s_2 = 9.5 MPa, 60 ; s_3 = 4 MPa, 150).

Table 4-1. Field data

BFZ 052903.1 Faults measured in rock face bounding east side of Hwy. 281, north of San Antonio, Texas, approx. 1 mile S of Hwy. 46 exit
Collected 29 May 2003

GPS location	**N end of scanline**	**UTM zone 14 meters NAD 27**	
Easting	**555743 m**	**Orientation of scanline:**	
Northing	**3294572 m**	**379**	**azimuth**
Elevation	**1199 feet**		

Number	meters along tape	Strike	Dip	Slickenline rake	Displacement, cm	Comments
1	0.25	52	74		2	
2	5.4	225	70	90	10	well developed slickenlines
3	23.05	54	56	90	15	well developed slickenlines
4	30.9	236	47	90	12	well developed slickenlines, offsets fault 5
5	31.75	48	50	96	3	offset by fault 4
6	35.3	48	57	88	15	well developed slickenlines
7	40.25	136	45	82	5	well developed slickenlines
8	42.7	47	65	96	220	this fault correlates with fault near south end of exposure across 281
		47	48	101		well developed slickenlines on hw surface
						gentle synthetic dip panel between faults 8 and 11
9	48.6	74	45	98	6	
10	52.4	251	80	85	3	
11	53.6	57	62	86	310	this fault appears to correlate with the other fairly large fault at the S end of exposure across 281
12	71.1	235	50	76	12	well developed slickenlines
13	71.5	223	45	76	30	faults 12 and 13 merge upward into a single fault with > combined displacement of 12 + 13
14	87.4	55	51	87.5	20	well developed slickenlines and local patches (2x10xm) of fibrous to prismatic calcite
15	130.7	227	47	86	12	well developed slickenlines
	149					END OF EXPOSURE

BFZ 052903.2 Faults measured in rock face bounding west side of Hwy. 281, north of San Antonio, Texas, approx. 1.5 miles S of Hwy. 46 exit
Collected 29 May 2003

GPS location	**N end of scanline**	**UTM zone 14 meters NAD 27**	
Easting	**555538 m**	**Orientation of scanline:**	
Northing	**3294180 m**	**25**	**azimuth**
Elevation	**1263 feet**		

Number	meters along tape	Strike	Dip	Slickenline rake	Displacement, cm	Comments
1	49.7	260	72	85	25	Clean break in limestone, well developed slickenlines
						3 subhorizontal dissolution tubes are present along fault, tube diameters are 3cm to 10 cm
2	68.1	48	51	92	125	expansive footwall fault surface exposure, well developed slickenlines
3	60.15	231	81	92	15	well developed slickenlines, fault corrugated wavelengths of 10's cm to m, corrugations plunge in slip directi amplitudes 5 to 30 cm
4	77.15	264	71	80	8	well developed slickenlines
5	86	247	58	88	25	well developed slickenlines
6	115.3	74	51	88	30	small dissolution cavity along fault (elongate in horizontal direction)
7	122.15	95	56	90	20	
	177					END OF EXPOSURE

BFZ 052903.3 Faults measured in rock face bounding west side of Hwy. 281, north of San Antonio, Texas, approx. 1.75 miles S of Hwy. 46 exit
Collected 29 May 2003

GPS location	**N end of scanline**	**UTM zone 14 meters NAD 27**
Easting	**555369 m**	**Orientation of scanline:**
Northing	**3293533 m**	**8 azimuth**
Elevation	**1269 feet**	

Number	meters along tape	Strike	Dip	Slickenline rake	Displacement, cm	Comments
1	28.2	277	64	85	30	No visible slickenlines
2	39.2	89	65		6	No visible slickenlines
3	106.4	280	45		700	No visible slickenlines, dissolution residuum in fault zone
						displacement estimate is a minimum based on probable correlation of highest exposed massive limestone i with lowest exposed massive limestone in hw
4	127.45	91	62		56	offset is visible, fault zone grungy
5	134.15	263	67		7	dissolution cavity along fault
6	136.95	277	62		10	dissolution cavity and residue along fault
	186.85					END OF EXPOSURE

BFZ 080703.1 Faults measured in rock face bounding east side of Hwy. 281, north of San Antonio, Texas, approx. 1.6 miles S of Hwy. 46 exit
Collected 8 Aug 2003

GPS location **N end of scanline** **UTM zone 14 meters NAD 27**

Easting **555462 m** **Orientation of scanline:**
Northing **3293830 m** **15 azimuth**
Elevation **1231 feet**

Number	meters along tape	Strike	Dip	Slickenline rake	Displacement, cm	Comments
1	38.95	77	73		10	no visible slickenlines
2	78.6	42	65	102	16	at northern edge of crossing fault array discussed in paper: FERRILL ET AL 2000 (AAPG)
3	78.95	108	71	88	9	
4	79.4	216	67	90	27	
5	81.8	226	58	88	3	fault featured in close up with slickolites and coarse calcite vein fill in crossing faults paper
6	82.6	223	58	85	1	
7	83	82	63	96	11	048/60 is average orientation for this fault in this exposure
8	85.35	230	52	85	1	
9	86	238	58	87	22	
10	86.9	158	45		2	no visible slickenlines
11	88.05	269	72	74	3	
12	89.15	218	56	95	30	
13	90.2	226	64	70	0.5	
14	90.65	225	75		0.5	75 and 54 are the steepest and gentlest dips respectively for this listric fault; no visible slickenlines
15	92.55	233	55	86	0.5	
16	92.85	222	58	74	0.5	
17	93.7	235	58	74	1	
18	94.3	43	60	99	150	
19	94.4	247	65	76	2	
20	95.05	235	81	78	1	
21	95.1	225	77	85	0.5	
22	95.45	71	39	90	0.5	
23	95.65	30	61	108	20	61 and 36 are the steepest and gentlest dips respectively for this listric fault
24	96.4	28	45	114	9	
25	97.2	62	40	110	7.5	
26	97.5	261	88	88	1	
27	97.7	65	65	90	8	
28	98.25	60	54	88	650	
29	99.2	229	61	93	5	
30	99.5	50	55	92	4	76 and 55 are the steepest and gentlest dips respectively for this listric fault
31	103.15	244	50	88	4	
32	108.15	62	90	90	5	
33	109.05	61	46	90	8	
34	109.7	219	75	86	1	
35	110.05	42	68	98	6	
36	110.8	242	83	89	3	

37	111.3	68	70	92	35	
38	112.05	51	71	90	40	
39	113.5	67	69	90	3	
40	113.65	284	64	90	6	
41	113.75	259	60	90	13	
42	115.05	270	62	90	7	
43	123.6	242	70	82	4	
44	133.3	279	72	91	1.5	
45	134.6	66	52	90	1	
46	137.1	84	44	92	8	
47	137.85	266	74	90	16	
48	146.25	63	60	90	6	
49	147.45	239	62	90	7	
50	163.7	40	60	88	10	
	182					END OF EXPOSURE

Faults measured in the rock face bounding the south side of HL Chapman work area on E side of Hwy. 281 S of Hwy 46 intersection
Collected 16 Jan 2003

GPS location	**E end of scanline**	**meters NAD 27**
Easting	**555824**	**Orientation of scanline:**
Northing	**3293921**	**264 azimuth**
Elevation	**358.4448**	

Number	meters along tape	Strike	Dip	Slickenline rake	Displacement, cm	Comments
1	1.9	41	38	90	11	
2	62.9	214	50	93	1.5	
3	64.4	223	41	90	21	
4	68.65	256	60	87	0	
5	79.1	223	50	90	9	
6	146.5	313	65	62	3	
7	152.4	227	46	100	220	
8	180.5	49	63	95	115	
9	191.65	54	75	93	45	
10	192.5	40	45	134	1	
11	202.6	16	76	90	28	
12	203.6	234	38	52	1	
13	205.6	13	56	90	5	
14	209.2	53	56	90	800	
15	210.8	46	50	na	5	
16	214.05	323	62	47	4	

17	287.8	210	46	na	50	
18	295.9	216	60	90	2	
19	298	216	45	90	1	
20	300.8	210	49	90	6	
21	305.6	235	70	90	2	
22	306.25	208	53	106	1	
23	312.8	46	40	93	15	
24	318.3	19	60	90	1	

Faults measured in the road cut bounding the east side of Ralph Fair Road north of San Antonio, Texas, approx. 1 mile N of IH 10
Collected 22 Jan 2003

GPS location	**N end of scanline**	**meters NAD 27**
Easting	**535691 m**	**Orientation of scanline:**
Northing	**3284946 m**	**180 azimuth**
Elevation	**411.1752 m**	

Number	meters along tape	Strike	Dip	Slickenline rake	Displacement, cm	Comments
1	100.2	219	58	102	94	
2	131	123	40	90	14	
3	131.15	214	75	85	25	
4	131.35	230	43	87	45	
5	131.6	204	80	85	2.5	
6	132.35	223	59	85	22	
7	224.3	221	63	75	10	
8	46.05	na	na	na	200	

Faults measured in the road cut bounding the east side of Ralph Fair Road north of San Antonio, Texas, approx. 2.5 miles south of Route 46
Collected 8 Aug 2003

GPS location	**N end of scanline**	**meters NAD 27**
Easting	**538936 m**	**Orientation of scanline:**
Northing	**3295504 m**	**180 azimuth**
Elevation	**1280 feet**	

Number	meters along tape	Strike	Dip	Slickenline rake	Displacement, cm	Comments
1	6.25	78	62	90	65	
2	14.2	55	54	88	70	
3	17	48	65	85	60	
4	20.45	48	80	90	8	Steepest dip is 80 gentlest is 55
5	23.35	4	68	79	2	
6	24.7	237	57	90	10	
7	33.85	274	64		35	Steepest dip is 64 gentlest is 38
8	42.2	209	61	90	unknown	
9	43.3	250	70		16	

See photograph CLS 021203_1

Number	Strike	Dip	Surface type	Slickenline rake	Displacement, cm	Comments
1						GPS UTM zone 14, NAD 27, E: 577810 m; N: 3303022 m; Elev: 868 ft.
2	48	5	bed	na		
3	226	46	fault	85	15	
4	56	80	fault	90	220	This fault marks the edge of the main fault damage zone
5	239	60	fault	90	15	
6	63	83	fault	nm	4	
7	104	9	bed	na	na	
8	223	48	fault	88	40	
9	63	85	fault	nm	108	same fault as in 1.11
10	248	59	fault	nm	4	
11	263	27	fault	100	25	same fault as in 1.09
12	44	49	bed	na	na	
13	53	9	fault	nm	40	
14	60	40	bed	na	na	
15	55	76	fault	nm	na	
16	42	25	bed	na	na	
17	63	68	fault	90	>15	Main fault zone
18	239	27	fault	100	13	
19	58	84	fault	na	na	Contact between limestone above and shale or argillaceous limestone below; an undulating surface cove with slickenlines in a variety of orientations

20	70	2	bed	na	na	
21	245	64	fault	90	nm	additional rake 4(

See Photograph 031303_1

Number	Strike	Dip	Surface type	Slickenline rake	Displacement, cm	Comments
1	58	73	fault	90	1.5	
2	110	3	bed	na	na	
3	63	65	fault	75	67	
4	230	45	fault	96	12	
5	85	12	bed	na	na	
6	208	75	fault	108	19	
7	60	69	fault	nm	2.5	calcite-filled and visible slickenlines. Displacement measured as down dip offset
8	244	44	fault	90	0.5	
9	58	70	fault	90	1	coarse calcite vein fill present along much of fault
10	54	40	fault	94	6	
11	243	76	fault	90	<1	
12	55	5	bed	na	na	
13	60	56	fault	90	1	
14	78	3	bed	na		
15	245	31	fault	90	2	
16	230	66	fault	104	6	
17	244	71	fault	90	1	
18	70	67	fault	50	1	cuts fault at 1.17
19	63	9	bed	na	na	
20	239	62	fault	96	0.5	
21	235	60	fault	98	1	
22	233	74	fault	90	0.5	
23	38	70	fault	nm	0.75	
24	105	74	fault	62	32	
25	78	73	fault	63	7	
26	75	76	fault	48	7	
27	71	84	fault	86	big	fault zone 50 cm wide, fault rock with organic smell, black with clasts <1 to 50 mm; measurements on smoo grooved hw surface
28	65	2	bed	na		
29						UTM zone 14 NAD 27; E: 577908 m; N: 3303102 m; Elev: 842 ft.
30						UTM zone 14 NAD 27; E: 577904 m; N: 3303098 m; Elev: 833 ft.
31						UTM zone 14 NAD 27; E: 577879 m; N: 3303088 m; Elev: 843 ft.
32	344	65	fault	88	15	
33	35	62	fault	88	10	
34	73	60	fault	94	10	

35	73	60	fault	90	12	
36	34	65	fault	90	13	
37	58	64	fault	90	15	
38	212	80	fault	93	4	
39	245	78	fault	90	10	
40	70	59	fault	nm	5	
41	56	68	fault	90	big	HW surface of fault core. Fault core 55 cm thick, cataclastic fault rock; lenses of cataclasite.
42	55	7	bed	na		
43	250	54	fault	90	10	Displacement increases down
44	275	45	fault	90	50	Displacement increases up
45	240	58	fault	90	10	
46	54	76	fault	90	45	
47	50	64	fault	88	55	
48	228	47	fault	90	45	
49	240	52	fault	90	34	
50	71	19	bed	na	na	
51	70	75	fault	90	4	
52	246	70	fault	90	7	
53	64	83	fault	90	57	
54	62	71	fault	90	55	low
	62	55	fault	90	na	mid
	62	71	fault	90	na	upper
55	242	60	fault	nm	20	
56	245	50	fault	87	13	
57	245	40	fault	90	4	
58	243	34	fault	90	52	
59	50	81	fault	85	23	
60	58	83	fault	85	7	
61	94	11	bed	na	na	
62	88	4	bed	na	na	
63	78	22	bed	na	na	
64	81	10	bed	na	na	

5 FAULT ZONE DEFORMATION

5.1 Introduction

In this section, we present the results of fault zone deformation investigations conducted in the Cretaceous limestone and shale section, with emphasis on investigations of the Glen Rose Limestone, and comparisons with fault zone deformation in the Edwards Limestone (Ferrill and Morris, 2003; Ferrill et al., 2003a). The overall *en echelon* geometry of the Balcones Fault System would, in general, be expected to produce poorly connected faults and result in well connected layers early in fault system development. Competing with this development is the apparent rapid lateral propagation of fault segments with increasing displacement, at least within stronger mechanical layers (Ferrill et al., 2003a). This rapid propagation is expected to result in relatively early interconnection of faults and loss of stratigraphic communication pathways due to development of through-going faults. Field observations show that vertical connectivity is tied to mechanical stratigraphy and that weak mechanical layers at the formation to member scale are capable of arresting fault tip propagation (Ferrill et al., 2003b).

Fault zone deformation involves mechanical and chemical alteration of rock properties, both in the principal displacement zone (fault core) and the zone of less intense fault damage (damage zone), developed adjacent to the fault core (Caine et al., 1996). The Glen Rose Formation consists of limestones and calcareous clays, and the Upper Glen Rose Formation in particular is alternating well-bedded limestones and calcareous clays. This lithological character leads to lower mechanical competence compared with the overlying Edwards limestones and coupled with the greater depth of burial during faulting results in gentler fault dips and a different faulting character than occurs in the Edwards limestones.

Deformation within fault zones results in faults serving as barriers to flow, pathways for flow, or both. Fault zone deformation is by definition localized along faults, and its distribution is therefore controlled by the architecture of the fault systems. The mechanisms of deformation within fault zones depend on the host lithologies, fault system architecture (e.g., Ferrill et al., 2003b), and deformational environment (e.g., Ferrill and Morris, 2003).

Although lateral displacement gradients appear to be relatively gentle throughout the Balcones Fault zone and in the Camp Bullis/Castle Hills areas in particular (Ferrill et al., 2003a), there is evidence that vertical displacement gradients are locally pronounced and controlled by stratigraphy. This stratigraphic control is to be expected where strongly contrasting mechanical layers are faulted. Normal faulting in single, mechanically strong layers has been the subject of intensive investigation by numerous workers over the past decade. These analyses have shown that folding prior to or during fault propagation along faults tends to be limited, and most commonly occurs between laterally or vertically overlapping fault tips (Grimshaw and Woodruff, 1986; Larsen, 1988; Peacock and Sanderson, 1994; Trudgill and Cartwright, 1994; Huggins et al., 1995; Childs et al., 1996; Ferrill et al., 1999a). A mechanically weak layer within the deforming stratigraphic section can serve as a décollement and result in disharmonic deformation. The presence of a weak décollement layer may result in significant monoclinal folding prior to fault breakthrough (Withjack et al., 1990). Thus, the most likely locations for fault tip monoclines to form is where faults in a strong mechanical layer intersect a weak mechanical layer. The style of deformation and structural disharmony depends on the effective mechanical contrast between the deforming layers under the conditions of deformation, and thicknesses of the contrasting units. Monoclines commonly develop structurally above faults that terminate below the ground surface and where the rate of fault propagation is relatively slow with respect to the rate of fault displacement. Consequently, folding occurs above and laterally beyond fault tip lines. Depending on the location of breakthrough, this process will leave synthetic dip panels (rock dipping in the same direction as the fault) in either the hanging wall or footwall, or both.

5.2 Faulting in the Edwards Group, Del Rio Formation, and Buda Formation

An exceptionally well exposed fault within the Kainer Formation (Edwards Aquifer) has been exhumed in Beckmann Quarry (see Ferrill et al., 2003a for quarry location). It is exposed along strike for a distance of approximately 100 m, and vertically in 3-dimensional exposure for a height of 15 m (49 ft) (Figure 5-1). The fault is part of an array of faults that are arranged *en echelon*. Most of the fault's exposed surface is parallel to the regional fault trend, although it changes strike by 80° at its southwestern end to intersect with another *en echelon* segment (Fault B in Figure 5-1a; also cf. Ferrill et al., 1999a). In the fault tip region, the fault is vertically segmented (similar to depiction of Childs et al., 1996), with offset distance between the mostly vertically overlapping segments on the order of tens of centimeters. Parts of the fault surface are obscured by fault rock which occurs in isolated festooned patches that appear to emanate from specific stratigraphic layers in the footwall (Figure 5-1c). These fault rock patches consist of cataclastic host rock material, and precipitated calcite. Two patches are dark gray in outcrop and emit a petroliferous odor when broken, indicating the presence of natural hydrocarbons. Corrugations, grooves, and striations are present on the fault surface, producing consistent indicators, at scales of millimeters to meters, of the dip slip displacement on the fault (Figure 5-1). Evidence of dissolution is not ubiquitous across the fault surface (Figure 5-1c). Instead, dissolution features on the fault plane consist of localized tubes and cavities, some of which have been filled or partially filled by *terra rosa* clay. *Terra rosa* is the clay residue from dissolution of limestone. These dissolution features are more than 50 meters (164 ft) below the pre-excavation ground surface, and based on their predominant down-dip long axis orientations, are indicative of down dip water movement. Flow paths are in some cases discontinuous or intermittently present down the fault plane in the visible footwall. This suggests that the flow paths in three dimensions may cross the fault core from footwall to hanging wall and back. The fault is not a simple conduit, and flow through and across the fault zone is unlikely to be uniform. Although the fault likely represents a zone of greater transmissivity than the surrounding unfaulted strata, the presence of well lithified fault rock implies that the fault does not have uniformly high transmissivity. Despite this occlusion of the fault surface by fault rock, there is little evidence of clay smear into the fault zone, and this is due to the relative paucity of clay-rich strata in the Edwards stratigraphic section. Layering adjacent to the fault and other nearby fault segments show little or no evidence of tilting associated with the faulting. Although this is typical of faults in the Edwards, other examples in Beckmann Quarry (discussed below) display localized layer tilting associated with normal faulting.

Over a distance of several hundred meters along one quarry wall in the northeast part of Beckmann Quarry in northwest San Antonio, Texas, six faults with maximum displacement of <6 m (20 ft) extend upward from the quarry floor through the dolomitic member of the Kainer Formation. All six faults terminate at or within the more clay-rich and thinly bedded Kirschberg evaporitic member of the Kainer Formation. Of the faults visible in the exposure, the fault with the largest displacement has a maximum observed displacement of 6 meters (20 ft) along its exposed profile length of 25 m (82 ft) (Figure 5-2). This fault has fairly uniform displacement of 4-6 m (13 - 20 ft) over 15 m (49 ft) of length. At its upward end, displacement drops from 4 m (13 ft) to 0 m over a vertical distance of 5 m (16 ft) (Figure 5-2). Above the fault tip, throw is accomplished by folding, forming a monocline in the Kirschberg evaporitic member above the fault tip. The other five faults that span the dolomitic member in the quarry wall have less displacement, with displacement ranging from decimeters to meters, and all of the faults tip upward in the same stratigraphic interval. Based on their consistent dip extent, but variable maximum displacements, these faults probably propagated through the dolomitic member relatively rapidly with respect to displacement accumulation and continued to accumulate displacement without commensurate upward propagation. The Kirschberg Evaporite member therefore arrests upward fault propagation by deforming in a ductile manner.

Although generally within the Edwards Group, mechanical contrasts are not sufficient to generate monoclines much larger than the one illustrated in Figure 5-2. The overlying Del Rio Clay is much weaker than the Edwards limestones. Consequently, fault propagation monoclines might be expected to develop at the interface between the Edwards Group and the Del Rio Clay. In the San Antonio area this stratigraphic interval is not well-exposed, however, the Sierra Del Carmen range of West Texas provides excellent, well exposed examples of the geometry and deformation processes likely to have occurred in and above the Edwards Aquifer during deformation (Ferrill et al., 2003a). The Sierra Del Carmen range lies along the eastern margin of Big Bend National Park and the contiguous western margin of Black Gap Wildlife Management Area. Range morphology is controlled by the resistant (ridge forming) Cretaceous Santa Elena Limestone (an Edwards Group equivalent), which has largely been exhumed by erosion of the overlying Del Rio Formation (Maxwell et al., 1967; Maxwell, 1968; Moustafa, 1988; Maler, 1990). In Big Brushy Canyon, the massive Santa Elena Limestone is displaced by at least 30 m (98 ft) on a NNW-SSE trending, down-to-the-east normal fault. The Del Rio Formation (clay-rich calcareous strata) which overlies the Santa Elena Limestone, is not completely cut by the fault, but is dramatically thinned over the fault tip (Ferrill et al., 2003a). Overlying the Del Rio Formation is the Buda Limestone, which contains limestone beds 1 to 2 m (3 to 7 ft) thick. The Buda Limestone beds are not faulted, but form a monoclinal fold over the fault. Buda Limestone layers are cut by bed-perpendicular extension fractures that have extended beds by several percent. The Buda and Edwards limestones, however, are not in physical contact with one another, nor is there a physical rupture through the Del Rio Formation that would allow communication between the two potential aquifers. The Del Rio Formation has been folded and perhaps smeared along the fault, and may remain an intact barrier to across-fault fluid communication.

In the San Antonio area, we conducted a detailed outcrop investigation of the Buda Limestone in a recently excavated exposure (near the intersection of Bandera Road and Loop 1604) in northwestern San Antonio. The limestone has been cut by several normal faults with tens of centimeters to more than a meter of displacement (Figure 5-3). These faults have in several cases been enlarged by dissolution, and cavities are filled by red clay. Examples of dilational normal faults (Ferrill and Morris, 2003) were identified in this outcrop. The contact between the Buda Limestone and the overlying Eagle Ford Formation (shale) is exposed at the southwest end of the outcrop. At this location, the contact steepens from nearly horizontal to 45° (Figure 5-3). Also associated with this steepening dip is locally intense extension fracturing, faulting, and dissolution along fractures and faults in the Buda Limestone. This locally intensive deformation may be the damage zone associated with a monocline in the Buda Limestone, similar to the upper part of a fault tip monocline. Fracturing in the limestone units represents a local increase in porosity and permeability parallel to the fault/monocline trend, whereas the monoclinally folded clay-rich Eagle Ford Formation may inhibit fluid flow communication between the Buda and Austin limestones.

5.3 Faulting in the Glen Rose Formation

Small-displacement (<10 centimeters (4 inches)) faults within the Glen Rose Formation generally have well developed slickenline lineations, and fault zones are commonly a single fracture (e.g., Ferrill et al., 2000). Faults with displacements greater than a few tens of centimeters are less likely to display clear slickenlines, and are more likely to consist of more than a single fracture. Features such as slickolites, re-precipitated calcite and cataclasite may also occur in faults of this size. Meter-scale displacement faults are rarely represented by a single fracture plane, and have damage zones that may be 0.5 to 1 m (1.6 to 3 ft) wide perpendicular to the fault. Slickenlines commonly occur on supplementary slip surfaces within the damage zone, and may or may not accurately reflect the displacement on the principal fault. Faults with displacements measured in tens of centimeters to meters in limestone layers commonly lose displacement in the more clay rich beds of the Glen Rose Formation. The steep displacement gradients associated with this loss of displacement is commonly expressed as monoclinal folding beyond the fault tip.

The more common occurrence of clay-rich beds within the Glen Rose Formation increases the likelihood of faults terminating within clay-rich layers (Figure 5-4). Larger faults may have monoclines that are several tens of meters across. The fault in the Canyon Lake Spillway Gorge is the largest fault investigated in this study and has a displacement of greater than 30 m (98 ft) (see Figure 1-3 for location). This fault has a synthetic dip panel in the adjacent footwall, and is characterized by a damage zone that varies from 1 m (3 ft) to greater than 5 m (16 ft) in width perpendicular to the fault. Depending upon which lithologies are involved in the fault zone, deformation features range from high fault and fracture densities (Figure 5-5) to monoclinal folding and extreme bed attenuation leading to clay smear (Figure 5-5). The fault zone is composed of fault segments that have linked to form a throughgoing feature. In addition to slip surfaces parallel to the main fault, there are large numbers of smaller faults with roughly parallel strikes but with variable dip (Figure 5-5). Bedding orientations adjacent to and within the fault zone define both synthetic dip panels and fault-strike-parallel dip panels indicative of relay ramps (Childs et al., 1996; Ferrill and Morris, 2001).

We have developed a conceptual model for the evolution of this fault based on detailed studies of sections through the fault zone (Figures 5-5, 5-6, and 5-7). Segmented faults propagating past each other initiate bedding panels that dip synthetically with and along the strike of the primary faults (Figure 5-7a). Because of the mechanical contrast between the limestone and clay-rich layers within the Glen Rose Formation and the relatively high proportion of clay-rich layers (especially in comparison with the Edwards lithologies), slip on existing fault surfaces could accumulate more rapidly than the fault tip could propagate. This results in steep dips in the beds beyond the tip lines of the primary faults, accommodated by small scale faulting in the thin limestone beds (Figure 5-7b, c). Ultimately the linking of the primary fault segments is achieved and the relict relay ramp becomes entrained in the fault zone as a steeply dipping panel (Figure 5-7d).

Fault zones that develop in this way are highly heterogeneous. They contain regions of clay smear where clay-rich beds have deformed into the fault zone without significant faulting. Where more competent limestone units have been faulted to accommodate the bulk bending strain they may become encased in more clay rich material (Figure 5-7) or if they are relict relay ramps they may form larger, highly tilted blocks of more-or-less intact limestone within the fault zone. Such a fault zone architecture represents a complex plumbing system for groundwater flow. Clay smear will likely reduce bulk permeability, and may seal blocks of more permeable limestone. Limestone blocks entrained in the fault zone are likely highly fractured and susceptible to dissolution by chemically aggressive ground water. The larger blocks, such as relict relay ramps are likely to provide significant flow pathways within the fault zone. This complex and heterogeneous structure is exemplified by the fault exposed in the Canyon Dam Spillway. Portions of the fault zone are clearly not recharge features and can pond surface water for considerable periods of time. Within a few meters of these features are fault zone segments that are very efficient recharge points and serve as sinks for surface water (Figure 5-8).

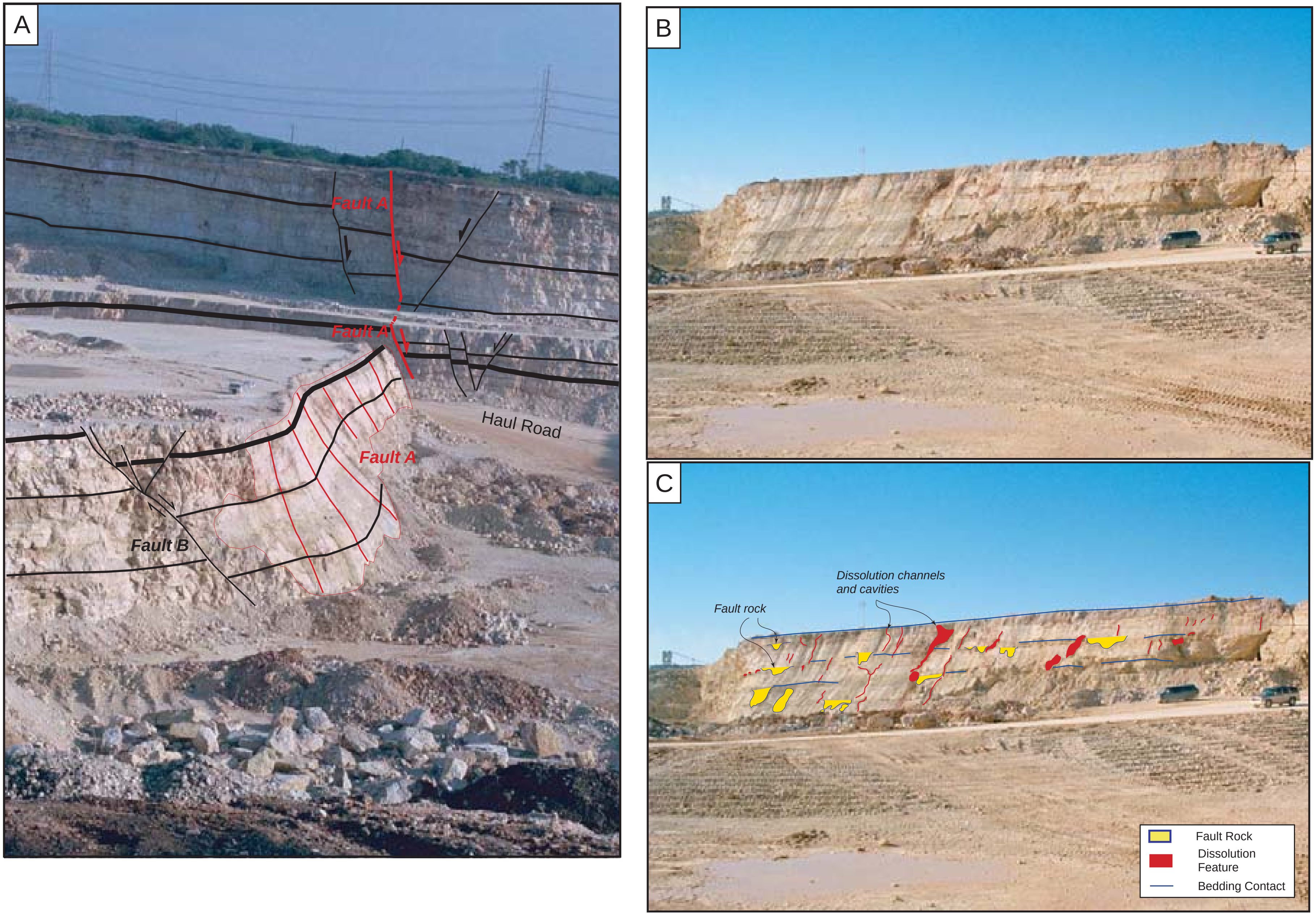

Figure 5-1. (a) Fault system exposed in Beckmann Quarry in northwest San Antonio (after Ferrill et al., 2003a). Note that faults cut across approximately 65 m (213 ft) exposed thickness of Edwards strata, and show evidence of only very minor tilting of layers adjacent to the fault. (b) Un-annotated and (c) annotated photographs showing striations and grooves, fault rock (yellow patches) and dissolution features (red) on Beckmann Quarry fault.

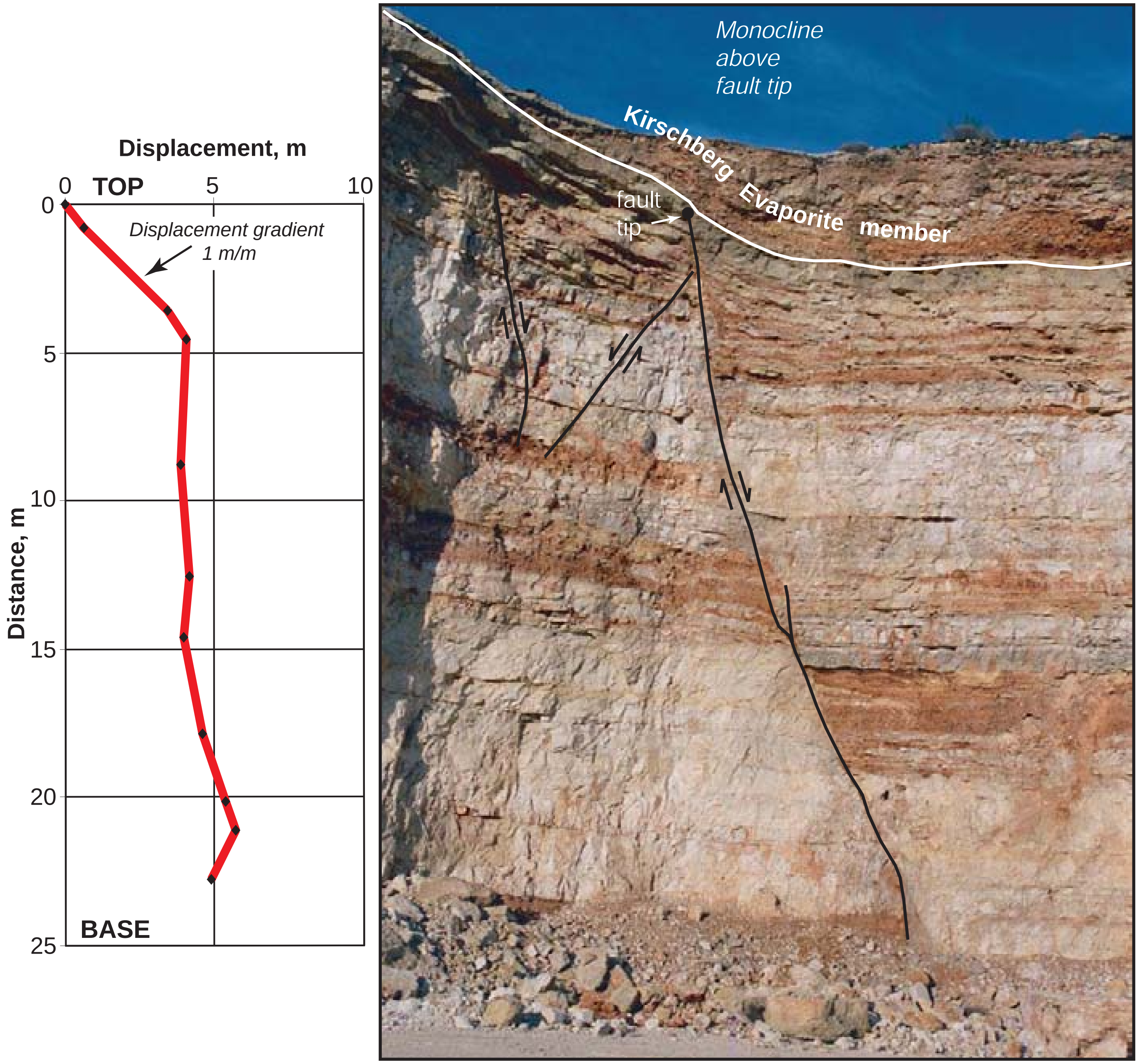

Figure 5-2. Fault in the dolomitic member of the Kainer Formation tips (terminates) upward into the Kirschberg Evaporite member. Displacement in the dolomitic member is replaced by monoclinal folding in the overlying Kirschberg Evaporite member. Photo from the Beckmann Quarry, San Antonio, Texas. View is to the ENE, along the direction of strike of the fault.

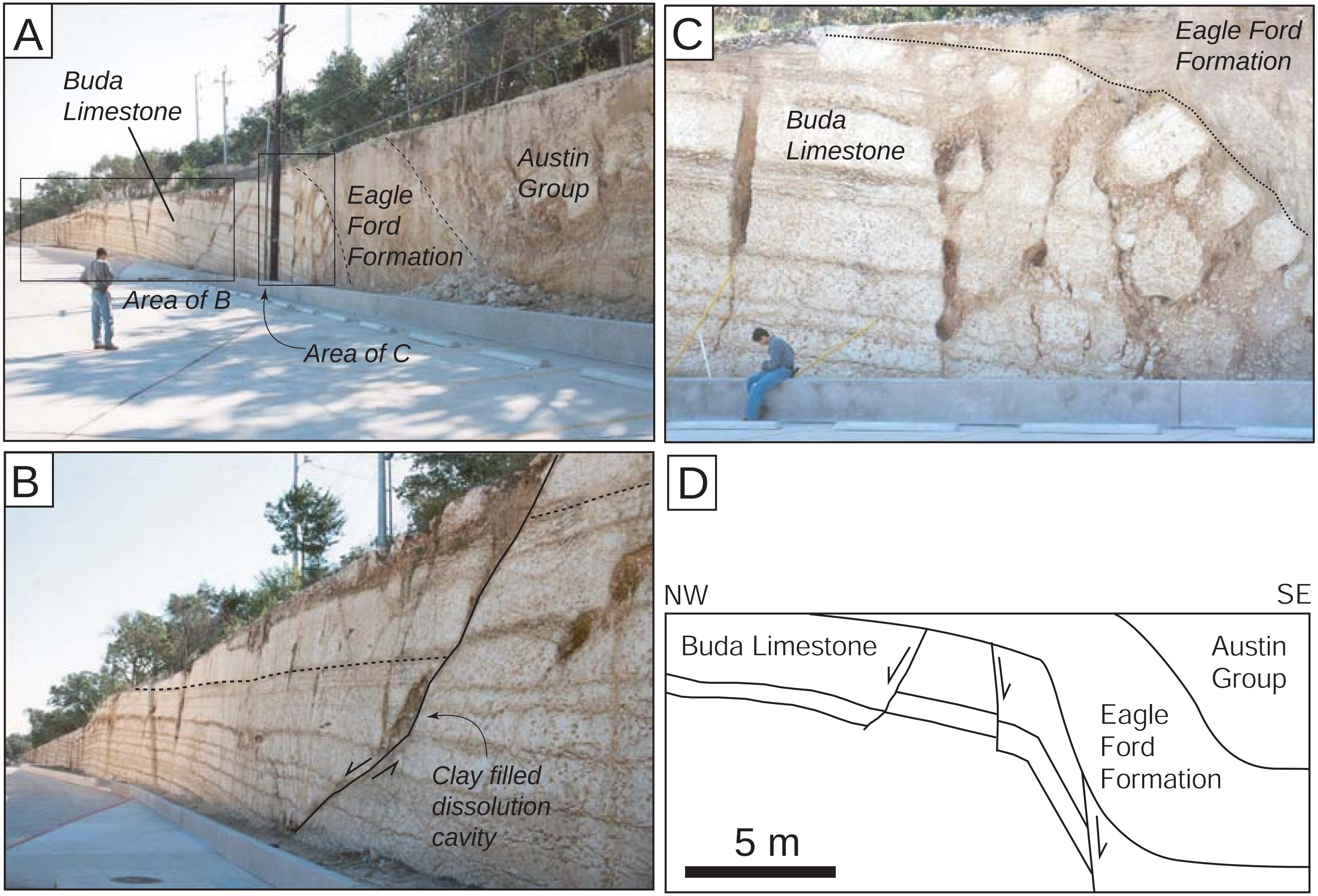

Figure 5-3. Field photographs of faults and dissolution features in the Buda Limestone, exposed near the intersection of Bandera Road (16) and Loop 1604, in northwest San Antonio, Texas. (A) Monoclinal fold developed in the clay-rich Eagle Ford Formation and the base of the Austin Group above the Buda Limestone. View is toward the east. (B) Dissolution cavity developed in a dilational segment of a small-displacement normal fault in the Buda Limestone. View is toward the east. (C) Dissolution cavities developed in extensional faults and fractures accommodating bending in the Buda Limestone. View is approximately toward the southeast. (D) Schematic cross section based on (A), (B), and (C).

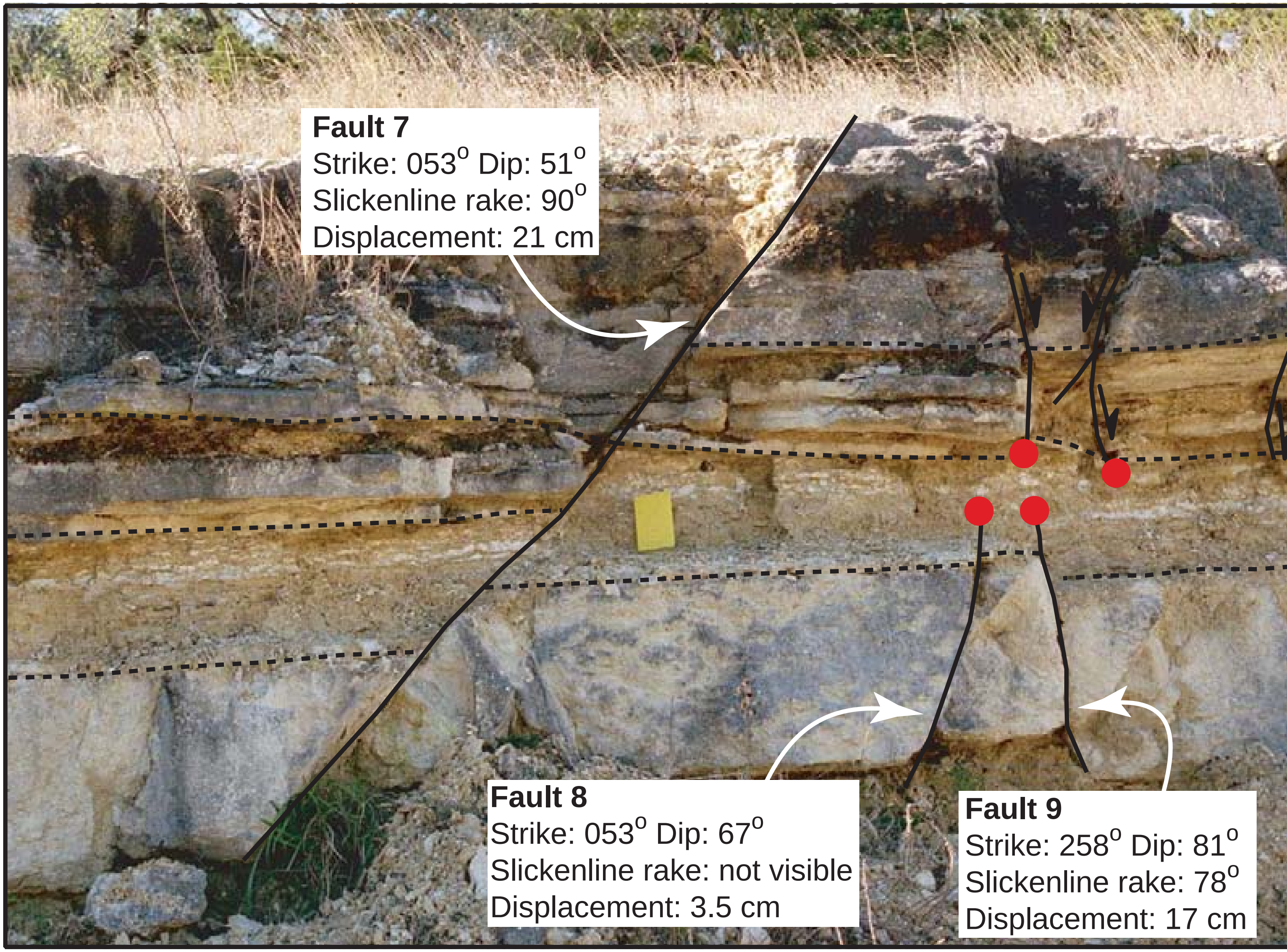

Figure 5-4. Faults exposed on Route 46. Red dots indicate fault tips. At this location more than half of the 13 measured faults tip in the shale layer illustrated in this photograph.

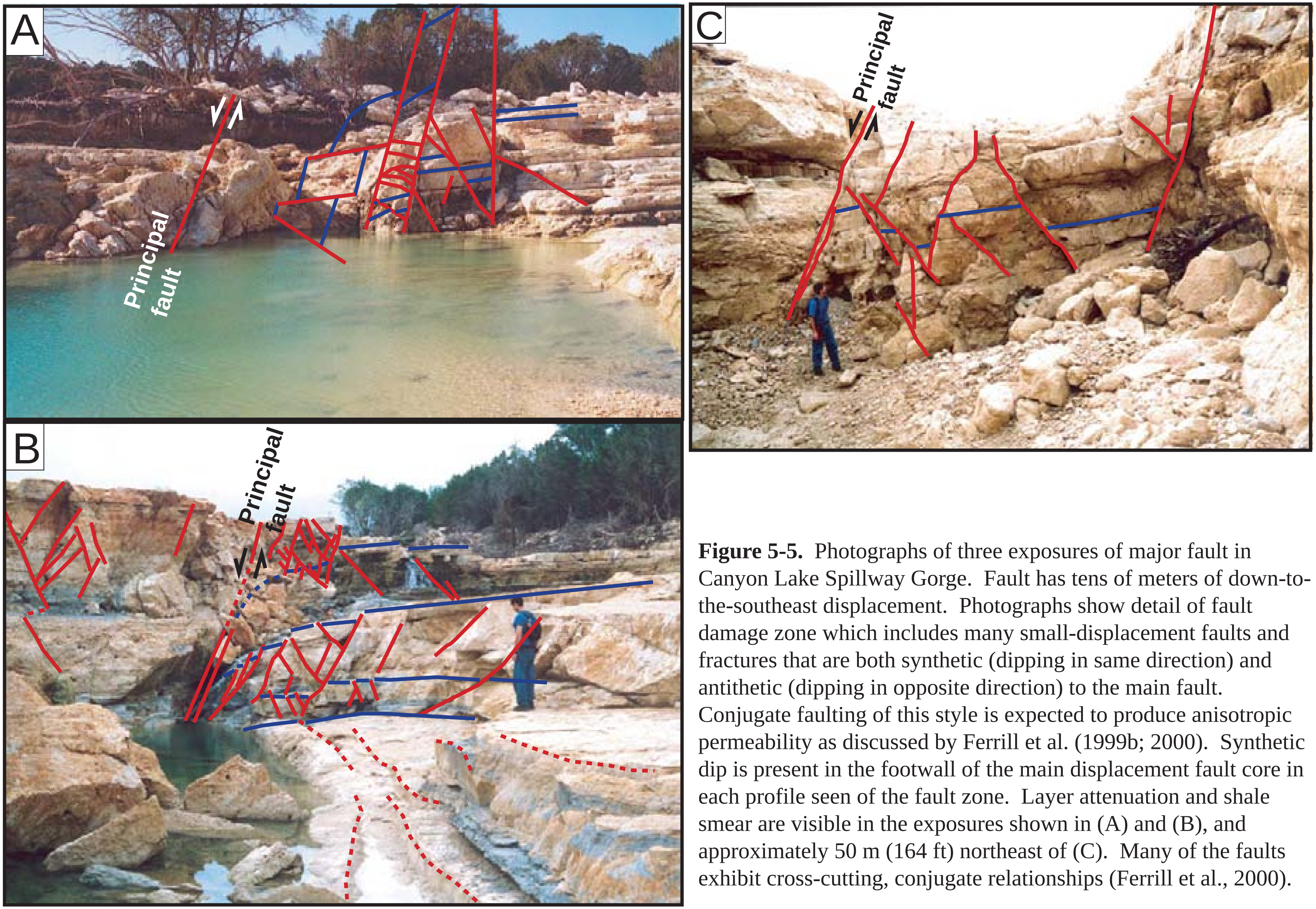

Figure 5-5. Photographs of three exposures of major fault in Canyon Lake Spillway Gorge. Fault has tens of meters of down-to-the-southeast displacement. Photographs show detail of fault damage zone which includes many small-displacement faults and fractures that are both synthetic (dipping in same direction) and antithetic (dipping in opposite direction) to the main fault. Conjugate faulting of this style is expected to produce anisotropic permeability as discussed by Ferrill et al. (1999b; 2000). Synthetic dip is present in the footwall of the main displacement fault core in each profile seen of the fault zone. Layer attenuation and shale smear are visible in the exposures shown in (A) and (B), and approximately 50 m (164 ft) northeast of (C). Many of the faults exhibit cross-cutting, conjugate relationships (Ferrill et al., 2000).

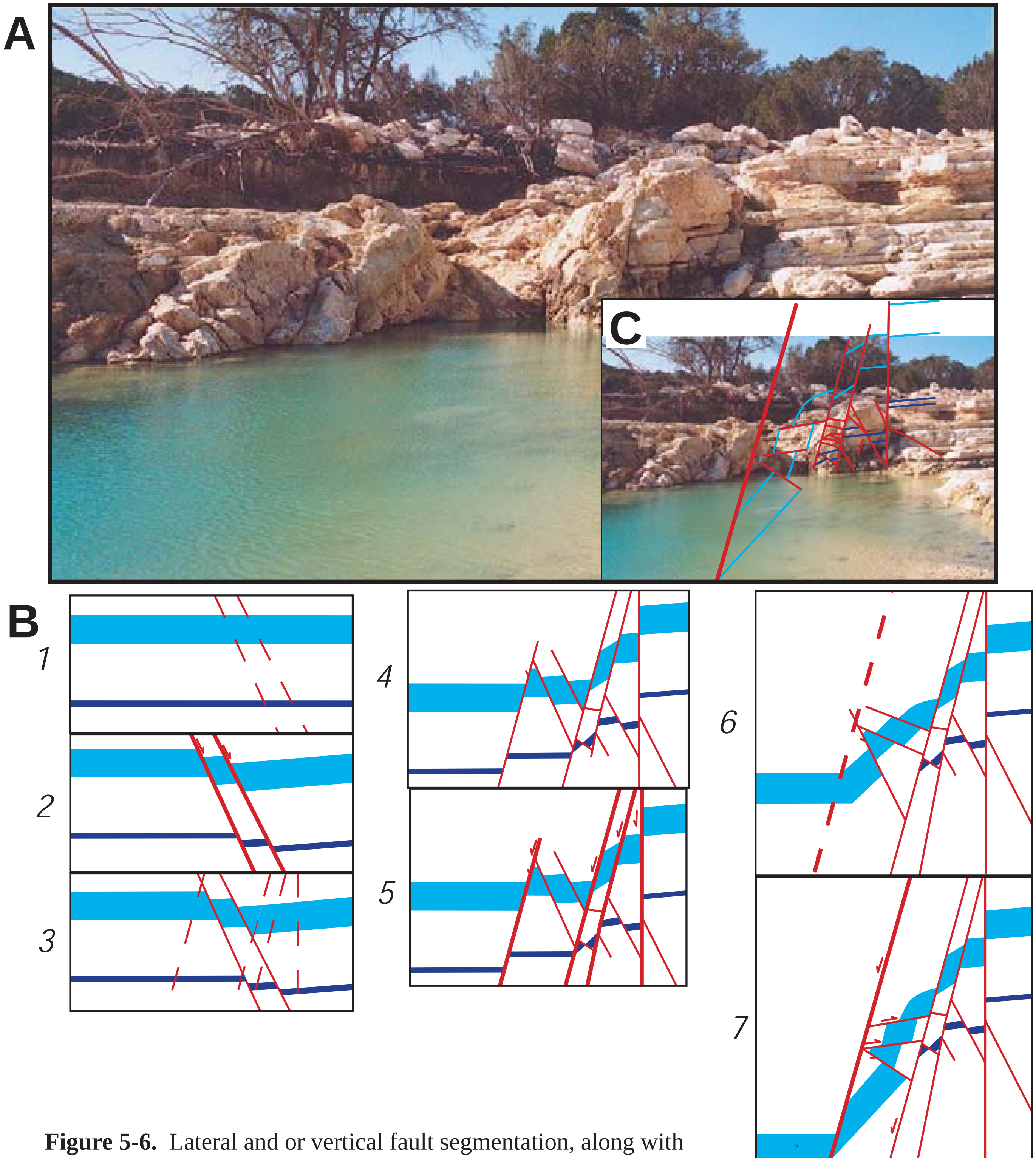

Figure 5-6. Lateral and or vertical fault segmentation, along with monoclinal folding associated with arrest of propagating fault tips in weak clay rich layers has led to significant tilting, extension, and thinning of limestone beds in fault zone exposed in the Canyon Lake Spillway Gorge. (A) Unannotated photograph of exposure. (B) Sequence 1 through 7 is the interpreted evolution of the structure in cross section (compare with Figure 5-7), blue layers are more competent than the white. (C) Annotated photograph of exposure, compare with Fig. 5-7.

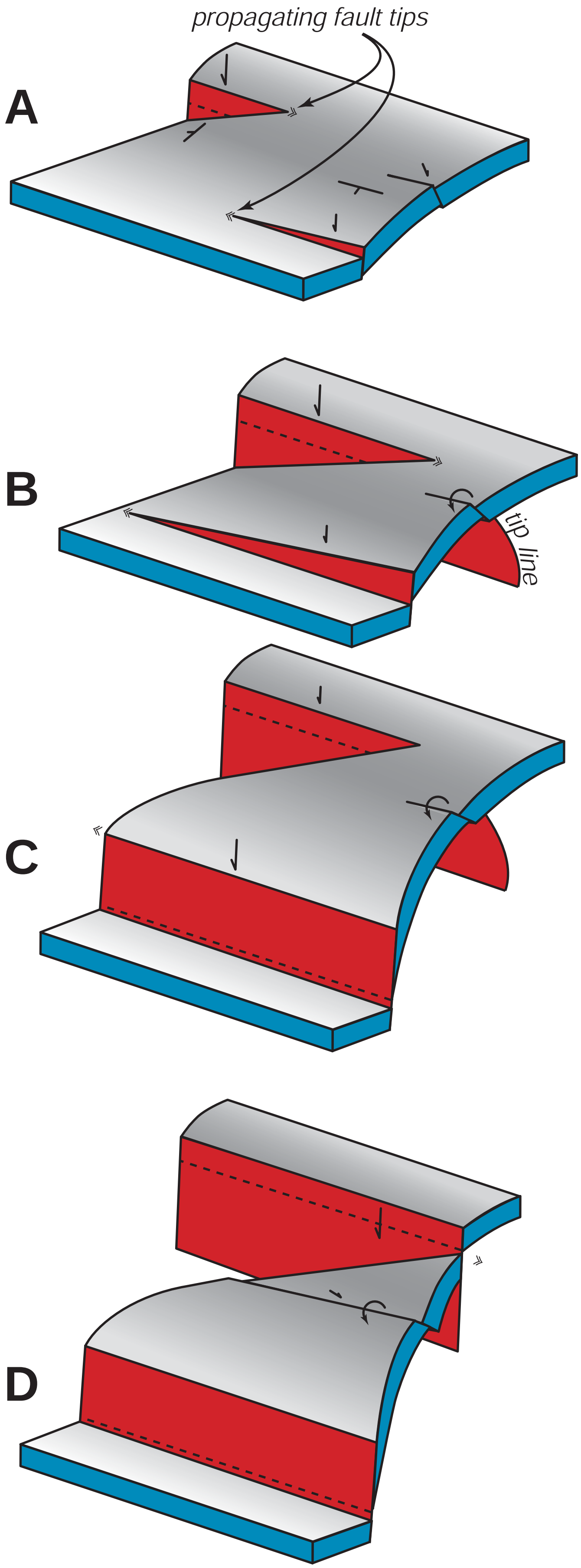

Figure 5-7

Lateral propagation of two normal faults (propagation direction indicated by chevrons) establishes a relay ramp between the terminal sections of the faults. Bending in the relay ramp causes development of small extensional faults.

Continued propagation of the bounding faults causes enlargement and increased bending of relay ramp. Early formed normal faults in ramp become rotated.

Continued propagation of one of the bounding faults, propagation of other fault is arrested. Ramp steepens, small faults within it rotate.

Temporarily arrested fault propagates further. Relay ramp has rotated into a synthetic dip panel and faults within it may be reactivated to accommodate down-dip extension.

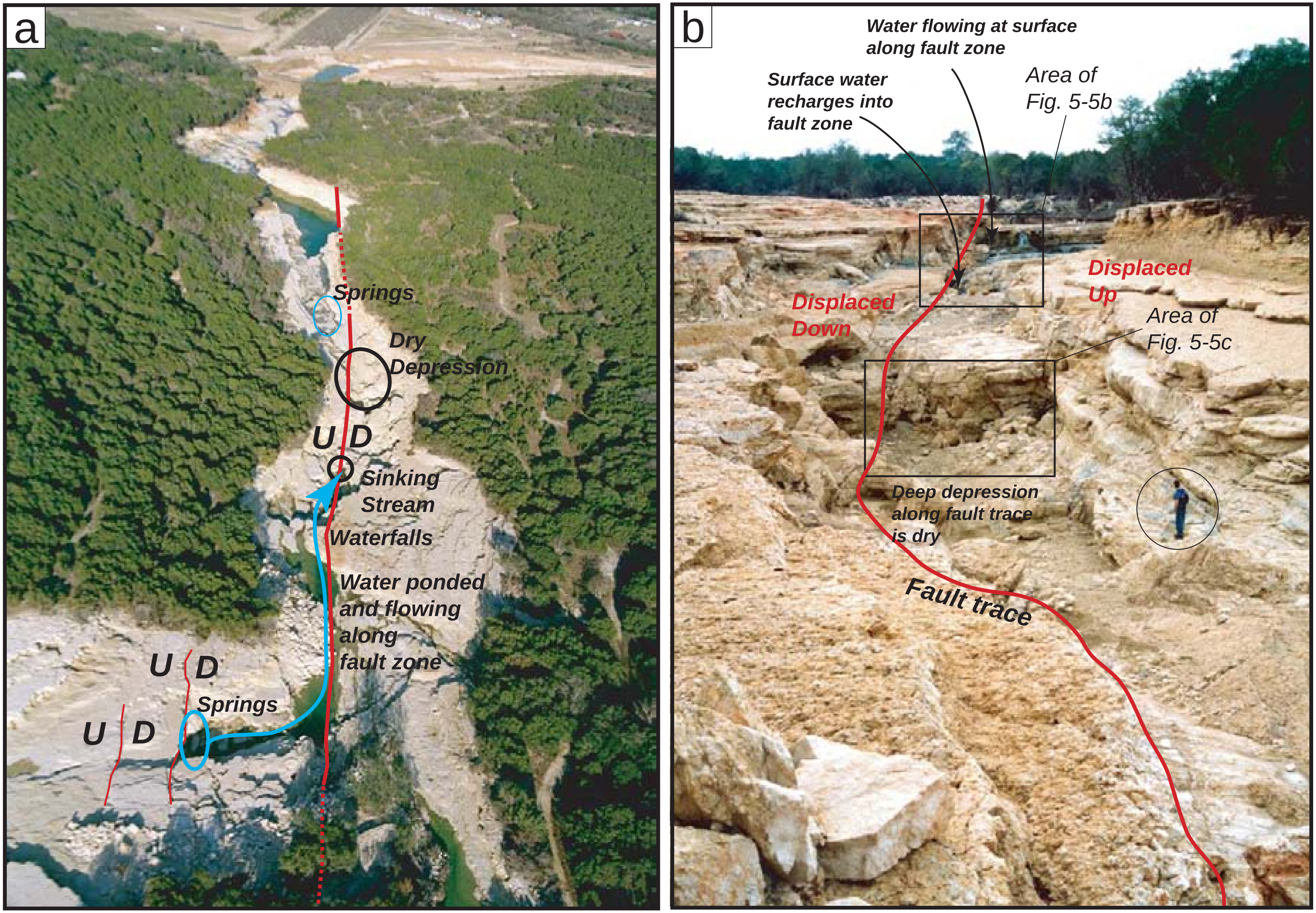

Figure 5-8. (a) Low altitude aerial photograph of Canyon Lake Spillway Gorge showing traces of faults, and locations of springs, pools, and infiltration points in channel. View is to the northeast. (b) Water flowing at the surface along the fault discharged from springs along the fault upstream. Water recharges into the fault within the field of view in the photograph and closed depression along the fault in the middle of the photograph has no surface outlet but is dry indicating infiltration of surface water. View is to the southwest.

6 FAULT BLOCK DEFORMATION

The magnitude of deformation and the orientations of small faults and fractures within fault blocks are major contributors to permeability anisotropy and connectivity within fault blocks (Sims et al., in press). The evolution of extensional fault systems is characterized by nucleation and growth of numerous faults, which then become linked into a network of faults (Walsh and Watterson, 1988; Trudgill and Cartwright, 1994; Childs et al., 1995; Dawers and Anders, 1995; Cartwright and Mansfield, 1998; Ferrill et al., 1999a). During extensional fault system development, faults typically have displacement gradients along their lengths, which lead to deformation within adjacent fault blocks (Figure 6-1) (Ferrill and Morris, 2001). Displacement variation along faults is common and displacement gradients are typically steeper near fault terminations (tips) than on the fault as a whole (Dawers et al., 1993; Trudgill and Cartwright, 1994; Dawers and Anders, 1995). The presence of a displacement gradient requires that, in most cases, either one or both of the hanging wall and footwall cutoff lines must differ in length from their original, prefaulting lengths (Figure 6-1). Factors that influence the magnitude and partitioning of strain between footwall and hanging wall cutoffs include (i) dip of fault, (ii) displacement gradient on fault, (iii) degree of footwall uplift versus hanging wall subsidence, and (iv) orientation of fault slip vector.

Ferrill and Morris (2001) developed a methodology that estimates fault block strain based on present-day geometry of the horizon/fault intersection lines (cutoff lines), original cutoff line orientations, and fault slip directions. We used this approach to calculate cutoff line elongations for cutoff lines from the three-dimensional model. Cutoff lines used in the analysis are from the top of the Lower Glen Rose Formation (Figure 6-2). We used 3DStress™ to calculate slip directions for all fault surfaces in fault gaps, using the 3-dimensional orientations for each fault segment, and the stress tensor determined based on fault analyses conducted in this project (see Section 4.3 for details) where σ_1' = vertical = 15 MPa, σ_2' = azimuth 060 = 9.5 MPa; σ_3' = azimuth 150 = 4 MPa). Resulting cutoff line elongations tend to be very small; only in rare cases do elongations exceed 2% (positive or negative). These small cutoff elongations reflect the low displacement gradients on faults as characterized in the Camp Bullis geologic framework model.

Observations at the scale of the three-dimensional geologic framework model of very gentle dips in competent units (e.g., massive limestones) are consistent with relatively rapid lateral and vertical propagation, until intersection with other faults occurs (laterally) or intersection with a weaker mechanical layer occurs. This lack of steep lateral displacement suggests rapid fault propagation with respect to the rate of displacement accumulation on the faults (Ferrill and Morris, 2001). Relatively rapid lateral propagation with respect to displacement accumulation resulted in comparatively small displacement gradients on faults, little cutoff elongation, and relatively minor influence on fault block deformation. Map scale faults at high angles to regional fault trends are mapped and may accommodate cutoff extension.

Small faults, with displacements of millimeters to <10 m (33 ft), in the Edwards Aquifer recharge zone most commonly parallel the regional fault tend. Although the faults of the

Balcones Fault System overall step strata down toward the Gulf of Mexico, major and minor faults with the regional southeast dip and conjugate faults dipping to the northwest are both very common (e.g., Figure 4-6). Our observations of approximately 5 km (3 miles) of exposure in quarries and roadcuts in Edwards Aquifer strata, indicate that systems of small faults are heterogeneously developed within fault blocks. Scanline studies in accessible roadcut exposures (two localities near the northwest corner of the Castle Hills Quadrangle in northwest San Antonio) within the Kainer Formation demonstrate this heterogeneity. In a roadcut exposure along Kyle Seale Parkway, extension by small-scale faults is 0.1% and fault intensity is 0.04 faults/meter, over an extension-parallel distance of 198 m. In a nearby roadcut exposure along La Cantera Parkway, adjacent to a mapped fault, extension by small-scale faults is 7.6% and fault intensity is 1.16 faults/meter, over an extension-parallel distance of 93 m. These two examples represent the end members of fault intensity variation that we have observed in Edwards Aquifer strata. We conclude that zones of high fault intensity are generally within 100 m (328 ft) (perpendicular to strike) of a large displacement (maximum displacement >10 m (33 ft)) fault.

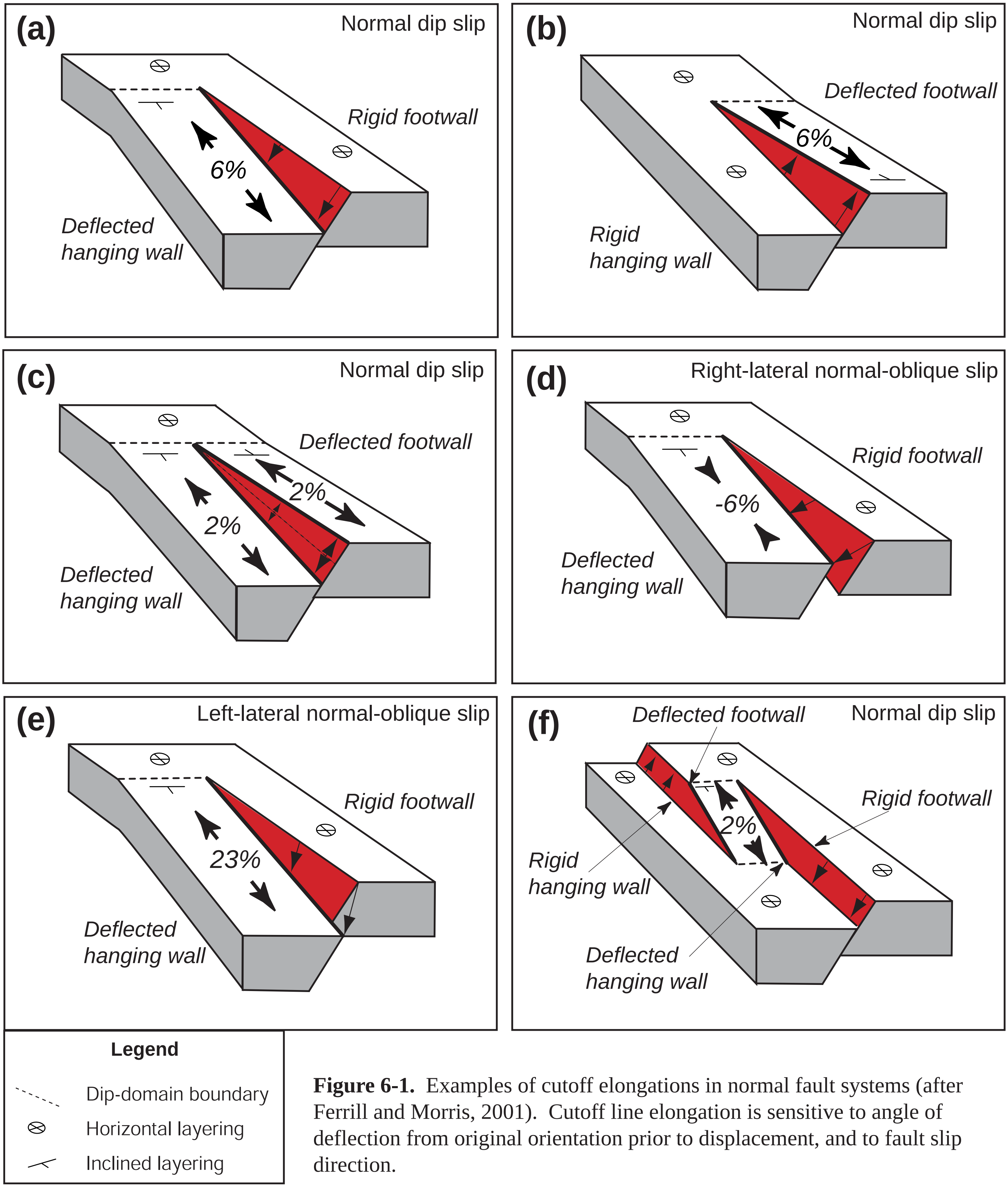

Figure 6-1. Examples of cutoff elongations in normal fault systems (after Ferrill and Morris, 2001). Cutoff line elongation is sensitive to angle of deflection from original orientation prior to displacement, and to fault slip direction.

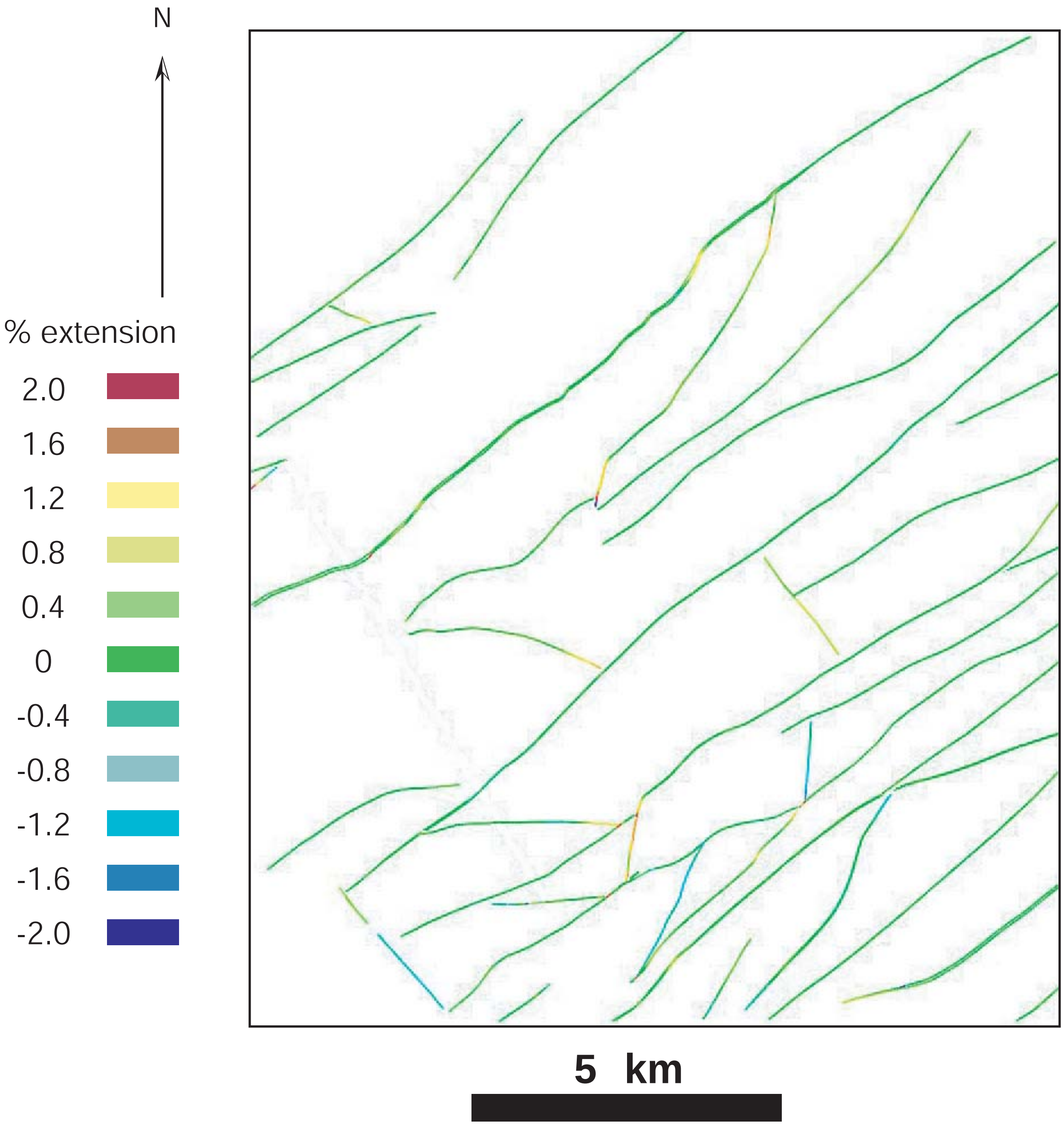

Figure 6-2. Fault cutoff elongation map for horizon at the top of the top of the Lower Glen Rose Fm. (base of the Upper Glen Rose Fm.) based on fault gaps in Camp Bullis geologic framework model.

7 STRUCTURAL ANALYSIS OF POTENTIAL COMMUNICATION BETWEEN TRINITY AND EDWARDS AQUIFERS

The contribution of water to the Edwards from the Trinity Aquifer has been the subject of a range of investigations that considered the geology, geochemistry and hydrologic modeling of the interface between the two aquifer systems. These investigations have resulted in a wide range of estimates of the contribution of water from the Trinity to the Edwards Aquifer (see discussion by Mace et al., 2000, in section on "Discharge" for a summary of the different interpretations). LBG-Guyton (1995) specifically discussed the aquifer interface along the Haby Crossing Fault where fault throw has fully juxtaposed the Edwards and Glen Rose Limestones. As we discussed in Section 4, fault throws of this magnitude are not present in the Camp Bullis and Castle Hills area. Instead, smaller fault displacements have resulted in juxtaposition of the Edwards limestones with the Upper Glen Rose Formation, with only very minor and local examples of basal Edwards placed units against the Lower Glen Rose Formation. The lack of fault juxtaposition of the recognized highly permeable units of the Edwards and Glen Rose Formation in the Camp Bullis and Castle Hills areas suggests that simple juxtaposition is not likely to be a major source of aquifer communication in this area.

We have shown that:

- Direct, across fault connections between the Edwards and Trinity Aquifers are rare in the Camp Bullis quadrangle.
- Fault displacements are generally less than the stratigraphic thickness of aquifer units, therefore units are thinned across faults, thus constricting hydraulic flow paths.

However:

- Fault zones in the Edwards and Trinity Aquifers serve as conduits for groundwater movement.
- Large fault surfaces that cut multiple layers depicted in the geologic framework model provide potential pathways for both vertical and lateral movement of water and communication between aquifers.
- At certain stratigraphic horizons there is the potential for clay smear to decrease hydraulic connectivity across faults.
- Damage zones associated with fault tips and relay ramps are sites of most intense small scale faulting and extension fracturing.
- Fault surfaces along with localized zones of relatively intense small scale faulting and extension fracturing, and limestone dissolution (karst conduit formation) provide likely communication pathways between the Trinity and Edwards Aquifers.

The southward trending contaminant anomaly in the Trinity Aquifer extending from the contaminant source along Lewis Creek suggests southward movement of groundwater towards the Edwards Aquifer. The structural analyses presented in this report provide the framework for more detailed investigations of groundwater levels, multiwell pumping (drawdown) tests, tracer studies, and geochemical investigations to further investigate potential groundwater communication between the Trinity and Edwards Aquifers in the Camp Bullis and Castle Hills Quadrangles.

8 SUMMARY

The purpose of the project reported here was to characterize the structural architecture of the Edwards and Trinity Aquifers for the area of the Camp Bullis 7 ½ minute quadrangle, and extending north to include Cibolo Creek in the southern part of the Bergheim 7 ½ minute quadrangle. Included in this analysis were tasks to generate a three-dimensional computer model of the Trinity and Edwards Aquifer, and perform field investigations to characterize the mechanisms and products of localized fault-related deformation in the Edwards Aquifer and Trinity Aquifer near the study area. An important objective was to analyze the potential for communication between the Edwards Aquifer and the Trinity Aquifers, taking into account fault-related deformation and juxtaposition of the aquifers across key faults. We investigated the geologic structure of the Trinity and Edwards Aquifers to assess the large scale aquifer architecture, analyze fault offset and stratigraphic juxtaposition relationships, evaluate fault zone deformation and dissolution and fault system architecture, and investigate fault block deformation and scaling of small scale (intra block) normal faults. The goal was to assess the structural controls on the aquifers at a broad range of scales that may influence water movement.

Comparing field observations and data from this project with results of two previous projects has led to a new understanding of fault related deformation for the limestones of the Glen Rose Formation that contrasts with the deformation style in the Edwards Group Limestone. Faults with displacements of 5 m (16 ft) to tens of meters in the Glen Rose Formation commonly have damage zones with widths on the order of meters, within which small faults and rotated fault blocks are common. Although faults with displacements of 5 m (16 ft) to tens of meters in the Edwards Group limestones typically have numerous associated small faults, block rotation and bed tilting is not common. This characteristic difference in structural style between the Edwards Group limestones and the Glen Rose Formation appears to be related to lithologic differences and the resulting differences in mechanical behavior of the two stratigraphic sections. The Glen Rose Formation is more heterolithic, containing competent massive limestone beds interbedded with incompetent argillaceous limestone and shale beds. Incompetent beds tend to arrest fault propagation during fault growth. Consequently, with increasing fault displacement, fault tips episodically propagate then arrest. Continued displacement on a fault with an arrested fault tipline will produce fault tipline folding and associated local deformation such as intense small scale faulting. Continued fault tip propagation breaks through the zone containing the tipline fold and locally intense faulting. During continued displacement, distributed deformation in the damage zone may continue to occur, rotating bedding and small faults and shear relatively incompetent beds. Resulting fault damage zones can be quite complex and variable along a fault, related to the structural position (including displacement magnitude) and the associated mechanical stratigraphy. Permeability in fault zones and fault blocks is likely to be strongly influenced by the different deformation styles in mechanical layers, and the deformation progression with increasing fault displacement.

Extensional deformation in the Camp Bullis study area has produced an extensive network of faults likely to influence intra-aquifer permeability due to the influence of fault zone processes producing permeability anisotropy with maximum transmissivity parallel to fault strike. This effect is accentuated by the fact that displacement on these faults has thinned the aquifer along each fault, further restricting aquifer connectivity perpendicular to fault strike. These faults do not however have major displacement. The maximum displacement mapped on any fault in the Camp Bullis study area is approximately 110 m. Displacements of this and smaller magnitude are not sufficient to separate the Upper Glen Rose Formation from itself across a fault, and are thus insufficient to juxtapose the highly permeable Edwards Aquifer with the relatively high permeability Middle Trinity Aquifer. However, the presence of the faults themselves and the higher transmissivity within the fault zones compared with the unfaulted strata increases the likelihood of along-fault communication between the aquifers.

9 REFERENCES

Allan, U.S., 1989, Model for hydrocarbon migration and entrapment within faulted structures: Bulletin of the American Association of Petroleum Geologists, v. 73, p. 803–811.

Antonellini, M., and Aydin, A., 1994, Effect of faulting on fluid flow in porous sandstones: Petrophysical properties: Bulletin of the American Association of Petroleum Geologists, v. 78, p. 355–377.

Arnow, T., 1963, Ground-water geology of Bexar County, Texas: U.S. Geological Survey Water-Supply Paper 1588, 36 p., 13 plates.

Ashworth, J. B., 1983, Ground-water availability of the lower Cretaceous formations in the Hill Country of South-Central Texas, Texas Department of Water Resources, Report 273.

Barker, R.A., Bush, P.W., and Baker, E.T., Jr., 1994, Geologic history and hydrogeologic setting of the Edwards-Trinity Aquifer system, west-central Texas: U.S. Geological Survey, Water-Resources Investigations Report 94–4039, 51 p.

Caine, J. S., Evans, J.P., and Forster, C.B. 1996, Fault zone architecture and permeability structure: Geology, v. 24, p. 1,025–1,028.

Cartwright, J.A., and Mansfield, C.S., 1998, Lateral displacement variation and lateral tip geometry of normal faults in the Canyonlands National Park, Utah: Journal of Structural Geology, v. 20, p. 3–19.

Chalk Butte Inc., 1994, U.S. Digital Topography for GIS. Boulder, Wyoming: Chalk Butte Inc.

Childs, C., Watterson, J., and Walsh, J.J., 1995, Fault overlap zones within developing normal fault systems: Journal of the Geological Society, London, v. 152, p. 535–549.

Childs, C., Nicol, A., Walsh, J.J., and Watterson, J., 1996, Growth of vertically segmented normal faults: Journal of Structural Geology, v. 18, p. 1389–1397.

Clark, A.K., 2000, Vulnerability of ground water to contamination, Edwards Aquifer recharge zone, Bexar County, Texas, 1998: U.S. Geological Survey Water-Resources Investigations Report 00-4149, 9 p., 1 sheet.

Collins, E.W., 1993, Fracture zones between overlapping *en echelon* fault strands: outcrop analogs within the Balcones fault zone, central Texas: Gulf Coast Association of Geological Societies Transactions, v. 43, p. 77–85.

Collins, E.W., 2000, Geologic map of the New Braunfels, Texas, 30×60 minute quadrangle: geologic framework of an urban-growth corridor along the Edwards Aquifer, south-central Texas: The University of Texas at Austin Bureau of Economic Geology Miscellaneous Map No. 39, 28 p., scale 1:100,000, 1 sheet.

Collins, E.W., and Hovorka, S.D., 1997, Structure map of the San Antonio segment of the Edwards Aquifer and Balcones fault zone, south-central Texas: Structural framework of a major limestone aquifer: Kinney, Uvalde, Medina, Bexar, Comal, and Hays Counties: The University of Texas at Austin, Bureau of Economic Geology, Miscellaneous Map No. 38, scale 1:250,000, 2 sheets.

Dawers, N.H., Anders, M.H., and Scholz, C.H., 1993, Growth of normal faults: Displacement-length scaling: Geology, v. 21, p. 1107–1110.

Dawers, N.H., and Anders, M.H., 1995, Displacement-length scaling and fault linkage: Journal of Structural Geology, v. 17, p. 607–614.

Deike, R.G., 1990, Dolomite dissolution rates and possible Holocene dedolomitization of water-bearing units in the Edwards Aquifer, south-central Texas: Journal of Hydrology, v. 112, p. 335–373.

Dynamic Graphics, Inc., 2001, EarthVision User's Guide, Version 6.0. Alameda, CA: Dynamic Graphics, Inc.

Ferrill, D.A., and Morris, A.P., 2001, Displacement gradient and deformation in normal fault systems: Journal of Structural Geology, v. 23, p. 619-638.

Ferrill, D.A., and Morris, A.P., 2003. Dilational normal faults. *Journal of Structural Geology* 25: 183-196.

Ferrill, D.A., Morris, A.P., Stamatakos, J.A., and Sims, D.W., 2000, Crossing conjugate normal faults: Bulletin of the American Association of Petroleum Geologists, v. 84, p. 1543–1559.

Ferrill, D.A., Sims, D.W., Waiting, D.J., Morris, A.P., Franklin, N., and Schultz, A. 2003a. Structural framework of the Edwards Aquifer Recharge Zone, South-Central Texas: Geological Society of America Bulletin, (in press).

Ferrill, D.A., Morris, A.P., Sims, D.W., Waiting, D.J., Hasegawa, S., 2003b. Development of synthetic layer dip adjacent to normal faults. In Sorkhabi, R. (Ed.), Traps and Seals. AAPG Memoir, American Association of Petroleum Geologists, Tulsa, OK, USA, (in press).

Ferrill, D.A., Stamatakos, J.A., and Sims, D.W., 1999a, Normal fault corrugation: Implications for growth and seismicity of active normal faults: Journal of Structural Geology, v. 21, p. 1027–1038.

Ferrill, D.A., Winterle, J., Wittmeyer, G., Sims, D.W., Colton, S., Armstrong, A., and Morris, A.P., 1999b. Stressed rock strains groundwater at Yucca Mountain, Nevada: GSA Today, v. 9, no. 5, p. 1–8.

Finkbeiner, T., Barton, C.A., and Zoback, M.D., 1997, Relationships among *in-situ* stress, fractures and faults, and fluid flow: Monterey Formation, Santa Maria Basin, California: Bulletin of the American Association of Petroleum Geologists, v. 81, p. 1975–1999.

Foley, L.L., 1926, Mechanics of the Balcones and Mexia faulting: Bulletin of the American Association of Petroleum Geologists, v. 10, no. 12, p. 1261–1269.

Grimshaw, T.W., Woodruff, C.M., Jr., 1986, Structural style in an *en echelon* fault system, Balcones fault zone, central Texas: geomorphologic and hydrologic implications: *in* Abbott, P.L., and Woodruff, C.M., Jr., eds. 1986. The Balcones Escarpment, Central Texas: Geological Society of America, p. 71–76.

Groschen, G.E., 1996, Hydrogeologic factors that affect the flowpath of water in selected zones of the Edwards Aquifer, San Antonio region, Texas: U.S. Geological Survey Water-Resources Investigations 96-4046, 73 p.

Hanson, J.A., and Small, T.A., 1995, Geologic framework and hydrogeologic characteristics of the Edwards Aquifer outcrop, Hays County, Texas: U.S. Geologic Survey Water-Resources Investigations Report 95-4265, 10 p.

Hayes, M.E., 2000, Major Aquifers of Texas (map), Texas Water Development Board (TWDB), Austin, Texas: website: http://www.twdb.state.tx.us/mapping/maps/pdf/aqu_maj_24x24.pdf

Hovorka, S.D., Mace, R.E., and Collins, E.W., 1998, Permeability structure of the Edwards Aquifer, South Texas—Implications for aquifer management: The University of Texas at Austin, Bureau of Economic Geology Report of Investigations, v. 250, 55 p.
Huggins, P., Watterson, J., Walsh, J.J., and Childs, C., 1995, Relay zone geometry and displacement transfer between normal faults recorded in coal-mine plans: Journal of Structural Geology, v. 17, p. 1741–1755.
Johnson, S., Esquilin, R., Mahula, D.M., Thompson, E.L., Mireles, J., Gloyd, R., Sterzenback, J., Hoyt, J.R., and Schindel, G., 2002, Hydrogeologic Data Report for 2001. Edwards Aquifer Authority, p. 1-3.
Kastning, E.H., 1981, Tectonism, fractures, and speleogenesis in the Edwards Plateau, Central Texas: *in* Beck, B.F., ed., Eighth International Congress of Speleology, Bowling Green, Ky., July 18–24, 1981, Proceedings, Hunstville, Alabama, National Speleological Society Bulletin, v. 2, p. 692–695.
Knipe, R.J., 1997, Juxtaposition and seal diagrams to help analyze fault seals in hydrocarbon reservoirs: Bulletin of the American Association of Petroleum Geologists, v. 81, p. 187–195.
Kuniansky, E.L., and Holligan K.Q. 1994. Simulations of flow in the Edwards-Trinity Aquifer system and contiguous hydraulically connected units, west-central Texas. U.S. Geological Survey Water-Resources Investigations Report 93-4039, 40 p.
LBG-Guyton Associates, 1995, Edwards/Glen Rose Hydrologic Communication, San Antonio Region, Texas.: Final report for the Edwards Underground Water District, 38 p. with 7 Tables, 13 Figures, and 4 appendices.
Larsen, P.-H., 1988, Relay structures in a lower Permian basement-involved extension system, East Greenland: Journal of Structural Geology, v. 10, p. 3–8.
Loucks, R.G., 1999, Paleocave carbonate reservoirs: origins, burial-depth modifications, spatial complexity, and reservoir implications: American Association of Petroleum Geologists Bulletin, v. 83, no. 11, p. 1795–1834.
Mace, R.E., Chowdhury, A.H., Anaya, R., and Way, S.-C. 2000. Groundwater availability of the Trinity Aquifer, Hill Country Area, Texas: Numerical simulations through 2050. Texas Water Development Board, Austin, Texas, 169 p.
Maclay, R.W., 1989, Edwards Aquifer in San Antonio: Its hydrogeology and management: South Texas Geological Society Bulletin, v. 30, no. 4, p. 11–28.
Maclay, R.W., 1995, Geology and Hydrology of the Edwards Aquifer in the San Antonio Area, Texas: U.S. Geological Survey Water-Resources Investigations Report 95-4186, 64 p., 12 plates.
Maclay, R.W., and Rettman, P.L., 1972, Hydrologic Investigations of the Edwards and Associated Limestones in the San Antonio Area, Texas, Progress Report, 1970–1971: U.S. Geological Survey Open-File Report 72-244, 24 p.
Maclay, R.W., and Small, T.A., 1976, Progress report on geology of the Edwards Aquifer, San Antonio area, Texas, and preliminary interpretation of borehole geophysical and laboratory data on carbonate rocks: U.S. Geological Survey, Open-File Report 76-627, 65 p.

Maclay, R.W., and Small, T.A., 1983, Hydrostratigraphic subdivisions and fault barriers of the Edwards Aquifer, south-central Texas, U.S.A.: Journal of Hydrology, v. 61, p. 127–146.
Maclay, R.W., and Small, T.A., 1984, Carbonate geology and hydrology of the Edwards Aquifer in the San Antonio area, Texas: U.S. Geological Survey Open-File Report OFR 83-537, 72 p., 14 sheets.
Maler, M.O., 1990, Dead Horse Graben: A west Texas accommodation zone: Tectonics, v. 9, no. 6, p. 1357–1368.
Maxwell, R.A., 1968, The Big Bend of the Rio Grande: A Guide to the Rocks, Landscape, Geologic History, and Settlers of the Area of Big Bend National Park: The University of Texas at Austin Bureau of Economic Geology, Guidebook 7, 139 p.
Maxwell, R.A., Lonsdale, J.T., Hazzard, R.T., and Wilson, J.A., 1967, Geology of the Big Bend National Park, Brewster County, Texas: University of Texas at Austin, Bureau of Economic Geology, Publication 6711, 320 p., 11 plates.
Mayer, J.R., and Sharp, J.M., Jr., 1998, Fracture control of regional ground-water flow in a carbonate aquifer in a semi-arid region: GSA Bulletin, v. 110, no. 2, p. 269–283.
Morris, A.P., Ferrill, D.A., and Henderson, D.B., 1996, Slip-tendency analysis and fault reactivation: Geology, v. 24, no. 3, p. 275–278.
Moustafa, A.R., 1988, Structural Geology of Sierra del Carmen, Trans-Pecos Texas: The University of Texas at Austin Bureau of Economic Geology Geologic Quadrangle Map No. 54, 28 p., scale 1:48,000, 3 sheets.
Murray, G. E., 1956, Relationships of Paleozoic structures to large anomalies of coastal element of eastern North America: Gulf Coast Association of Geological Societies Transactions, v. 6, p. 13–24.
Murray, G. E., 1961, Geology of the Atlantic and Gulf Coastal Province of North America: New York, Harper and Brothers, 692 pp.
Palmer, A.N., 1991, Origin and morphology of limestone caves: Geological Society of America Bulletin, v. 103, p. 1-21.
Peacock, D.C.P., and Sanderson, D.J., 1994, Geometry and development of relay ramps in normal fault systems: Bulletin of the American Association of Petroleum Geologists, v. 78, p. 147–165.
Reeves, R.D., 1972, Maps showing outcrops of the Edwards and associated limestones in the principal recharge area of the Edwards Aquifer in Bexar County, Texas: U.S. Geological Survey Open-File Report OF 72-0310, 6 sheets.
Rose, P.R., 1972, Edwards Group, surface and subsurface, central Texas: University of Texas, Bureau of Economic Geology Report of Investigations 74, 198 p.
Sharp, J.M., Jr., and Banner, J.L., 1997, The Edwards Aquifer: A resource in conflict: GSA Today, v. 7, p. 1–9.
Shaw, S.L., 1978, Structural Geology of the Edwards Aquifer in the Castle Hills Quadrangle, Northwestern San Antonio, Texas: The Texas Journal of Science, v. XXX, no. 2, p. 125–131.
Sims, D.W., Morris, A.P., Ferrill, D.A., and Sorkhabi, R. 2003. Extensional fault system evolution and reservoir connectivity. In Sorkhabi, R. (Ed.), Traps and Seals. AAPG Memoir, American Association of Petroleum Geologists, Tulsa, OK, USA, (in press).

Small, T.A., 1984, Identification and Tabulation of Geologic Contacts in the Edwards Aquifer, San Antonio Area, Texas: U.S. Geological Survey Open-File Report 84-075, 54 p.
Small, T.A., 1985, Identification and Tabulation of Geologic Contacts in the Edwards Aquifer, San Antonio Area, Texas: U.S. Texas Department of Water Resources, LP-199, Austin, Texas.
Small, T.A., and Clark, A.K., 2000, Geologic Framework and Hydrogeologic Characteristics of the Edwards Aquifer Outcrop, Medina, County, Texas: U.S. Geological Survey Water-Resources Investigations Report 00-4195, 10 p., 1 plate.
Small, T.A., and Hanson, J.A., 1994, Geologic framework and hydrogeologic characteristics of the Edwards Aquifer outcrop, Comal County, Texas: U.S. Survey Water-Resources Investigations Report 94-4117, 1:75,000 scale, 10p., 1 plate.
Stein, W.G., and Ozuna, G.B., 1996, Geological framework and hydrogeologic characteristics of the Edwards Aquifer recharge zone, Bexar County, Texas. U.S. Geological Survey Water-Resources Investigations Report 95-4030, 1:75,000 scale, 8 p., 1 plate.
Texas Natural Resources Information System (TNRIS), 1997, Digital coverage of Major Texas Aquifers source Texas Water Development Board, Austin, Texas: TNRIS, website: ftp://ftp.tnris.state.tx.us/Water_Resources/Ground_Water/Maj_Aqu_DD/
Trudgill, B., and Cartwright, J., 1994, Relay-ramp forms and normal-fault linkages, Canyonlands National Park, Utah: Geological Society of America Bulletin, v. 106, p. 1143–1157.
Waiting, D.J., Ferrill, D.A., Sims, D.W., 2003, Development of a high-resolution geological framework model for the Edwards Aquifer Recharge Zone: Data, assumptions, procedures, and workflow, South Texas Geological Society Bulletin, v. XLIII, no. 7, p. 13-24.
Walsh, J.J. and Watterson, J. 1988, Dips of normal faults in British coal measures and other sedimentary sequences: Journal of the Geological Society London, v. 145, p. 859-873.
Waterreus, P.A., 1992. Hydrogeology of the Camp Bullis Area, northern Bexar County, Texas [Masters Thesis]: The University of Texas at San Antonio, 186 p.
Weeks, A. W., 1945, Balcones, Luling, and Mexica fault zones in Texas: Bulletin of the American Association of Petroleum Geologists, v. 29, p. 1733–1737.
Wermund, E.G., and Cepeda, J.C., 1977, Regional relation of fracture zones to the Edwards Limestone Aquifer, Texas. in Tolson, J.S., and Doyle, F.L. Proceedings of the Twelfth International Congress Karst Hydrogeology. UAH Press, University of Alabama in Huntsville, Huntsville Alabama, USA, p. 239–253.
Wermund, E.G., Joseph, C.C., and Luttrell, P.E., 1978, Regional distribution of fractures in the southern Edwards plateau and their relationship to tectonics and caves: The University of Texas at Austin Bureau of Economic Geology Geologic Circular 78-2, 14 p.
Withjack, M.O., Olson, J., and Peterson, E., 1990, Experimental models of extensional forced folds: Bulletin of the American Association of Petroleum Geologists, v. 74, p. 1038–1054.
Yielding, G., Freeman, B., Needham, D.T., 1997, Quantitative fault seal prediction: Bulletin of the American Association of Petroleum Geologists, v. 81, p. 897–917.
Young, K., 1972, Mesozoic history, Llano region, *in* V.E., Barnes, W.C. Bell, S.E. Clabaugh, P.E. Cloud, Jr., R.V. McGehee, P.U. Rodda, and K. Young, eds., Geology of the Llano

Region and Austin Area, Field Excursion: The University of Texas at Austin Bureau of Economic Geology Guidebook 13, 154 p.

Zahm, C.D., Marrett, R., and Sharp, J.M., Jr., 1998, Prediction of regional groundwater flow and permeability using fractured outcrop exposures, Edwards Aquifer, Central Texas: in Gambling with Ground Water – Physical, Chemical, and Biological Aspects of Aquifer-Stream Relations (eds., Brahana, J.V., Eckstein, Y., Ongley, L.K., Schneider, R., and Moore, J.E.), Proc., Joint Meeting. American Institute of Hydrology and XXVIII Congress I.A.H., Las Vegas, p. 697-705.

10 GLOSSARY

cataclasite - rock composed of broken rock fragments, resulting from fault slip
cataclastic - of or belonging to a cataclasite
cut-off line - line of intersection between a bed or horizon and a fault surface
décollement - detachment; surface (often near horizontal or parallel to bedding) that permits easy sliding (as of a fault), such as shale or salt
dilation - act of opening to form a void, as of a fracture
displacement gradient - rate at which displacement across a fault varies with position on the fault
en echelon - an array of parallel elements arranged in a zone that is oblique to each element

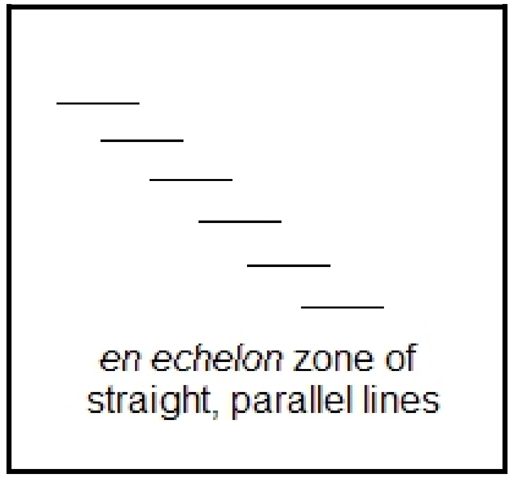

fault tip - point (in two dimensions) or line (in three-dimensions) that marks the end of a fault; bounding point or line of a fault beyond which there is no displacement
fault throw - vertical component of fault displacement
fault heave - horizontal component of fault displacement
footwall - displaced fault block that lies below the fault plane
hanging wall - displaced fault block that lies above the fault plane
hydrostatic stress - stress tensor in which all three principal stresses are equal; equivalent to pressure; stress acts equally in all directions as in a fluid
isochore - a line of equal value, e.g., contour, isobar etc.; **reference-isochore** - the isochore from which others are measured
isopach map - map of lines of equal thickness for a given geological interval, layer, or formation
listric fault - concave upward fault surface (from Greek for shovel); also **anti-listric** - convex upward fault surface
lithostatic stress - the hydrostatic component of a stress tensor at some depth within the earth that results from the weight of overlying rock
mechanical stratigraphy - rock layers defined by their mechanical properties (strength, tendency to brittle or ductile behavior) rather than by their lithology or fossil content
monocline - rock layers dipping (tilted) in one direction; often separates areas where the rock layers are horizontal
normal fault - fault on which displacement has caused the hanging wall to move down relative to the footwall; usually associated with horizontal extension and a stress tensor that has vertical maximum principal stress
occlusion - something which obscures or covers up
pole - the pole to a surface is a line drawn perpendicular to that surface

relay ramp - region of intact rock that connects the hanging wall of a fault with its footwall

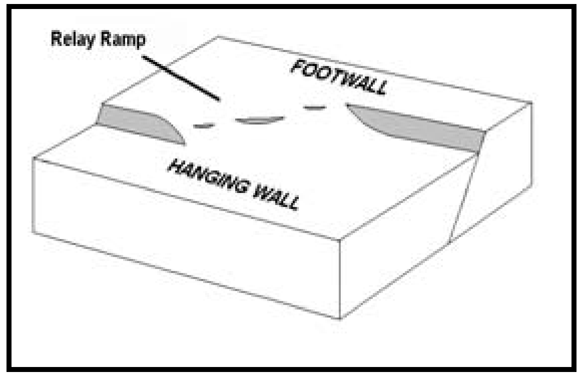

slickenlines - lines on a fault surface, either grooves or mineralized lineations, that indicate slip direction; may feel slick to the touch
slickolites - slickenlines that show evidence of mineral precipitation and dissolution
stress tensor - roughly synonymous with "stress system" and usually confined to homogeneous stress systems; most commonly defined by giving the magnitudes and orientations of the three mutually perpendicular principal stresses; specifying these implies a complete description of all possible stresses within the system
strike - the compass azimuth of a horizontal line drawn in a non-horizontal plane; the line of intersection between a plane and a horizontal surface
synthetic dip panels - rock layers adjacent to a fault or faults that have the same dip direction as the fault